INVESTIGATING THE FUNCTION OF KCNE4 IN CARDIAC PHYSIOLOGY

By

Erin Julia Ciampa

Dissertation

Submitted to the Faculty of the

Graduate School of Vanderbilt University

in partial fulfillment of the requirements

for the degree of

DOCTOR OF PHILOSOPHY

in

Pharmacology

May, 2011

Nashville, Tennessee

Approved:

Dr. Ronald B. Emeson

Dr. James R. Goldenring

Dr. Bjorn C. Knollmann

Dr. Christopher B. Brown

Dr. Alfred L. George, Jr.

ACKNOWLEDGEMENTS

I feel very fortunate to have had the opportunity to complete my dissertation under Dr. Alfred George, whose mentorship both guided me smoothly through my thesis work and has provided me with an excellent model for how to effectively lead a lab team. The supportive, stimulating environment he fosters in his laboratory has been an ideal setting for my training as a scientist. Great thanks are also due to all of my colleagues in the George lab, especially Dr. Carlos Vanoye, Jennifer Kunic, Lauren Manderfield, and Melissa Daniels, who helped me so willingly throughout every step of my project. Each member of my Dissertation Committee has also provided great wisdom and guidance that contributed to a graduate school experience that I could not be happier with.

My time in the Vanderbilt Medical Scientist Training Program has amounted to a life-changing experience, thanks to my mentors and classmates. I would especially like to thank our program director, Dr. Terry Dermody, for his enthusiasm and dedication to all trainees and for the personal support he has provided me ever since offering me a position to train at Vanderbilt. My career has been forever shaped for the best thanks to my opportunity to be a part of this program.

I also thank my family for their endless support as I pursue my career goals. My parents instilled in me a love of education at an early age that has become a defining

element of my self-identity and drives so much of what I do on a daily basis and as I plan

for my future. Finally, I cannot adequately express my gratitude to my husband, Phil, for

continually inspiring me to do meaningful work and take on important challenges.

TABLE OF CONTENTS

Chapter

LIST OF TABLES

LIST OF FIGURES

CHAPTER I

INTRODUCTION

Ion channels are integral membrane proteins or protein complexes that are critical for cell functions that depend on properly maintained electrical and chemical gradients. Their direct involvement in a cell's ability to generate electrical activity implicates ion channels in muscle contraction and movement, sensation, and cognition, among other complex physiologic functions. Additionally, their contributions to the regulation of electrolyte distribution across the cell membrane makes ion channels necessary for fundamental processes such as growth and fluid balance. As a result, disruption of normal ion channel function can have wide-ranging and substantial consequences, and the so-called "channelopathies" include epilepsy, cardiac arrhythmias, cystic fibrosis, and many others[1].

Voltage-gated potassium (K_V) channels

K_V channels comprise one family of ion channels. As voltage-gated channels, they respond to alterations in membrane potential with conformational changes that allow potassium ions to move down their electrochemical gradient into or out of a cell. K_V channels constitute a diverse class of membrane proteins, and the channels in this subset are known to have an essential role in membrane excitability, cellular proliferation, synaptic transmission, and epithelial transport.

K_V channel structure

K_V channel structure

The minimal functional unit of a K_V channel is a homo- or hetero-tetramer of pore-forming subunits. There exist more than 75 genes encoding K_V channel α subunits (categorized into 12 subfamilies, K_V1-12), each possessing unique biophysical, pharmacological, and assembly properties, and with diverse physiologic functions. KCNQ1, also known as K_V7.1 or K_VLQT1, is an important K_V channel α subunit in many physiologic systems but is best known for its contributions to cardiac electrophysiology, which are discussed below. Briefly, in cardiac myocytes KCNQ1 is a component of the channel complex responsible for I_{Ks}, a critical repolarizing current in the cardiac action potential[2,3]. KCNQ1 is also implicated in solute transport across the membranes of a number of epithelial tissues, including pancreas[4,5], kidney[6,7], the inner ear[8,9], and components of the gastrointestinal tract[7,9-13].

Figure 1 illustrates basic structural features of the KCNQ1 monomer and homotetramer, which are typical of many K_V channels. Limited success at purifying KCNQ1 has so far prohibited solving its structure directly. However, our collaborators recently published computationally validated models of KCNQ1 monomers and homotetramers in the open and closed states, based on KCNQ1 homology to other K_V channels whose crystal structures were used as templates in computational predictions[14]. These models are useful for developing hypotheses about the mechanics of channel opening and closing and its modulation by other proteins. Notably, each KCNQ1 monomer has an intracellular N-terminus, four transmembrane segments (S1 through S4) that constitute the voltage-sensing domain of the functional tetramer, a pore domain
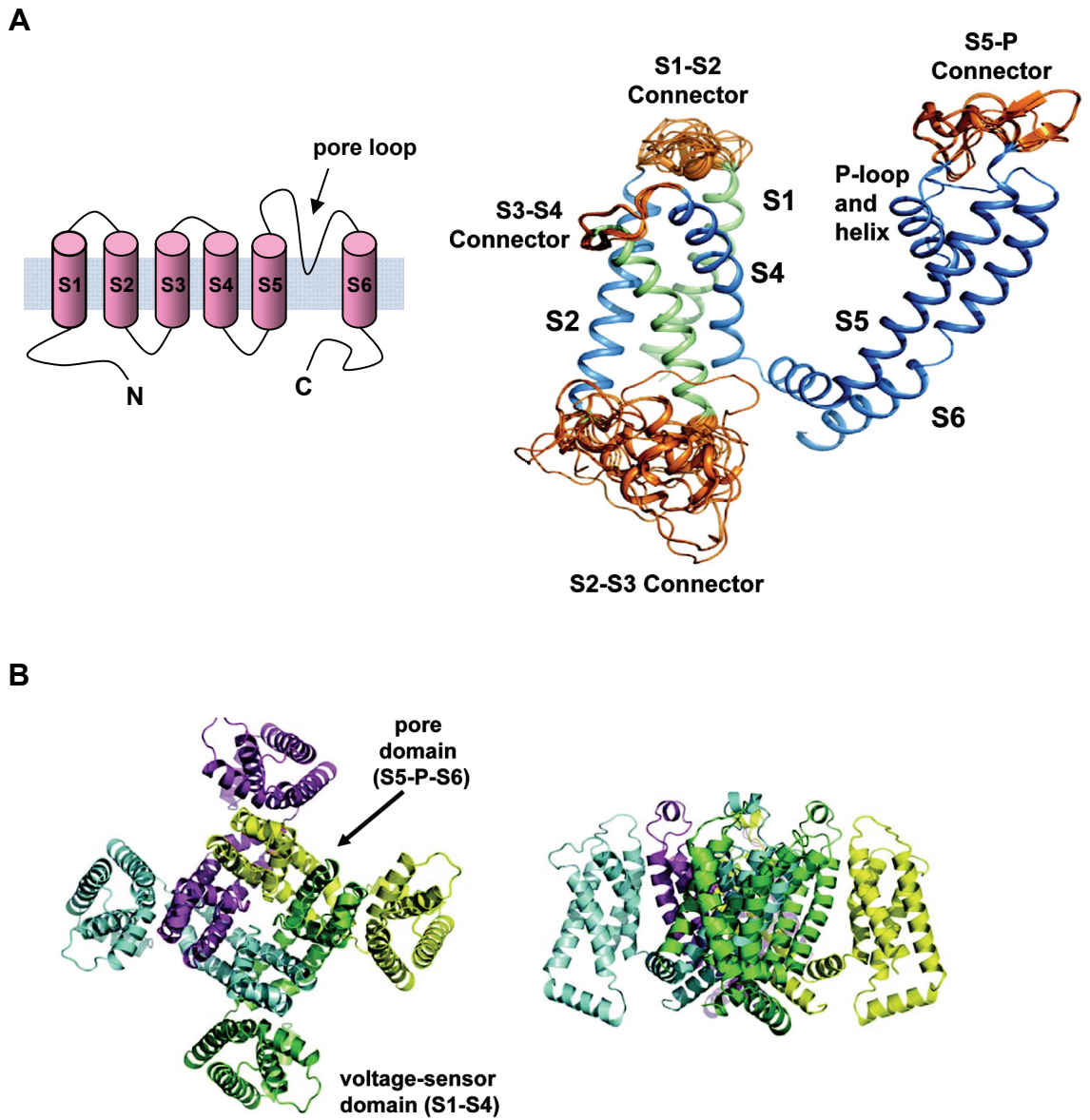
Figure 1. Structural features of KCNQ1. A, Topology map (left) and open-state model (right) of KCNQ1 monomer viewed from membrane plane, with transmembrane segments designated S1 through S6. Blue denotes regions derived from $K_V1.2$ crystal structure template; green denotes regions derived from crystal structure backbone coordinates and predicted side chain assignments; orange denotes regions modeled *de novo* using Rosetta. B, Open state model for KCNQ1 homotetramer (each monomer assigned a unique color). Left, extracellular view; right, view from membrane plane. Modeling data in A and B from Smith et al. *Biochemistry*, 2007 Dec 11;46(49):14141-52.

comprised of the two N-terminal transmembrane segments plus the linker ("pore loop") between them (S5-P-S6), and a long intracellular C-terminus.

Biophysical profile of K_V current

Unlike the other K_V7 subtypes ($K_V7.2 - K_V7.5$, or KCNQ2 –KCNQ5), which can form heterotetramers in various combinations, KCNQ1 only assembles into homo-tetramers[15-19]. Whole-cell voltage-clamp recordings allow characterization of the current generated by KCNQ1 tetramers in heterologous expression systems, as shown in Figure 2. Applying a series of step depolarizations from a holding potential of -80 mV to more positive membrane potentials in 10 mV increments, we record a set of rapidly activating outward currents of increasing amplitude. Upon returning the membrane to a repolarized potential (-30 mV) after each step depolarization, we observe that KCNQ1 channels partially inactivate after opening, which is apparent as a "hook" in the tail currents, reflecting recovery from the inactivated state before deactivation takes place.

From the currents recorded under this voltage-clamp protocol, we can calculate average peak current density at each depolarizing test potential. Further, we can assess the voltage-dependence of activation for KCNQ1 channels, by normalizing peak tail current for each test potential to the maximal value for each cell, and plotting normalized peak tail current versus voltage. These activation curves can then be fitted with a Boltzmann function $y = [1 + \exp(V-V_{1/2}/k)]^{-1}$ to determine the voltage for half-maximal activation ($V_{1/2}$) and a slope factor (k). This set of basic biophysical properties of KCNQ1 currents is displayed in Figure 2.

A

Protocol:

B

C
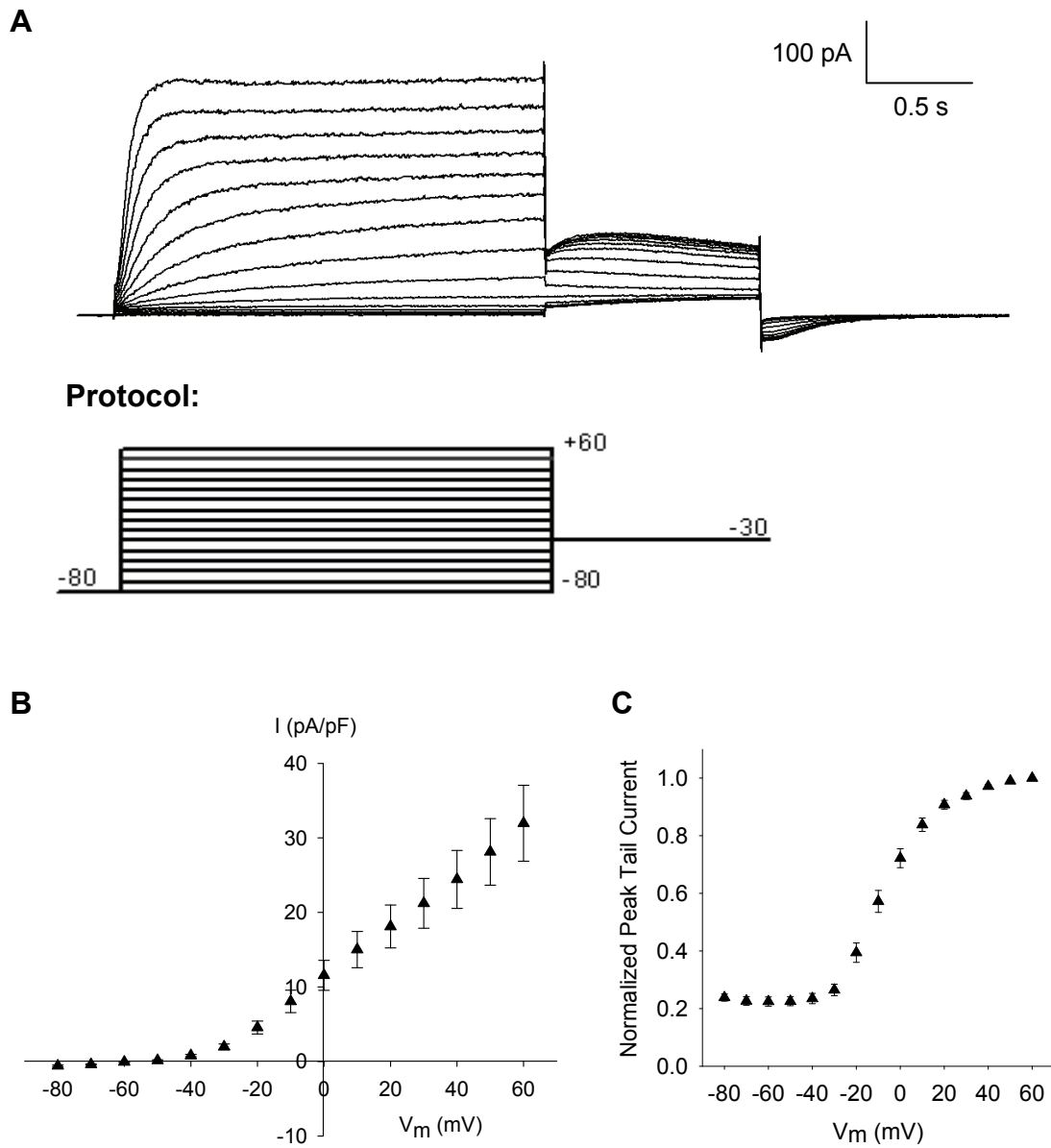
Figure 2. Biophysical properties of KCNQ1 current. A, Representative whole-cell currents elicited in CHO cells transiently transfected with KCNQ1 upon applying a series of test potentials as illustrated in the voltage-clamp protocol (membrane voltage indicated in mV). B, Average peak current-density versus voltage plot (n = 9 cells). C, Voltage-dependence of activation. $V_{1/2}$ = -7.0 ± 1.9 mV, k = 10.4 ± 0.5 mV.

Regulation of K_V channels

Research is demonstrating that *in vivo*, few (if any) K_V channels function independently of modulatory subunits or other regulatory factors within the cell. Rather, they exist as dynamic protein complexes whose constituents include a wide variety of proteins and signaling molecules. KCNQ1 channels are no exception; thus, characterization of the biophysical properties of KCNQ1 homotetramers under baseline conditions provides a critical reference point for assessing their modulation by other proteins, signaling molecules, and intracellular conditions.

Adrenergic stimulation has been identified as one important regulator of KCNQ1-containing channel complexes[20]. Adrenergic agonists stimulate cyclic AMP (cAMP) activation of protein kinase A (PKA), which phosphorylates a serine in the N terminus of KCNQ1, altering its activity[21,22]. KCNQ1 regulatory activity has also been assigned to phosphatidylinositol-4,5-bisphosphate (PIP_2), which has been found to stabilize the open state and increase current amplitude, as well as slow deactivation[23,24]. Additionally, cell swelling[25] and extracellular acidification[26] have each been observed to stimulate KCNQ1 current.

Recent studies have also implicated the ubiquitous Ca^{2+}-sensing protein calmodulin (CaM) as a modulator of KCNQ1 activity[27,28]. A domain in the C-terminus of KCNQ1 appears to mediate a biochemical interaction with CaM, and pharmacological disruption of the KCNQ1-CaM interaction was found to cause complete suppression of KCNQ1 current, suggesting that CaM is required for KCNQ1 activity. Further, KCNQ1 voltage-dependence of activation is shifted toward more negative potentials under conditions of high intracellular $[Ca^{2+}]$. This KCNQ1 Ca^{2+} sensitivity may be conferred by its

interaction with CaM, as overexpression of a Ca^{2+}-insensitive CaM mutant shifts the voltage-dependence of activation of KCNQ1 toward more positive potentials.

K_V Channel Accessory Subunits

The diversity of K_V channel composition and activity is also expanded through association of pore-forming α-subunit tetramers with accessory subunits, of which there are three main classes: $K_V\beta$, KCHIP, and KCNE. These accessory proteins can have profound effects on channel biophysical properties, pharmacological responses, tissue distribution, trafficking, and regulation by other cellular factors[29].

KCNE proteins

There are five *KCNE* genes, each encoding a short protein (103-177 residues in length) with a single membrane-spanning domain (Figure 3). The KCNE proteins do not generate current when they are expressed alone, but they are characterized by their ability to modulate the biophysical properties of potassium channels when coexpressed with K_V α subunits. In addition to structural similarity, the *KCNE*s share promiscuity in their interactions with K_V channel complexes. Lists of K_V α subunits that each KCNE protein has been shown to modulate to date are illustrated in Figure 4. It is important to note that these lists reflect a compilation of findings based on a candidate approach to studying the targets of modulation of each KCNE protein, and they will likely be proven incomplete as research continues.

A

B

```
KCNE1                                     MILSNTTAV  TPFLTKLWQE  TVQQGGNMSG
KCNE2                                     MSTLSNFTQT  LEDVFRRIFI  TYMDNWRQNT
KCNE3   METTNGTETW  YESLHAVLKA  LNATLH----  -SNLLCRPGP  GLG----PDN
KCNE4                                      MLKMEPLN  STHPGTAASS
KCNE5      MNCSES-   -QRLRTLLSR  LLLELHHRGN  ASGLGAGPRP  SMGMGVVPDP


KCNE1   LARRSPRSSD  GKLE-----A  LYVLMVLGFF  GFFTLGIMLS  YIRSKKL-EH
KCNE2   TAEQEALQAK  VDAENFYYVI  LYLMVMIGMF  SFIIVAILVS  TVKSKRR-EH
KCNE3   QTEERRASLP  GRDDNSY---  MYILFVMFLF  AVTVGSLILG  YTRSRK-VDK
KCNE4   SPLESRAAGG  GSGNGNEY--  FYILVVMSFY  GIFLIGIMLG  YMKSKRR-EK
KCNE5   FVGREVTSAK  G--DDAY---  LYILLIMIFY  ACLAGGLILA  YTRSRKLVEA


KCNE1   SNDPFNVYIE  SDAWQEKDKA  YVQARVLESY  RSCYVVENHL  AIEQPNTHLP
KCNE2   SNDPYHQYIV  ED-WQEKYKS  --QILNLEES  KAT-IHENIG  AAGFKMSP
KCNE3   RSDPYHVYI-  KNRVSMI
KCNE4   KSSLLLLY--  KDEERLWGEA  MKPLPVVSGL  RSVQVPLMLN  MLQESVAPAL
KCNE5   KDEPSQACA-  EHEWAPGGAL  TADAEAAAGS  QAEGRRQLAS  EGLPALAQGA


KCNE1   ETKPSP
KCNE2
KCNE3
KCNE4   SCTLCSMEGD  SVSSESSSPD  VHLTIQEEGA  DDELEETSE  TPLNESSEGSS
KCNE5   ERV


KCNE1                  129 aa
KCNE2                  123 aa
KCNE3                  103 aa
KCNE4   ENIHQNS        170 aa
KCNE5                  142 aa
```

Figure 3. Basic structural features of KCNE proteins. A, Topology of a KCNE protein with extracellular N-terminus and cytoplasmic C-terminus. B, Amino acid sequence alignment of human isoforms of KCNE1-KCNE5. Colors denote predicted domains: purple – extracellular, red – transmembrane, blue – intracellular.

KCNE1 → KCNQ1, HERG, $K_V2.1$, $K_V3.1$, $K_V3.2$, $K_V4.3$, $K_V12.2$

KCNE2 → KCNQ1, HERG, KCNQ2, KCNQ3, $K_V2.1$, $K_V3.1$, $K_V3.2$, $K_V4.2$, $K_V4.3$

KCNE3 → KCNQ1, HERG, KCNQ4, $K_V2.1$, $K_V3.1$, $K_V3.2$, $K_V3.4$, $K_V4.2$, $K_V12.2$

KCNE4 → KCNQ1, BK, $K_V1.1$, $K_V1.3$, $K_V4.2$, $K_V4.3$

KCNE5 → KCNQ1, $K_V4.3$
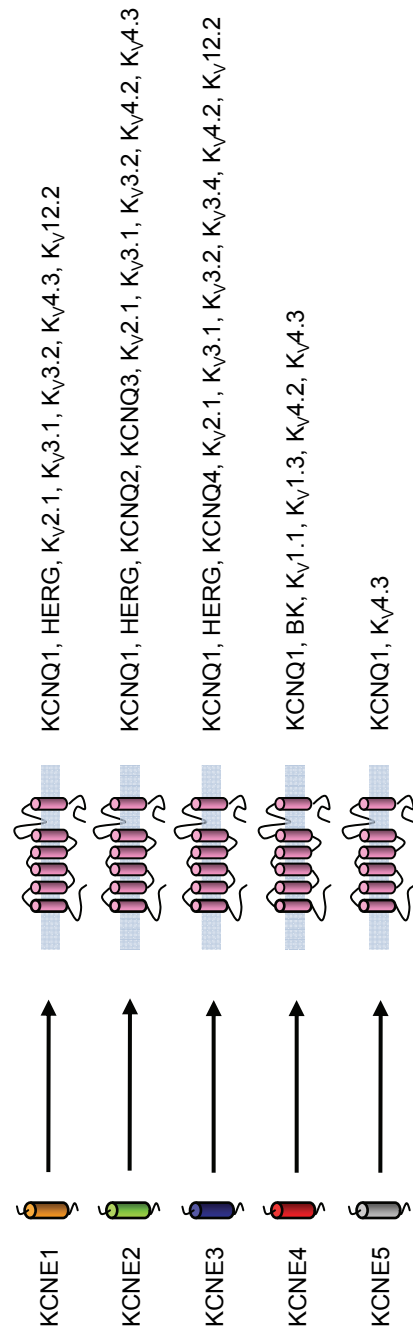
Figure 4. K_V channel α subunits demonstrated to be biophysically modulated in heterologous expression systems by KCNE1-5.

Biophysical modulation of KCNQ1 by KCNE1-KCNE5

As illustrated in Figure 4, each KCNE subunit is capable of modulating KCNQ1. We performed whole-cell voltage-clamp recordings in CHO cells co-expressing each KCNQ1-KCNE pair, which allows us to directly compare the modulatory properties of the KCNE family members (Figure 5). As the current traces illustrate, each subunit exerts a different modulatory effect on KCNQ1. Our findings, described below, are consistent with other published characterizations of the KCNQ1-KCNE channel complexes.

KCNE1 (also known as minK, "minimal K$^+$ channel protein") interacts with KCNQ1 to increase its current amplitude, slow its activation and deactivation rates, remove its inactivation state, and shift its voltage dependence of activation to more positive potentials[2,30]. When KCNE2 (or MiRP1, MinK-related protein 1) is co-expressed with KCNQ1, it decreases its current amplitude but renders the channel constitutively open[31]. By contrast, KCNE3 (MiRP2) dramatically increases KCNQ1 current amplitude and also confers near-instantaneous activation[32,33]. KCNE4 (MiRP3) and KCNE5 (MiRP4) each dramatically inhibit KCNQ1 channel activity at all physiologic voltages, though for KCNQ1 plus KCNE5 at supra-physiologic depolarizations an outward current with slowed activation properties is restored[34,35]. Together, these data reflect great diversity in the modulatory properties of the various KCNE subunits when they interact with KCNQ1.
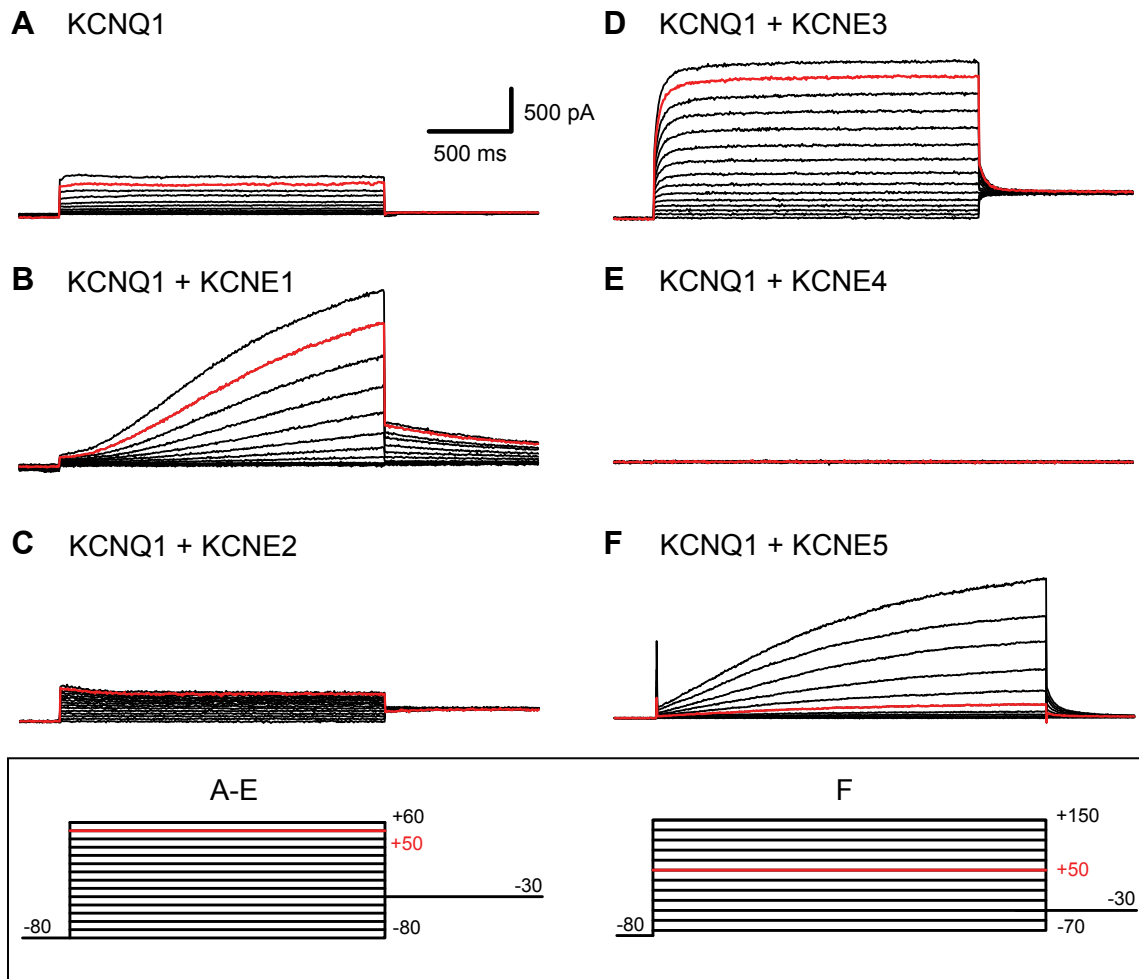
Figure 5. Whole-cell currents recorded in CHO cells co-transfected with *KCNQ1* and *KCNE1-5*. Each set of traces recorded using voltage-clamp protocol as indicated in box. Currents recorded upon +50 mV test depolarization illustrated in red for reference.

Mechanisms of K_V channel modulation by KCNE proteins

We have an incomplete understanding of the mechanisms by which KCNE subunits exert their modulatory effects on K_V channel α subunits such as KCNQ1. One obstacle arises from conflicting evidence regarding the number of KCNE proteins that associate with a given tetramer of K_V channel α subunits. The KCNQ1-KCNE1 channel complex has most commonly been the focus of previous investigations into subunit stoichiometry.

Two studies approached the problem with the use of the K^+ channel inhibitor charybdotoxin (CTX). Chen *et al* compared CTX on- and off-rates for cells expressing KCNQ1 and KCNE1 monomers (which assemble into their natural channel complexes) and cells expressing KCNQ1-KCNE1 concatamers that force defined stoichiometries[36]. Morin and Kobertz performed KCNE1 counting by iterative cell-surface modification[37]: they linked CTX to a cysteine-modifying agent via a cleavable linker, such that upon addition of this reagent to cells expressing KCNQ1-KCNE1 channels the compound blocks the channel and modifies a cysteine engineered into the extracellular domain of KCNE1. Excess reagent is washed out, and CTX is tethered to the channel complex via the KCNE1 cysteine, irreversibly blocking the channel until the linker is chemically cleaved, leaving one KCNE1 subunit labeled. This process is repeated until the reagent becomes a reversible blocker without cleaving the linker, indicating that all the KCNE1 subunits have been modified. Both studies provided strong evidence of a fixed 4:2 KCNQ1-to-KCNE1 subunit ratio.

However, other studies (whose main limitations include their reliance on isolated subdomains of KCNQ1 and KCNE1 or chimeras tethering KCNQ1 to other protein domains for structural anchoring, as opposed to native proteins) have suggested that

multiple configurations are possible (from one to four KCNE1 subunits per KCNQ1 tetramer), depending on the relative expression of each gene[38,39]. Without a clear understanding of subunit stoichiometry it is difficult to work toward a comprehensive understanding of the mechanism of KCNE modulation of KCNQ1 or any K_V channel complex.

KCNE structure-function relationships

We also lack data clearly defining the relative positioning of KCNE subunits within a K_V channel complex. No direct crystallographic analysis has been achieved for any member of the KCNE family (alone or in complex with a K_V channel), but our collaborators recently published a 3-dimensional characterization of KCNE1 based on NMR spectroscopy of KCNE1 purified into micelles, plus models for KCNE1 docking to KCNQ1 in open and closed states based on a number of experimentally derived restraints[40]. Though the authors themselves consider their models "best regarded as being medium-resolution in nature, both because of the imperfect precision of structures that satisfy the experimental restraints used in docking and because of uncertainty regarding some of the assumptions made in the restrained docking calculations", they provide valuable new information about the general locations of KCNE1 subdomains with respect to KCNQ1. For example, in the closed state, KCNE1 is found to sit in a cleft between the S5-P-S6 pore domain of one KCNQ1 subunit and the voltage sensor of an adjacent subunit; in the open state, the N-terminus of the KCNE1 transmembrane domain is in contact with three different subunits: S1 from one, S5 and the pore helix from a second, and S6 from a third.

In many cases, findings from the structural analysis support mechanistic postulations derived from previous studies of structure-function correlates for how KCNE1 slows KCNQ1 channel activation and enhances conductance. For example, previous studies had identified a specific residue in the KCNE1 transmembrane domain, Thr58, to be sufficient for conferring the slow activation properties of KCNE1 to KCNE3 (in which a valine occupies the equivalent site) and vice versa[41-43]; in the structural models the side chain of Thr58 was found to be well-positioned to interact with KCNQ1. Further, the cleft KCNE1 was found to occupy in the open state encompasses the sites of four KCNQ1 gain-of-function mutations[44-47], supporting a postulation from the structural model that KCNE1 may enhance conductance in part by stabilizing the open state of KCNQ1 via contact of its transmembrane domain with KCNQ1 residues in this cleft.

Structural models of the KCNQ1-KCNE1 channel complex may prove to be a useful template for understanding some properties universal to all KCNE proteins, but given the unique structural and functional features of each KCNE protein, we must ultimately study them individually to determine the mechanisms that underlie their specific modulatory effects on K_V channels. KCNE4 is distinct among the KCNE proteins both for its long C-terminus and for its dramatic inhibition of KCNQ1. Our lab used KCNE1-KCNE4 and KCNE3-KCNE4 chimeras to study which KCNE4 domains are critical for its inhibition of KCNQ1. Notably, the transmembrane residues sufficient for swapping activation properties among KCNE1 and KCNE3 were not found to impart KCNE1- or KCNE3-like properties to KCNE4 (nor KCNE4-like complete inhibition of KCNQ1 to KCNE1 or KCNE3).

Instead, the intracellular C-terminus of KCNE4 (residues 59 through 170) conferred inhibitory properties to KCNE1 and KCNE3, and also was also found to be necessary for KCNE4 inhibition of KCNQ1, as chimeras that replaced the C-terminus of KCNE4 with that of KCNE1 or KCNE3 failed to inhibit KCNQ1[48]. Importantly, this study also demonstrated that the KCNE4 C-terminus is not sufficient for inhibition of KCNQ1, using a chimera that tethered the KCNE4 C-terminus to a surrogate single transmembrane domain protein, the lymphocyte CD8 receptor. The CD8-KCNE4 C-terminus chimera did not inhibit KCNQ1 current, despite confirmation that the chimeric protein reached the membrane and that it interacts biochemically with KCNQ1. These data and findings from several other studies[49-51] contribute to an emerging model of cooperativity between the transmembrane domain and C-terminus for a KCNE protein to exert its modulatory effect on a K_V channel.

Other studies have lent further insight into the particular mechanism of KCNE4 inhibition of KCNQ1. These include early observations that delayed injection of *KCNE4* mRNA into oocytes previously injected with KCNQ1 does not impair the ability of KCNE4 to inhibit KCNQ1 current, suggesting that its inhibitory effect is not dependent on early KCNQ1-KCNE4 assembly in the secretory pathway, but could take place in the plasma membrane[35]. Further, we[52] and others[35] have demonstrated that expression of KCNQ1 at the cell surface is not affected by KCNE4 expression, suggesting that KCNE4 exerts its inhibitory effect on KCNQ1 via true biophysical modulation of channel gating, as opposed to disrupting KCNQ1 trafficking to the membrane or enhancing its internalization from the cell surface. These findings each provide additional clues as to the mechanism by which KCNE4 exerts its impressive inhibitory effect on KCNQ1.

Expression patterns of KCNE1-KCNE5

All five of the *KCNE* genes are widely expressed in mammalian tissues. Our lab used real-time RT-PCR to quantify relative expression levels of *KCNQ1* and *KCNE1-5* in commercially available panels of cDNA derived from normal human subjects[53]. Figure 6 illustrates the findings across 15 tissues. Consistent with previous studies in human and other mammalian tissues[35,54-56], all of the KCNEs were detected in the heart. *KCNE1* is also prominently expressed in kidney[57,58], testes[59], and uterus[60,61]. *KCNE2* expression was found to be most significant in colon and small intestine, to complement previous findings of its high relative expression in stomach[62,63]. We found strongest *KCNE3* expression in human kidney, liver, prostate, colon, spleen, ovary, placenta, and leukocytes (consistent with previous findings[62,64-67]), whereas its expression has also been previously demonstrated in the trachea[67], nasal epithelia[64], and portal vein[68]. Prominent expression of *KCNE4* was detected in kidney, skeletal muscle, testis, prostate, spleen, ovary, and uterus, which overlaps to some extent with a previous report of *KCNE4* expression in mouse[35]. Finally, we found particularly high *KCNE5* expression in brain, thymus, ovary, and placenta, whereas previous studies have mostly focused on its expression in various regions of the central nervous system[55,68].

Our lab has also characterized KCNE4 expression at the protein level[52]. Lysates from sixteen human tissues were probed with anti-KCNE4, as shown in the representative Western blots in Figure 7. Modest protein expression was detected in many of the tissues that demonstrated robust *KCNE4* mRNA expression, including brain, heart, small intestine, kidney, liver, ovary, pancreas, skeletal muscle, spleen, testis, thymus, and uterus. Overall, the mRNA and protein data we have collected provide a
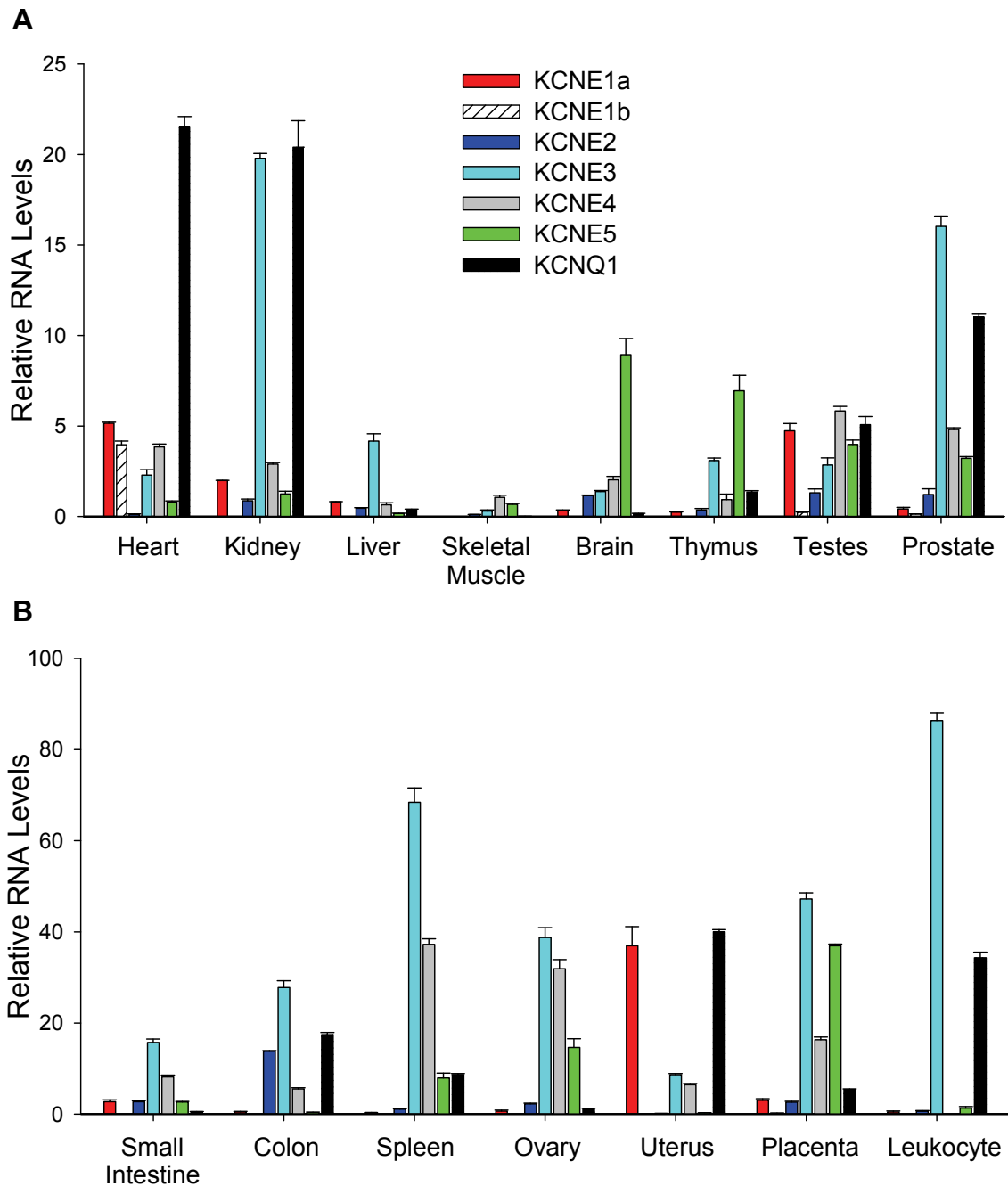
Figure 6. Relative expression of *KCNQ1* and *KCNE* genes in human tissues. Several human tissues were examined by real-time quantitative RT-PCR. Tissues were grouped by low (A) and high (B) overall expression for display purposes (note differences in the y-axis scale). All data were quantified by gene specific standard curves and results were normalized by GAPDH expression. Data are presented as mean ± SEM for at least 6 replicates from 2 different pooled (2 or more individuals) cDNA samples isolated from healthy individuals. From Lundquist *et al*. Genomics. 2006 Jan;87(1):119-28.
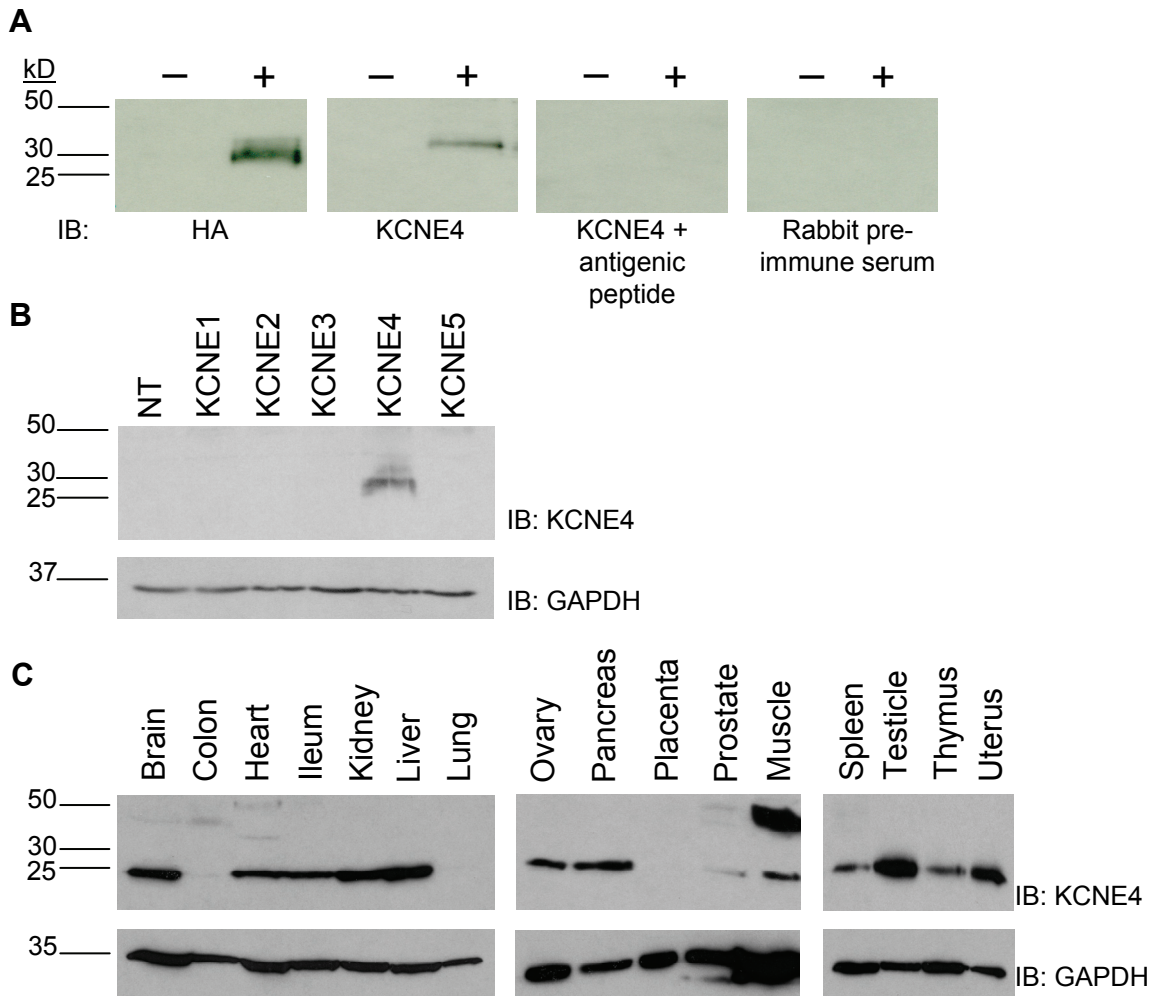
Figure 7. Expression of KCNE4 protein in human tissues. A, Whole cell lysates from COS-M6 cells transfected with HA epitope-tagged KCNE4 (+) or non-transfected cells (−) were subjected to SDS-PAGE and western blotting with the indicated immunoreagent. A specific protein with a molecular mass of approximately 28 kDa was identified by immunoblotting with either anti-HA or anti-KCNE4. B, Western blot of lysates derived from non-transfected cells (NT) or cells expressing each individual KCNE protein probed for KCNE4. All lysates were also probed for GAPDH in order to demonstrate protein expression. C, Western blot of lysates derived from specified human tissues probed for KCNE4. Brain lysates were derived from the cerebellum. Colon lysates were derived from the descending colon. Heart lysates were derived from the left ventricle. Muscle lysates were derived from skeletal muscle (quadriceps). All lysates were also probed for GAPDH. From Manderfield *et al*. FEBS J. 2008 Mar;275(6):1336-49.

foundational understanding of the distribution of *KCNE* expression, but further studies with increasing specificity (eg. identifying which subregions or specific cell types within a tissue express a given *KCNE* gene) are also needed.

Physiologic functions of KCNE1-KCNE5

It has become possible to assign physiologic functions to the KCNE proteins, based on various combinations of the following findings: disease association with human mutation(s) in a *KCNE* gene, phenotypic findings in *Kcne* knockout mouse models, recapitulation of the biophysical and pharmacological properties of a physiologic current upon heterologous expression of the candidate K_V-KCNE channel complex, and confirmation of native expression of the *KCNE* gene and its target of modulation by the appropriate tissue. In many cases, a single *KCNE* gene has been implicated in multiple physiologic processes, which is not surprising based on the broad expression of *KCNE* genes and their promiscuity in modulating diverse K_V channel complexes. Findings to date are summarized below.

Cardiac physiology

K_V channels are critical for generation and propagation of action potentials in the heart. A generic ventricular cardiac action potential is displayed in Figure 8, along with underlying potassium currents. The exact waveform of the action potential varies within subregions of the heart, concurrent with variations in the biophysical properties of the underlying currents and expression of ion channel subunits. This electrical heterogeneity
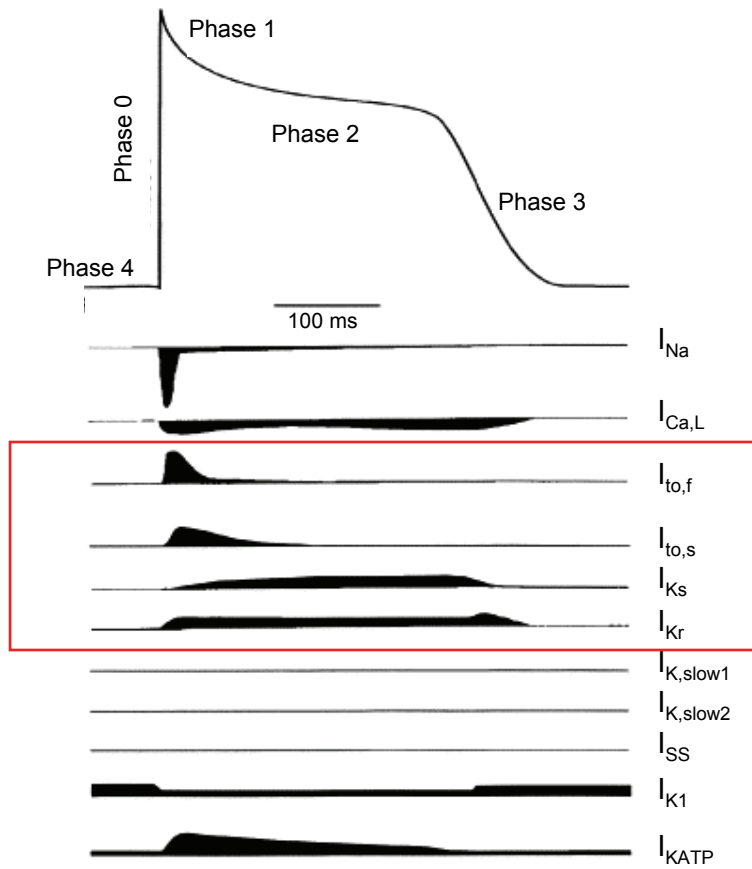
Figure 8. Generic human ventricular action potential waveform. X-axis, membrane potential; y-axis, time. Underlying currents identified below; red box highlights major repolarizing K^{+} currents. Adapted from Nerbonne JM *Trends Cardiovasc Med* **14**, 83-93 (2004).

across the heart is critical for coordination and fine control of action potential propagation, but can also be a substrate for arrhythmia[69].

I_{to}, I_{Ks}, and I_{Kr}, the major outward K^+ currents expressed by ventricular myocytes, are activated at depolarized potentials and contribute to repolarization of the myocyte. This directly implicates I_{to}, I_{Ks}, and I_{Kr} in determining the length of the action potential and the ability of myocytes to adapt to factors such as changing heart rate. Dysregulation of these currents can have significant consequences, as delayed repolarization (which translates to a lengthened QT interval on electrocardiogram) may allow for premature reactivation of inward calcium and sodium currents, permitting early afterdepolarizations and the potential for ventricular fibrillation, arrhythmia, and sudden death. Discovery of genetic mutations associated with inherited long QT syndrome (LQTS) has helped identify genes that encode the cardiac K^+ channel subunits responsible for the various repolarizing currents in the human cardiac action potential.

All five of the *KCNE* genes are expressed to varying degrees and with distinct regional patterns in the heart[70] (Figure 9). Over the years, several KCNE proteins have been identified as critical modulators of repolarizing K^+ currents in the cardiac action potential. As mentioned previously, the pore-forming unit of I_{Ks}, the 'slowly activating' repolarizing K^+ current, is a KCNQ1 tetramer, originally identified via association of KCNQ1 mutations with the most common inherited form of LQTS[71]. However, recapitulation of the pharmacological and biophysical properties of I_{Ks} requires co-expression of KCNQ1 with KCNE1[2,3], giving rise to the slowly activating and deactivating current displayed in Figure 5, first observed in 1996. Shortly thereafter, *KCNE1* mutations were identified in families with inherited LQTS, which when
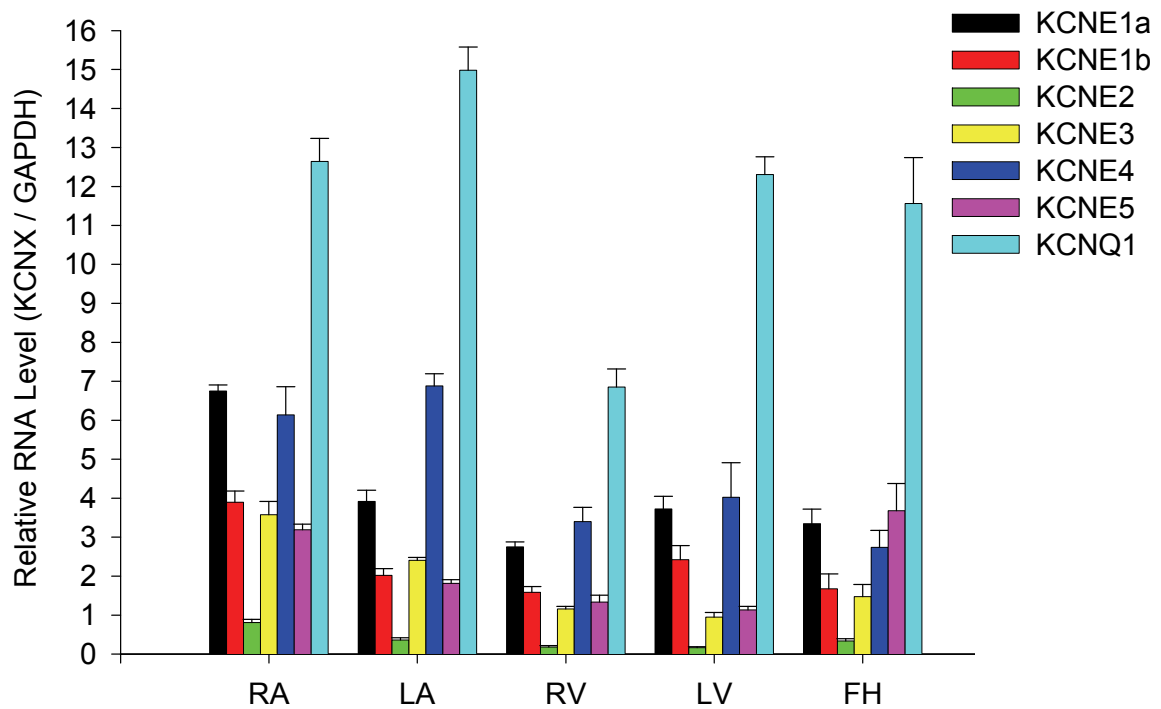
Figure 9. Relative expression of *KCNQ1* and *KCNE* genes in human heart. Five human cardiac tissues were examined by real-time quantitative RT-PCR: right atrium (RA), left atrium (LA), right ventricle (RV), left ventricle (LV), and fetal heart (FH). All data were quantified by gene-specific standard curves and values were normalized to GAPDH expression. Data are presented as mean ± S.E.M. of at least six replicates from two different pooled cDNA samples derived from multiple individuals. From Lundquist AL *et al*. J Mol Cell Cardiol. 2005 Feb;38(2):277-87.

characterized in heterologous expression systems were found to reduce I_{KS} current by shifting the voltage dependence of activation and accelerating deactivation. Lengthened QT interval in the mutation carriers can thus be accounted for by delayed repolarization due to reduced I_{Ks}. KCNE1 mutations are now recognized to account for approximately 3 % of inherited LQTS cases[72], and cardiac I_{Ks} is universally accepted to be generated by a channel complex comprised of KCNQ1 and KCNE1 subunits.

A recent study from our lab assessed whether the other KCNE proteins can modulate I_{Ks}[70]. A stable I_{Ks}-expressing cell line was generated by genomic integration of a bicistronic KCNE1-IRES2-KCNQ1 cassette, allowing uniform expression of *KCNQ1* and *KCNE1* from a single genomic locus, and generating a consistent level of I_{Ks} current in all cells. These I_{Ks}-expressing cells were then transfected with cDNA encoding each of the KCNE subunits, and potassium currents were recorded upon applying a standard voltage-clamp protocol (Figure 10). Cells expressing I_{Ks} plus EGFP, KCNE1, or KCNE2 exhibited slowly-activating current with gating properties indistinguishable from the transient co-expression of KCNQ1 and KCNE1 in CHO cells. By contrast, expression of KCNE3 accelerated activation of I_{Ks} while co-expression of either KCNE4 or KCNE5 suppressed the current. These observations indicate that KCNE3, KCNE4 and KCNE5 are capable of modulating KCNQ1-KCNE1 channel complexes *in vitro* and may contribute to fine-tuning of I_{Ks} *in vivo*.

I_{Kr}, the 'rapidly activating' repolarizing K^+ current, was first associated with the K_V α subunit hERG ('human ether-a-go-go related gene', also known as KCNH2 or $K_V11.1$) in 1995[73,74], and dominant-negative hERG mutations were identified in LQTS soon after[75]. However, heterologous expression of hERG alone has revealed differences in the
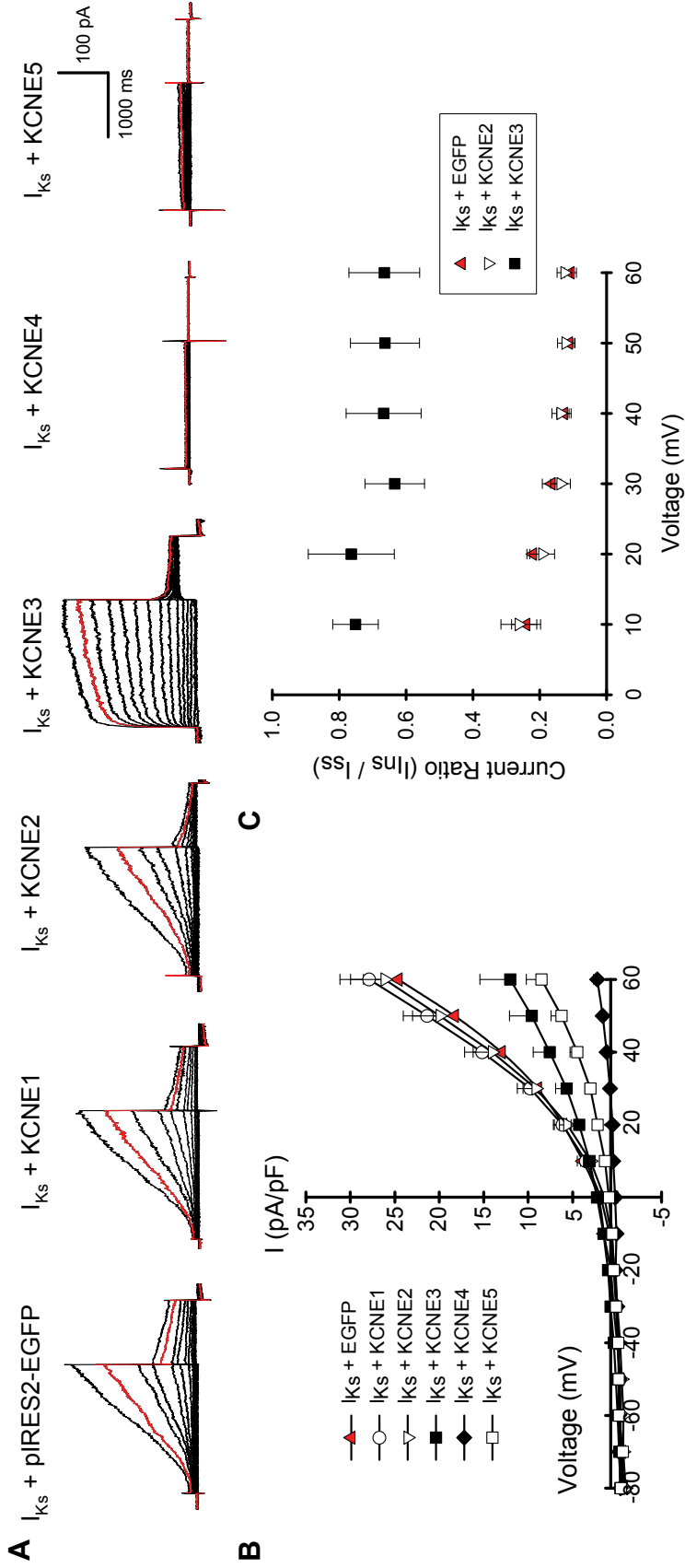
Figure 10. Heterologous expression of KCNE subunits in a stable I$_{Ks}$ cell line. A, Representative traces illustrating potassium currents observed in an I$_{Ks}$ cell line transiently transfected with vector alone (EGFP), KCNE1, KCNE2, KCNE3, KCNE4 or KCNE5. Data were recorded at test potentials ranging from –80 to +60 mV stepped in 10 mV increments from the holding potential of –80 mV for 2000 ms. B, Current–voltage relationships for potassium currents (normalized to membrane capacitance) measured in I$_{Ks}$ cells expressing EGFP ($n = 14$), KCNE1 ($n = 11$), KCNE2 ($n = 11$), KCNE3 ($n = 8$), KCNE4 ($n = 8$) or KCNE5 ($n = 12$). Current density is significantly reduced at all test potentials between –10 and 60 mV for I$_{Ks}$ + KCNE4 ($P <$ 0.01) and KCNE5 ($P <$ 0.05), but only at 60 mV for I$_{Ks}$ + KCNE3 ($P <$ 0.05). C, Alteration of I$_{Ks}$ activation kinetics by KCNE2 and KCNE3. The activation rate was assessed qualitatively by the ratio of the instantaneous current (I$_{Ins}$) to the steady state current (I$_{SS}$) measured at 150 and 1900 ms after the start of the voltage pulse, respectively. Data are shown as mean ± S.E.M. ($n = 8$). Current ratios are significantly different between I$_{Ks}$ + EGFP and I$_{Ks}$ + KCNE3 at all test potentials ($P <$ 0.01). From Lundquist AL *et al.* J Mol Cell Cardiol. 2005 Feb;38(2):277-87.

biophysical and pharmacological profiles of its K^+ current from those of native I_{Kr}[73,74,76-81], suggesting that cardiac I_{Kr} channels may be comprised of hERG plus accessory subunits. KCNE1 and KCNE2 have each been proposed as modulators of hERG in human heart.

In heterologous expression systems, KCNE1 can be co-immunoprecipitated with hERG and was found to increase hERG current density (with little effect on gating kinetics or single channel conductance)[82], and native ERG and KCNE1 have been co-immunoprecipitated from horse heart[83]. Co-expression of KCNE2 and hERG yields currents that resemble those of I_{Kr}, with more rapid deactivation and less sensitivity to external K^+ than hERG alone. Further, *in vitro* translated hERG has been found to preferentially assemble with KCNE2 over KCNE1[84], and native KCNE2 and ERG have been co-immunoprecipitated from dog heart[85]. Loss-of-function mutations in both KCNE1 and KCNE2 have been associated with LQTS[84,86-90], providing additional evidence that either of these subunits could be important for modulating I_{Kr} in cardiac physiology.

I_{to}, the 'transient outward' K^+ current, accounts for early repolarization in the human cardiac action potential. $I_{to,fast}$, the predominant component of I_{to} in most regions of mammalian myocardium, is thought to be composed of some combination of $K_V4.2$ or $K_V4.3$ α subunits plus the KChIP2 accessory subunit, depending on the species[91-94]. Findings of altered I_{to} current in the *Kcne2* knockout mouse plus co-immunoprecipitation of KCNE2 and $K_V4.2$ from mouse heart[95] implicate KCNE2 as a potential I_{to} modulator. KCNE3 has been demonstrated to be capable of modulating $K_V4.2$ in heterologous expression studies, and association of a missense *KCNE3* mutation with LQTS provides

further evidence that KCNE3 could modulate I_{to} *in vivo*[96]. Finally, $K_V4.2$-KChIP2 channels[97] and $K_V4.3$-KChIP2 channels[98] have both been demonstrated to be modulated *in vitro* by KCNE4, suggesting it too could function as a native modulator of I_{to}. Further, KCNE4 was found to co-localize with $K_V4.2$ to transverse tubules of rat cardiac myocytes and it was co-immunoprecipitated with $K_V4.2$ and KChIP2 following heterologous expression in tsA201 cells[97].

These findings reflect our preliminary understanding of possible roles for the KCNE subunits in cardiac physiology, but in many cases further investigation is needed. Particularly compelling evidence could emerge from demonstration of native co-assembly of the candidate channel subunits in cardiac myocytes, characterization of additional disease-associated mutants, or findings from knock-down studies in animal models whose cardiac electrophysiology closely recapitulates that of humans.

Central nervous system (CNS) physiology

Like the heart, the main function of the central nervous system requires generation and propagation of electrical signals, and thus depends on a wide range of ion channel subunits to elicit currents with varying biophysical properties. Expression of all five *KCNE* genes has been demonstrated in human brain[53], promoting the possibility that any of them could play important roles in modulating neuronal excitability. The M-current, a muscarinic-sensitive voltage-and time-dependent K^+ current expressed in many regions of the brain[99], has been the focus of most investigations into possible CNS targets of KCNE modulation. Heteromultimers of KCNQ2 and KCNQ3 subunits are thought to contribute to M-current channels[16,19], and mutations in each have been associated with

familial epilepsy[100-102]. It has been observed that the expression pattern of KCNE2 in the brain overlaps significantly with that of KCNQ2 and KCNQ3, that coexpression of KCNE2 with KCNQ2-KCNQ3 heteromultimers in COS cells recapitulates many biophysical properties of the native M-current, and that the three subunits can be co-immunoprecipitated following co-expression in COS cells[103].

Studies have also provided evidence for possible contributions of KCNE1 and KCNE3 to central nervous system electrophysiology, via possible interactions with $K_V2.1$ and $K_V3.1$ which may each constitute important neuronal K_V channels. Kcne3 was co-immunoprecipitated with $K_V2.1$ and $K_V3.1$ from rat brain, and KCNE3 has been demonstrated to modulate both of these a subunits in CHO cells[66]. A subsequent study also demonstrated modulation of $K_V3.1$ and $K_V3.2$ channels by KCNE1, KCNE2, and KCNE3 in CHO cells, further expanding the range of biophysical profiles of K^+ currents that can be generated by these neuronal channels[104].

Additionally, KCNE4 has been proposed as a modulator of CNS K_V channels composed of $K_V1.1$ and $K_V1.3$ subunits, based on observations that KCNE4 dramatically inhibits these channels in both oocytes and HEK cells[105]. Like its modulation of KCNQ1, KCNE4 is thought to inhibit the K_V1 channels via biophysical modulation of channel gating at the plasma membrane (as opposed to impairing trafficking of the channel subunits), as delayed injection of KCNE4 cDNA was effective at inhibiting channels at the membrane, and cell-surface expression of the α subunits was not found to be impaired by co-expression of KCNE4. The native functions of K_V1 channels in the brain are not known, and it is important to note that $K_V1.1$ and $K_V1.3$ are also expressed in

peripheral tissues (in many cases with patterns overlapping those of KCNE4) including lung, kidney, colon, and uterus.

Together, these findings provide early leads into potential roles for KCNE subunits in the electrophysiology of the central nervous system, but thus far no mutation in any *KCNE* gene has been associated with CNS deficits in humans or experimental models, limiting our ability to draw any firm conclusions.

Skeletal muscle physiology

Another excitable tissue that relies on diverse ion channel activity is skeletal muscle. An important study published in 2001 directly implicated KCNE3 in maintenance of resting membrane potential in skeletal muscle, via its interaction with $K_V3.4$ subunits[65]. In this study, KCNE3 protein was detected by Western blot in native rat sartorius muscle and in the C2C12 skeletal muscle cell line, and was found to co-localize with $K_V3.4$ in C2C12 cells by immunofluorescence. Further, KCNE3 was detected following co-immunoprecipitation with $K_V3.4$ from COS cells co-transfected with the two subunits. Evidence of $K_V3.4$ modulation by KCNE3 also emerged from voltage-clamp studies performed in CHO cells co-transfected with $K_V3.4$ and KCNE3, and the biophysical properties of the $K_V3.4$-KCNE3 channel complex matched those of native currents recorded in C2C12 cells. Finally, screening of patients with inherited muscle disorders without mutations in known disease-associated genes identified a KCNE3 mutation in two unrelated individuals with periodic paralysis. When characterized by co-expression with $K_V3.4$ in CHO cells, this KCNE3 mutation was found to reduce K^+ current and alter resting membrane potential, supporting a causative

role for the mutation in pathogenesis and for KCNE3 in normal skeletal muscle physiology.

Smooth muscle physiology

Limited data have been generated to suggest specific physiologic functions performed by KCNE subunits in smooth muscle cells, but their expression has been confirmed in a number of cell types. For example, expression of *Kcne2* and *Kcne3* has been detected in mouse portal vein myocytes[68]. ERG channels are thought to contribute to K^+ conductance and electrical activity of these cells, but native currents differ from those recorded upon heterologous expression of ERG subunits alone. Observations that *Erg1* and *Kcne3* transcripts co-localize at the cell membrane[68] support postulations that KCNE3 may modulate ERG currents *in vivo* as part of the electrophysiologic profile of these vascular smooth muscle cells.

Expression of *KCNE1, KCNE3,* and *KCNE4* has been demonstrated in mouse[106] and human myometrium[53]. Studies in mouse have shown upregulation of *Kcne1* (along with *Kcnq1* and *Kcnq5*) at the metestrous phase of the estrous cycle[106]. Further, *Kcne1* levels have been observed to increase dramatically during late pregnancy in rodents[60], though the physiologic significance of these findings is not known.

Epithelial physiology

Although they have been primarily studied for their contributions to the physiology of excitable tissues, K_V channels expressed in the membranes of epithelial cells have also

proven to participate in transepithelial K^+ secretion and recycling as a driving force behind other channels and transporters.

One important example of a significant role for K_V channels and KCNE subunits in epithelial physiology is the observation that *KCNQ1* and *KCNE2* are necessary for gastric acid secretion by parietal cells, which is coupled to K^+ intake via the H^+/K^+-ATPase. KCNQ1 was originally identified as the channel responsible for K^+ recycling that supports the H^+/K^+ exchanger in a 2001 study[107]. KCNQ1 expression in parietal cells was localized to the tubulovesicles and apical membrane by immunofluorescence. Further, inhibition of KCNQ1 current in parietal cells by chromanol 293B was found to completely block acid secretion. *KCNE2* was also observed to be abundantly expressed in the stomach, and the K^+ current measured in COS cells coexpressing *KCNQ1* and *KCNE2* showed electrophysiologic and pharmacologic similarities to the K^+ current observed in parietal cells. A subsequent study[108] confirmed that KCNE2 is necessary for gastric acid secretion, reporting that a *Kcne2$^{-/-}$* mouse model displays a gastric phenotype characterized by achlorhydria and hypergastrinemia.

Similar roles for KCNQ1 and KCNE subunits have been established in the colon and small intestine. In colonic crypt cells, a basolateral K^+ efflux is responsible for recycling K^+ in conjunction with Na-K-2Cl cotransport into the cell at the basolateral membrane, and for hyperpolarizing the membrane; both phenomena contribute to the driving force for luminal Cl^- secretion through CFTR at apical membrane. *In situ* hybridization and immunohistochemical studies confirmed the expression of *KCNQ1* and *KCNE3* in colonic crypt cells, and electrophysiologic studies demonstrated numerous similarities between K^+ currents of colonic crypt cells with those of transfected

KCNQ1/KCNE3 channels[109]. These findings suggest that a KCNQ1/KCNE3 channel may account for the basolateral K^+ current that is important for cAMP-stimulated Cl^- secretion, and thus may also play a role in the pathophysiology of cystic fibrosis and secretory diarrhea.

Preliminary studies have implicated KCNQ1-KCNE1 channel complexes in the physiology of the exocrine pancreas. Both subunits are abundantly expressed in pancreatic acinar cells[58], and a slowly activating K^+ current with biophysical properties resembling I_{Ks} has been recorded in rat pancreatic cells[5]. Further, pancreatic acinar cells from the *Kcne1* knockout mouse displayed significant reduction of a chromanol 293B-sensitive, cholinergic-stimulated, slowly activating K^+ current[61], suggesting that an I_{Ks}-like current generated by KCNQ1-KCNE1 channel complexes may contribute to the electrochemical driving forces that underlie pancreatic secretion of electrolytes and enzymes.

KCNE2 has been directly implicated in thyroid hormone biosynthesis. A 2009 study[110] demonstrated KCNQ1 and KCNE2 form a TSH-stimulated K^+ channel in thyrocytes responsible for a constitutively active K^+ current at the basolateral membrane. *Kcne2* knockout mice demonstrated a dramatic defect in I^- accumulation in thyrocytes, which is a critical step in thyroid hormone biosynthesis. As a consequence, pups from homozygous *Kcne2*$^{-/-}$ crosses exhibited cardiomegaly, dwarfism, and alopecia, concurrent with decreased serum thyroid hormone and increased thyroid stimulating hormone.

In many segments of the nephron, K^+ flux is critical for maintaining appropriate electrochemical gradients that drive the tightly regulated distribution of fluid and electrolytes across the membrane. Colocalization of Kcnq1 and Kcne1 has been observed

in the luminal membrane of proximal tubules of mouse kidney, and the *Kcne1* knockout mouse displayed abnormal K^+ flux in proximal and distal tubules plus enhanced urinary excretion of fluid, Na^+, Cl^-, and glucose compared to wild-type mice[111]. KCNE4 has been localized to the apical membrane of intercalated cells of the nephron, which are only known to express one K^+ channel, the voltage- and calcium-dependent BK channel[112]. Subsequent analysis by heterologous expression of BK plus KCNE4 in CHO cells revealed that KCNE4 shifts the voltage-dependence of activation of BK channels toward more positive potentials, and reduces macroscopic current but not single-channel conductance (suggesting that KCNE4 may accelerate turnover of BK channels, which was corroborated by biotinylation and pulse-chase experiments).

Finally, vestibular dark cells of the inner ear are known to rely on functional KCNQ1-KCNE1 channel complexes for normal endolymph production. The expression of KCNQ1 and KCNE1 has been observed at the apical surface of vestibular dark cells[113], and *Kcne1* knockout mice are profoundly deaf and demonstrate signs of dysfunction of the vestibular organ[61]. These phenotypes are likely attributable to impaired endolymph production, death of sensory hair cells, and degeneration of spiral ganglion neurons, which have all been observed in *Kcne1* knockout mice, concurrent with mislocalization of Kcnq1 in dark cells[114]. The inner ear phenotype displayed by these mice is similar to that in patients with Jervell-Lange-Nielsen syndrome caused by mutations in human KCNQ1 or KCNE1.

Objective

As summarized above, the KCNE proteins have already been implicated in a wide range of physiologic processes, but our understanding of their exact function is incomplete, particularly in the case of KCNE4. Though the modulatory effect KCNE4 has been observed to exert on some K_V channel complexes *in vitro* - total extinction of the current - is perhaps the most striking among the KCNE subunits, we have yet to determine how that effect is achieved or for what purpose(s) in physiology.

In vitro observations of the functional properties of KCNE4 and studies of its expression in human heart provide strong, specific leads in cardiac physiology: *KCNE4* may be an important regulator of I_{Ks} and/or I_{to} and contribute to fine-tuning of the cardiac action potential, with implications for heart rhythm and contractility. Additionally, it is important to consider that *KCNE4* may have an important function in skeletal muscle or in the CNS, tissues that robustly express *KCNE4* and that require coordinated activity of ion channels for normal function. Finally, based on the extensive expression of *KCNE4* in epithelial tissues and the emerging recognition of roles for members of the *KCNE* family in epithelial physiology, it is conceivable that *KCNE4* may participate in K_V channel activity in epithelial cells and contribute critically to their proper biological function.

In heterologous expression systems, the most commonly observed modulatory effect of KCNE4 on K_V channels of varying compositions is dramatic inhibition of current. In any physiologic setting, this could implicate KCNE4 as a negative regulator of endogenous K^+ currents and the cellular functions they contribute to. Grunnet et al.[105] have postulated that, based on the time course of K^+ current inhibition by KCNE4 (ie.

within hours of its expression), it may provide subacute regulation of cellular functions. They also note that this time frame is consistent with typical responses to hormonal regulation. Given that KCNE1 has previously been demonstrated to be subject to hormonal regulation, this is an intriguing possibility to consider for KCNE4. Speculation along these lines draws warranted attention to the fact that we have an extremely limited understanding of how KCNE4 is regulated, and new data shedding light on any regulatory factors would also be valuable toward understanding its physiologic functions.

Based on the broad expression of *KCNE4* by human tissues we hypothesized that *KCNE4* performs physiologically significant functions *in vivo*. In this project, we aimed to first consider the specific leads in cardiac physiology. Questions that address some crucial limitations of our understanding of function of *KCNE4* include: What are the protein interacting partners of KCNE4 in native cells? What are the consequences of the absence of *KCNE4* on heart rhythm and contractility, and cardiomyocyte electrophysiology? This thesis describes a set of multidisciplinary experiments that make use of a *Kcne4* knockout mouse and are designed to answer these questions and advance our understanding of the physiologic function of *KCNE4*.

CHAPTER II

DISCOVERY OF NOVEL KCNE4 PROTEIN INTERACTING PARTNERS

The physiologic function of KCNE4 may require interactions with other cellular proteins. From studies in heterologous expression systems, we know that the KCNE subunits do not generate current when expressed alone; they are instead characterized by their ability to modulate currents generated by K_V channel α subunits. We can study individual α subunits to see which are susceptible to functional modulation by KCNE4, but this candidate approach is inefficient for generating a comprehensive list of channels KCNE4 can modulate. In addition to potential targets of its modulation, we might expect KCNE4 to have numerous other protein interacting partners, falling into a variety different categories. Among the possibilities are up- or down-stream signaling proteins, chaperone proteins required for appropriate trafficking, or scaffolding proteins that enable KCNE4 to adopt a specific position relative to other components of a given K_V channel complex.

Discovery of any of these potential interacting partners is an important early step toward determining the native physiologic function of KCNE4. Establishing a complement of KCNE4 interacting partners whose physiologic functions are already known could provide useful context when considering potential roles for KCNE4. Further, studies of KCNE4 activity in heterologous expression systems will be most effective when we can ensure that other proteins relevant to its native function are present.

Studying biochemical interactions among membrane proteins has historically been difficult because of their hydrophobic nature. K_V channel α subunits and accessory subunits are no exception. No reliable evidence exists even for the biochemical interaction of KCNQ1 and KCNE1 in native tissue, while it is universally accepted (based on robust biophysical findings) that they form the K^+ channel complex responsible for I_{Ks}. Years of attempts by our lab and others that have failed to reliably demonstrate an interaction between the KCNE proteins and K_V alpha subunits in native cells using traditional biochemical assays (such as co-immunoprecipitation) provided additional motivation for employing an alternative approach: a recently developed screening tool to discover novel KCNE4 protein interacting partners.

Methods

The split-ubiquitin membrane-based yeast two-hybrid (MbYTH) system is a screening tool for identifying biochemical interactions among membrane proteins[115,116]. MbYTH is a modified version of the traditional yeast two-hybrid screen that does not require translocation of the bait and prey to the nucleus, and instead takes advantage of the ubiquitin-based split protein sensor (USPS) originally developed by Johnsson and Varshavsky[117,118]. In MbYTH, the bait and prey are fused to complementary halves of ubiquitin: Cub ("C-terminal ubiquitin") and NubG ("N-terminal ubiquitin G"; G denotes a single amino acid substitution, I13G, that decreases the affinity of Nub for Cub, to prevent spontaneous association). Upon interaction of bait and prey, NubG and Cub come together and the reconstituted "split-ubiquitin" is recognized by ubiquitin-specific proteases, resulting in cleavage of an artificial transcription factor (LexA-VP16) also

built into the bait-Cub fusion construct. The transcription factor then enters the nucleus, activating reporter genes that signal an interaction between bait and prey (Figure 11).

The specific reporter genes used in this screen include two auxotrophic growth markers (*HIS3* and *ADE2*) and *lacZ*, which encodes the enzyme β-galactosidase. The yeast reporter strain carries these genes under the control of LexA operators, such that they are expressed only when the artificial transcription factor LexA-VP16 is cleaved from split ubiquitin, allowing it to translocate to the nucleus. Upon binding of the transcription factor to LexA DNA binding domains upstream of these genes, the VP16 transactivator domain recruits RNA polymerase and initiates their transcription. Thus, the interaction between bait and prey is transduced into transcriptional events that can be assayed by growth of yeast on media lacking histidine or adenine, or by color development in a β-galactosidase assay.

Further, when *ADE2* is not transcribed and the yeast adenine synthesis pathway is blocked, a red-colored metabolic intermediate accumulates. Thus, in the absence of a protein-protein interaction, yeast colonies are pinkish in color. By contrast, the presence of two interacting proteins activates the *ADE2* gene, leading to completion of the adenine synthesis pathway and yeast colonies appear faint pink to white, depending on the strength of the interaction.

MbYTH has been successfully implemented in numerous studies by independent groups for small-scale and library-screening applications[119-125]. Two publications by the group that pioneered development of the protocol are dedicated to describing detailed methodology[115,116]. The series of steps we completed are described briefly here:
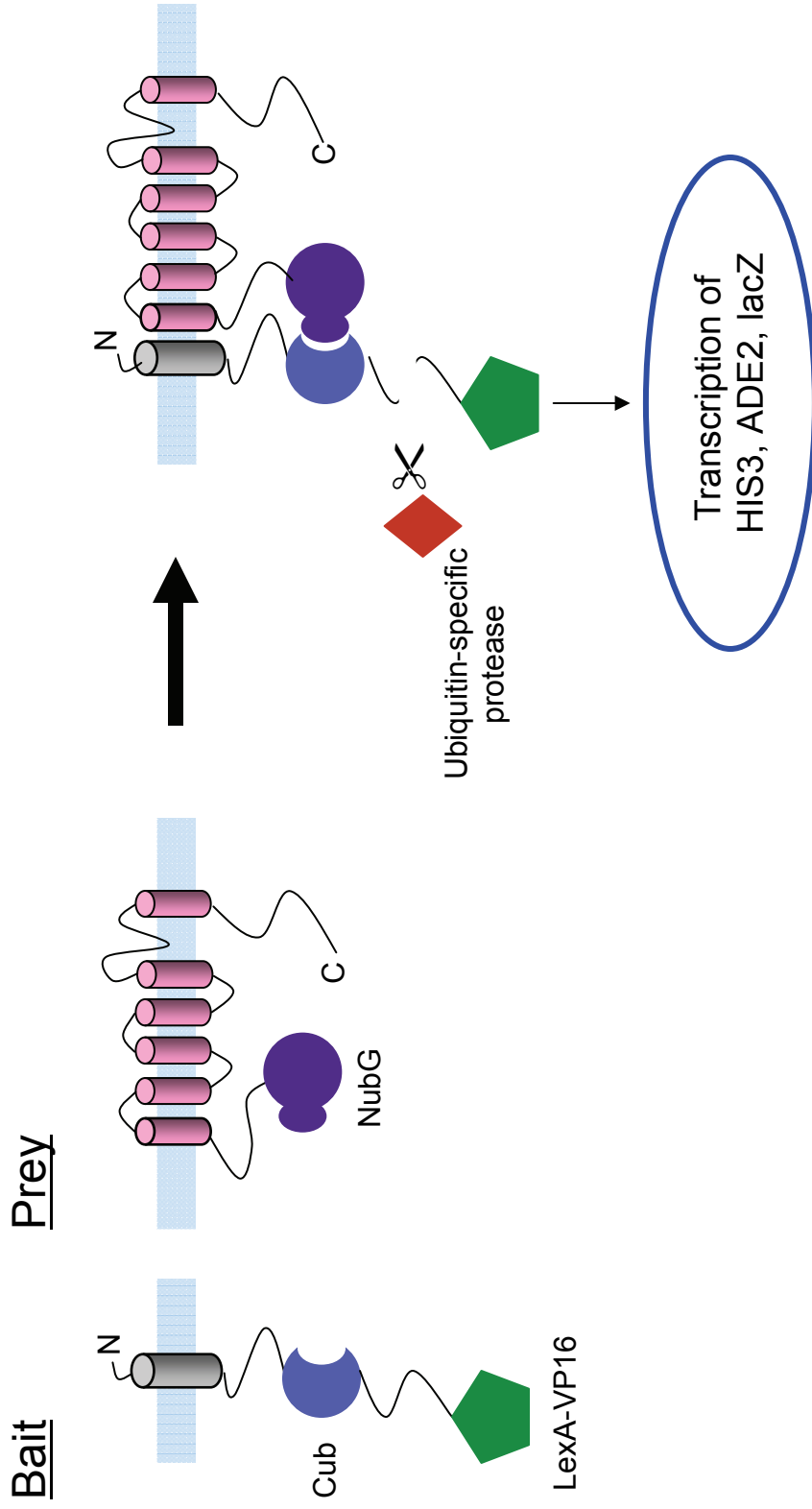
Figure 11. Schematic of principle behind MbYTH screen for biochemical interactions among membrane proteins. (Based on figure from Iyer, K et al. *Science STKE* **2005**.)

Generation of KCNE4-Cub bait construct

KCNE4 cDNA was subcloned into the pBT3-STE bait vector (acquired from Dualsystems Biotech, Schlieren, Switzerland) for type I integral membrane proteins such that KCNE4 is expressed under the weak CYC1 promoter and at the 3' end is in-frame with the Cub-LexA-VP16 cassette. The bait vector also includes the yeast *STE2* leader sequence for improved targeting of the heterologous bait protein to the yeast membrane. Following transformation in *E. coli,* positive clones were selected via Kan[R] expression and bait insertion was confirmed by PCR and sequencing. The bait vector also includes the auxotrophic marker *LEU2*, allowing for selection in yeast by growth on leucine-dropout (leu-) media.

Biochemical validation of bait fusion protein expression in yeast

The *S. cerevisiae* reporter strain NMY51 was transformed with the bait construct or one of two control constructs: pCCW-Alg5 (positive control bait vector, expresses yeast ER protein Alg5 as fusion protein with Cub-LexA-VP16 cassette under the CYC1 promoter), and pPR3-N (negative control empty prey vector, expresses NubG under CYC1 promoter). Yeast expressing the KCNE4 or control bait constructs were selected on leu- dropout media, whereas yeast expressing pPR3-N were selected on tryptophan-(trp-) dropout media. Protein lysates were prepared from each strain and used for SDS-PAGE. Western blots were performed using polyclonal rabbit anti-KCNE4 or monoclonal mouse anti-LexA to probe for the bait fusion proteins (predicted molecular weights: KCNE4-Cub-LexA-VP16, approximately 60 kDa; Alg5-Cub-LexA-VP16, approximately 77.5 kDa).

Functional validation of KCNE4-Cub bait construct by control co-transformations

Expression and functionality of the bait protein were assessed in yeast using the "NubG/NubI" test. In this test, NMY51 yeast were cotransformed with the KCNE4 or Alg5 control bait plus control prey plasmids that express control prey proteins Alg5-NubG or Alg5-NubI. (NubI is the wild-type N-terminal portion of ubiquitin that has strong affinity for Cub). Coexpression of Alg5-NubI with a bait-Cub-LexA-VP16 fusion protein will result in reconstitution of split ubiquitin and activation of the transcription factors if the bait-Cub-LexA-VP16 protein is properly expressed in the ER or plasma membrane. Coexpression of Alg5-NubG with the bait-Cub-LexA-VP16 fusion protein is not expected to result in reconstitution of split ubiquitin (unless the bait protein interacts with Alg5).

After verifying proper expression and functionality of our KCNE4-Cub-LexA-VP16 bait, we sent the bait construct to Dualsystems Biotech, where the remaining steps of the library screen were completed:

Bait self-activation test

Dualsystems assessed whether our bait displayed self-activation of the reporter complex. Yeast reporter strain NMY32 was transformed with the bait, grown in parallel on trp-leu- dropout media and trp-leu-histidine-adenine (trp-leu-his-ade-) dropout media, and assessed for adeneine and histidine prototrophy and β-galactosidase activity.

Bait functional analysis

Dualsystems performed a functional analysis of our bait using the control prey clones described in Table 1. Yeast reporter strain NMY32 was co-transformed with our bait plus each of these prey clones and growth on trp-leu-, trp-leu-his-, and trp-leu-ade-dropout media was assessed to determine if our bait was functional in the interaction assay.

Pilot screen for optimization of screening stringency

Prior to the library screen, Dualsystems performed a series of pilot screens to identify optimal screening conditions, by monitoring background interaction and interaction with positive controls while varying amounts of 3-amino-1,2,4-triazole (3-AT) to modulate the sensitivity of the HIS3 reporter gene.

Library transformation and selection of interactors

Dualsystems next screened their library of cDNAs from adult human brain in the pPR3-N vector (in the NubG-*x* conformation, with the prey fused to the 3' end of NubG). The library contains approximately 2.0×10^6 independent clones, with average insert size 1.7 kb. Yeast reporter strain NMY32 expressing our bait were sequentially transformed with prey clones, and primary selection was performed via growth assay on trp-leu-his-ade- dropout media.

Table 1. Control prey clones used in Dualsystems functional assessment of KCNE4 bait prior to library screen. ER, endoplasmic reticulum; PM, plasma membrane; MOM, mitochondrial outer matrix. Adapted from Science STKE 2005, pl3 (2005).

Control prey	Localization	Affinity for Cub	Interpretation of outcome
pOst1-NubI	ER	strong	Positive control; if no growth is observed on selective media, indicates insufficient bait protein expression or failure to pass through secretory pathway
pOst1-NubG	ER	weak	Negative control; if growth is observed on selective media, indicates bait overexpression, nonspecific cleavage, or interaction of bait with OST1
pAlg5-NubI	ER	strong	Positive control; if no growth is observed on selective media, indicates insufficient bait protein expression or failure to pass through secretory pathway
pAlg5-NubG	ER	weak	Negative control; if growth is observed on selective media, indicates bait overexpression, nonspecific cleavage, or interaction of bait with ALG5
pFur4-NubI	PM	strong	Positive control; if no growth is observed on selective media, indicates insufficient bait protein expression or failure to pass through secretory pathway
pFur4-NubG	PM	weak	Negative control; if growth is observed on selective media, indicates bait overexpression, nonspecific cleavage, or interaction of bait with FUR1
pTom20-NubI	MOM	strong	Positive control for mitochondrial proteins; if no growth is observed on selective media, indicates insufficient bait protein expression at mitochondrial outer matrix
pTom20-NubG	MOM	weak	Negative control; if growth is observed on selective media, indicates bait overexpression, nonspecific cleavage, or interaction of bait with TOM20
empty vector-NubG	cytosol	weak	Negative control; if growth is observed on selective media, indicates bait self-activation

β-galactosidase activity assay

Putative positive interactors from the primary growth assay were further studied via high-throughput β-galactosidase assay for the expression of *lacZ*. Briefly, yeast cultures were grown to late exponential phase, pelleted, and resuspended in lysis buffer plus X-gal substrate. Color development was monitored over time.

Plasmid recovery and retransformation in E. coli

Prey plasmids with the highest levels of β-galactosidase activity were isolated from the primary yeast clones (in duplicate for each hit) and amplified in *E. coli*. Restriction digests using *SfiI* were performed to determine insert size. If both plasmids isolated from a given primary clone were identical in size, one plasmid was processed further. If two different sizes were noted (suggesting that the yeast cell may have taken up multiple prey plasmids during transformation), both plasmids were further processed.

Confirmation of positive interactors

After plasmid purification, each vector was reintroduced into the reporter strain expressing the bait (in parallel with yeast expressing an empty vector control bait), and the transformants were each retested for growth on selective media and for β-galactosidase activity. The clones that demonstrated reproducible signs of interaction with KCNE4 were then sequenced at the junction between NubG and the cDNA to determine the reading frame and to identify the encoded protein by BLAST analysis.

Results

Biochemical validation of KCNE4 bait

After cloning KCNE4 into the bait vector pBT3-STE, we made a few attempts to validate its expression in yeast by Western blot but as advised by Dualsystems we did not apply major efforts toward optimization. Dualsystems reports that they typically detect only 10-20% of all baits by Western blot due to any of a number of possible limitations, including low expression in yeast due to the weak Cyc1 promoter, limited solubility of the protein, or non-specific proteolytic activity. Dualsystems relies much more heavily on the functional validation assays for assessing whether a bait construct is properly expressed and can be used in a library screen.

The results of our biochemical validation studies are found in Figure 12. Following SDS-PAGE and immunoblot, the KCNE4 fusion protein should be detectable with a molecular weight of approximately 60 kDa. A band of this size is apparent in both the anti-KCNE4 and anti-LexA blots, but the identity of this band is unclear without additional analysis via blocking peptides, a blot probed with secondary antibody alone, or a parallel blot of lysates from non-transfected yeast, none of which we performed. Protein lysates from yeast transfected with pCCW-Alg5 and pPR3-N served as a positive and negative control, respectively, for the LexA antibody. The Alg5-Cub-LexA-VP16 fusion protein should be detectable with anti-LexA and has predicted molecular weight of 77.5 kDa; pPR3-N does not express any proteins that should be detectable in an anti-LexA blot. A band slightly smaller than 75 kDa unique from the bands in the other lanes was detectable in the pCCW-Alg5 lane and could represent the control bait.
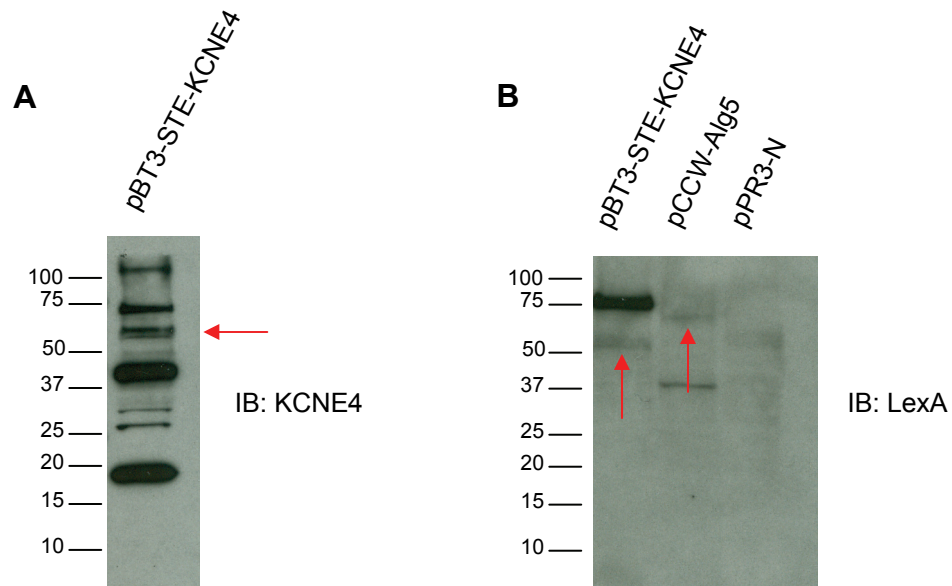
Figure 12. Biochemical validation of bait expression in yeast. A, Anti-KCNE4 immunoblot (IB) in protein lysates from yeast transformed with pBT3-STE-KCNE4. B, Anti-LexA immunoblot in protein lysates from yeast transformed with pBT3-STE-KCNE4, pCCW-Alg5, or pPR3-N. Arrows indicate putative bands of interest.

Functional validation of KCNE4 bait

We relied instead on a functional assay, the "NubG/NubI" test, for ultimate validation of correct expression of the bait. This assay revealed that co-expression of our KCNE4 bait with the NubI control prey yielded robust growth of white yeast colonies on trp-leu-his- and trp-leu-his-ade- plates (100% and 62% of growth on non-selective trp-leu- plates, respectively), suggesting that the bait was properly expressed with the Cub-LexA-VP16 complex in the cytosol, and split ubiquitin was reconstituted leading to the transcription of *HIS3* and *ADE2* (Table 2). Further, co-expression of our KCNE4 bait with the NubG control prey yielded little growth on the selective plates (22% and 13 % of growth on non-selective plates), suggesting that our bait is not self-activating and NubG must be tethered to a KCNE4 interacting partner for transcription of *HIS3* and *ADE2*. The results of this assay gave us confidence to proceed with our library screen so we provided Dualsystems with our KCNE4 bait construct.

Dualsystems performed additional functional validation assays using our KCNE4 bait. They reported that our bait was negative for self-activation in yeast strain NMY32 as observed via studies of adenine and histidine prototrophy and by an assay of β-galactosidase activity (data not shown). Further, growth assays following co-transformation of NMY32 with our KCNE4 bait and a panel of control prey clones show robust growth of white yeast colonies upon co-expression of our KCNE4 bait with plasma membrane-bound control prey clones tethered to NubI but not NubG (Figure 13). Finally, Dualsystems reported that the optimal screening conditions for our bait include selection on trp-leu-his-ade- media with 20 mM 3-AT, as was indicated by a pilot screen.

Table 2. Results of functional validation assay with KCNE4-Cub bait construct.
For each of four co-transformations, number and percentage of colonies counted four
days after plating as indicated for selective (trp-leu-his- and trp-leu-his-ade-) versus
non-selective (trp-leu-) media.

bait	prey	trp-leu-his- \# colonies (%)	trp-leu-his-ade- \# colonies (%)	trp-leu- \# colonies
KCNE4-Cub	Alg5-Nubl (+ control)	722 (>100)	340 (62)	548
KCNE4-Cub	Alg5-NubG (- control)	131 (22)	80 (13)	600
Alg5-Cub (+ control)	Alg5-Nubl (+ control)	300 (71)	356 (84)	424
Alg5-Cub (+ control)	Alg5-NubG (- control)	100 (29)	268 (78)	344
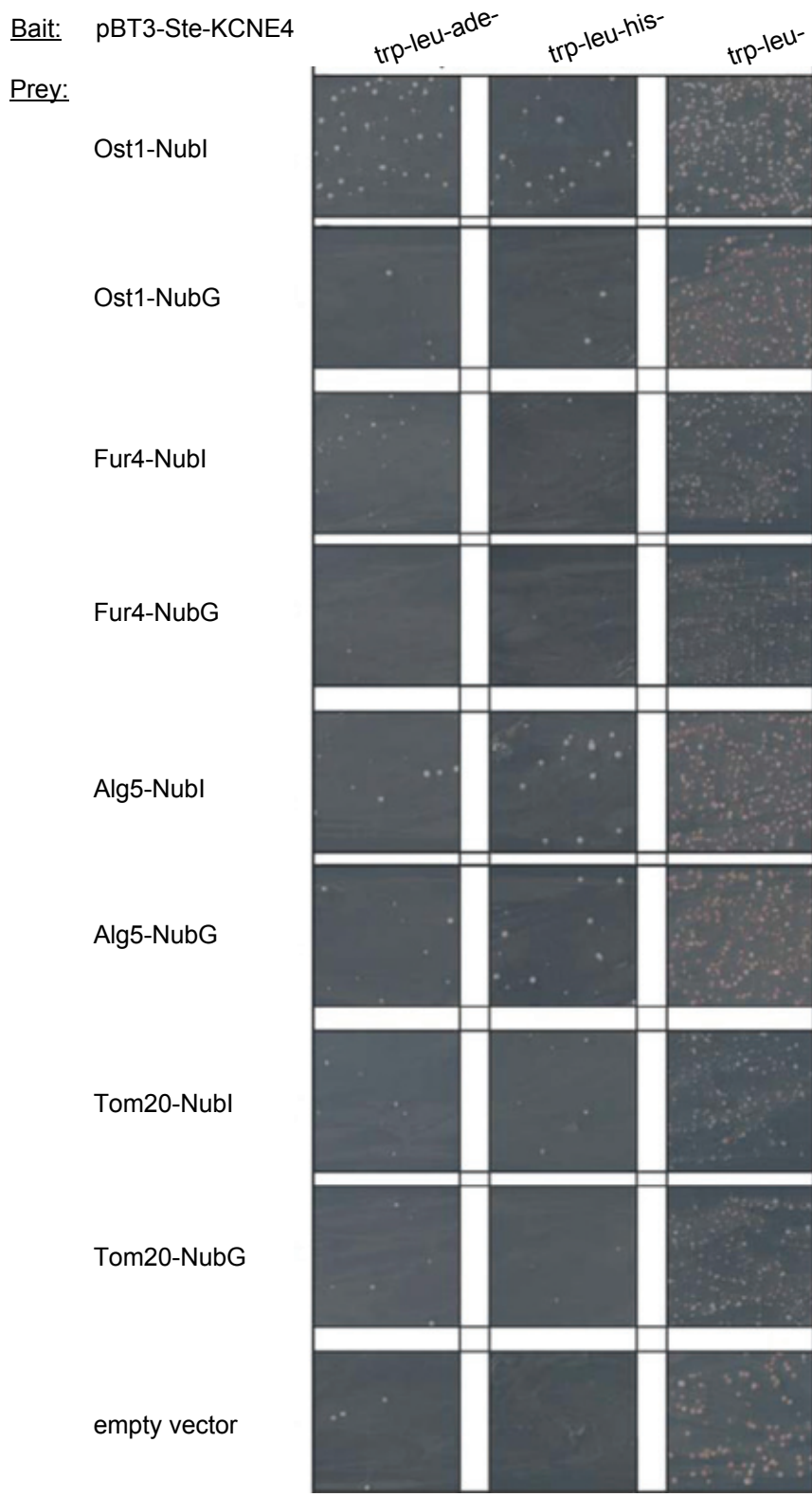
Figure 13. Functional validation of pBT3-Ste-KCNE4 bait by co-transformation with control prey plasmids. Panels show representative growth of yeast on selective (trp-leu-ade- or trp-leu-his-) versus non-selective (trp-leu-) media following co-transformation with the bait and prey plasmids indicated. Data provided by Dualsystems Biotech.

Library screen

We requested that Dualsystems screen our KCNE4 bait with their human adult brain cDNA library because human adult heart was not available, and as an excitable tissue, brain seemed to be the most appropriate option among the alternatives. We anticipated that many of the KCNE4 interacting partners identified by screening an adult brain cDNA library would be proteins that might perform similar functions in a cardiac myocyte and have corresponding relevance to the function of KCNE4. In the library screen, Dualsystems reported that the transformation efficiency was 9.5 x 10^4 cfu/µg DNA. In total, they screened 2.7 x 10^6 transformants and identified 108 putative interactors by a primary growth assay on trp-leu-his-ade- media. Those 108 clones were then tested in a high throughput assay for β-galactosidase activity, which indicated that 98 of the clones were also positive for lacZ expression (Figure 14).

Analysis of putative interactors

We selected 20 clones that appeared to be strong interactors (based on qualitative assessment of the intensity of blue color in Figure 14) for follow-up analysis. In duplicate for each prey clone, Dualsystems isolated the plasmids, amplified each in *E. coli*, and performed a restriction digest using SfiI to assess the size of each insert. For each prey clone except two (14 and 28), the duplicate samples yielded inserts of identical size (Figure 15), suggesting that the yeast cells responsible for those clones had been transformed with just one prey clone each. Two separate plasmids were recovered each from clones 14 and 28, and these were handled independently going forward, bringing the total number of putative positive prey clones for further analysis to 22.
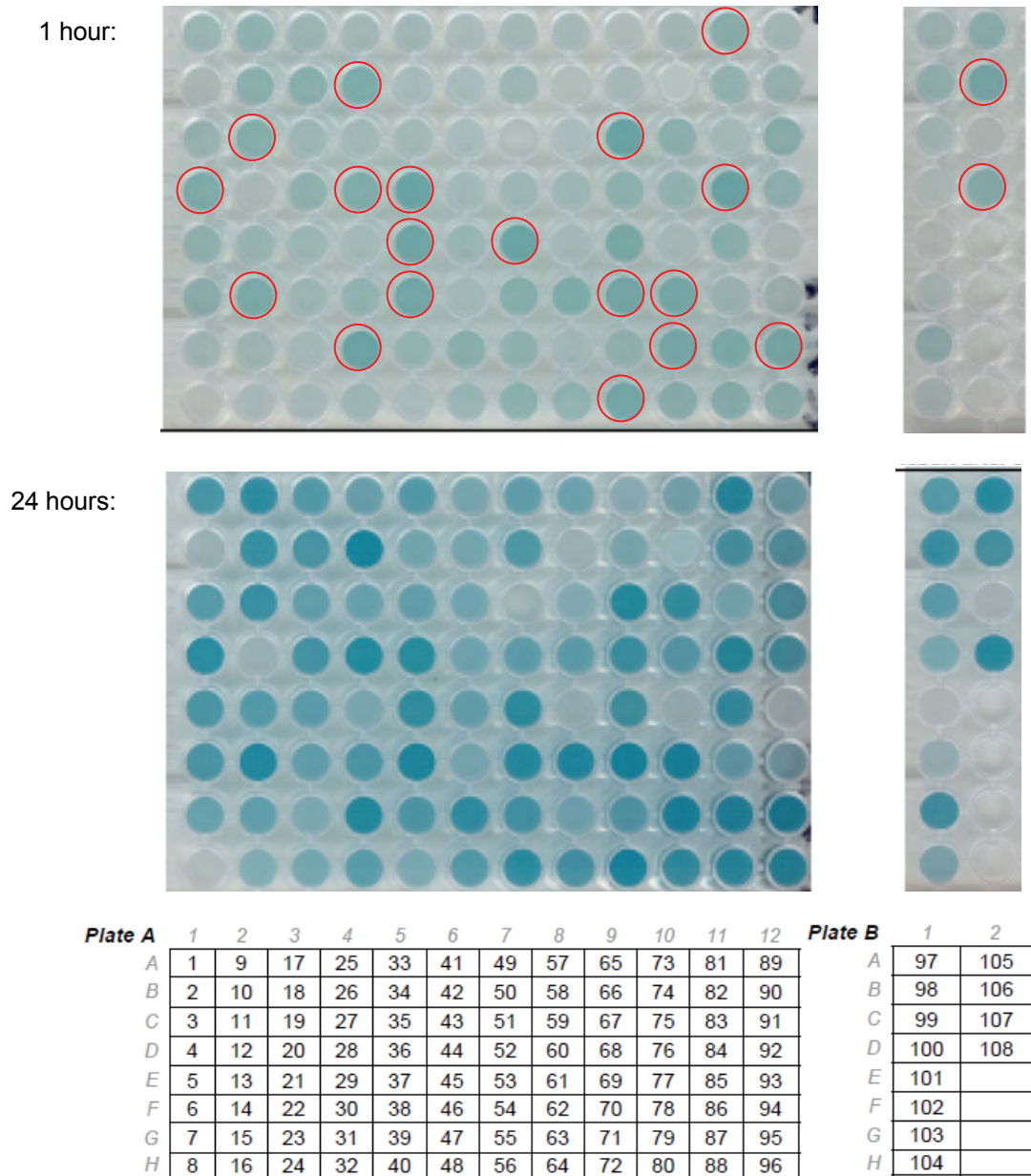
Figure 14. Results from β-Galactosidase assay in 108 putative positive prey clones. Development of blue color indicates β-galactosidase activity and reflects strength of the bait-prey interaction. Images captured 1 hour (top) and 24 hours (bottom) after adding X-Gal substrate to yeast lysates. Red circles indicate twenty clones selected for further analysis. Legend provides ID number assigned to each clone as used in subsequent figures. Data provided by Dualsystems Biotech.
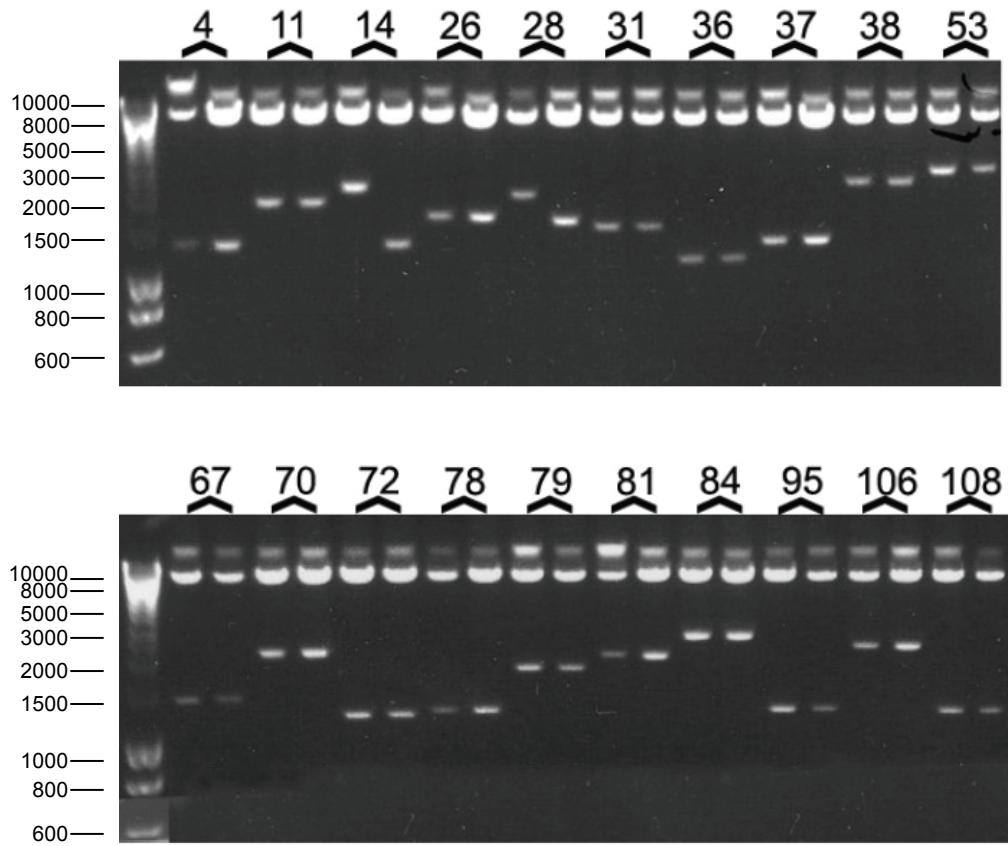
Figure 15. Prey plasmid insert sizes following *SfiI* digestion. Plasmids from each prey clone run in duplicate and identified by numbers above gel lanes. Marker sizes indicated in base pairs. Data provided by Dualsystems Biotech.

To confirm the interaction between each of the prey constructs and our KCNE4 bait, Dualsystems next co-transformed yeast with our bait plus each of the 22 prey clones isolated following the screen and repeated the growth and β-galactosidase assays. Figure 16 illustrates results of the growth assay, comparing yeast growth on non-selective versus selective media following co-transformation of NMY32 with either our KCNE4 bait or a control empty bait vector p415CYC plus each of the 22 prey clones. Each prey conferred histidine prototrophy to yeast transformed with our KCNE4 bait (compared with no growth on trp-leu-his- dropout media when co-transformed with the control bait, which suggests that none of the prey clones is self-activating). The change in color of the yeast colonies from red to white upon coexpression with KCNE4 bait suggests each prey also activates the *ADE2* gene, although observable growth on trp-leu-his-ade- dropout media was only evident for four of the prey clones (28-1, 36, 78, and 95). Results of the repeat β-galactosidase assay (Figure 17) also confirm expression of *lacZ* for all prey clones except one (79) when coexpressed with KCNE4 bait (but no *lacZ* expression when coexpressed with the empty vector control bait). From this set of assays, Dualsystems concluded that all of our selected prey clones gave reproducible signs of interaction with KCNE4 except clone 79.

Finally, the insert sequence of each prey clone was determined, and BLAST analysis revealed the identity of the parent genes (Table 3). The insert sequences were between 1211 and 1274 base pairs long, and 20 out of 21 each matched a human mRNA sequence with at least 97 % identity over a span of 520 to 1102 base pairs (one prey, 84-2, matched only a human BAC clone with no associated gene). The 20 identified prey proteins included 5 membrane-associated proteins (MBP, PDZD11, ANXA5, CALM2,
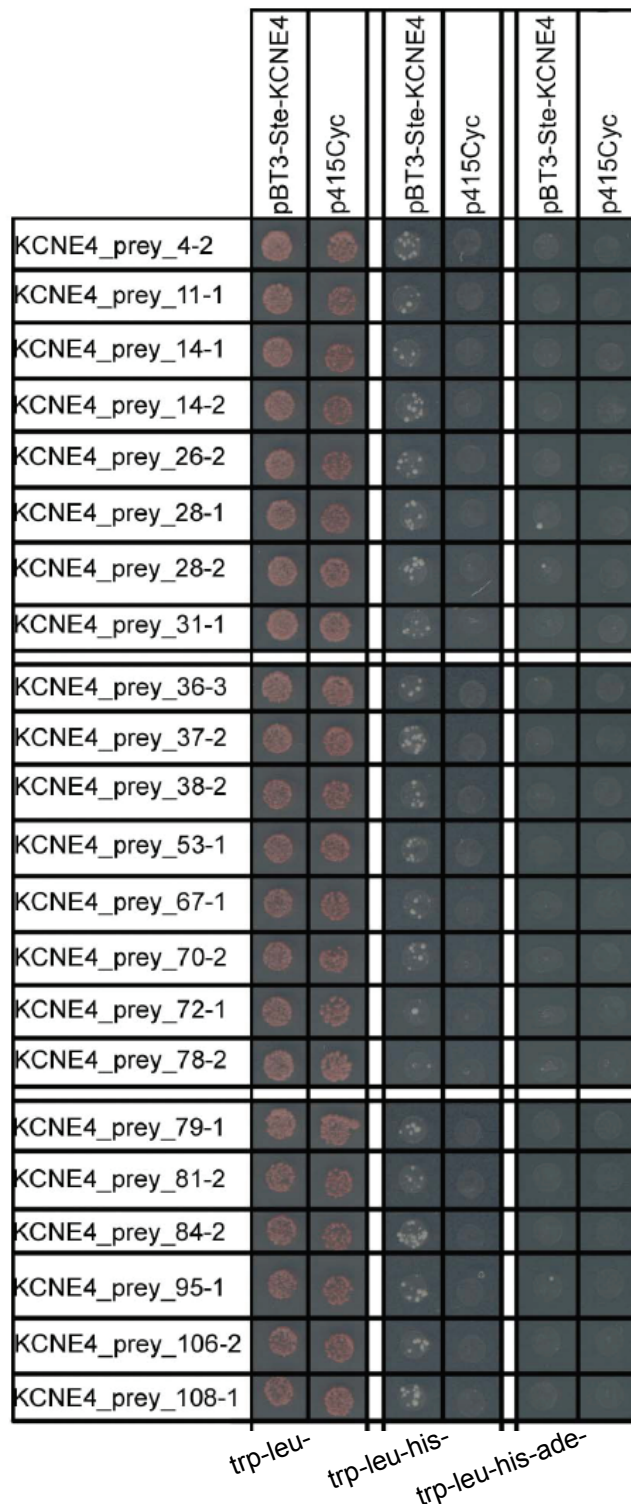
Figure 16. Repeat growth assay for interaction between KCNE4 bait and 22 select prey clones. Images of yeast colonies following co-transformation with indicated prey plus either KCNE4 or control bait (p415CyC), grown on non-selective versus selective media. Data provided by Dualsystems Biotech.
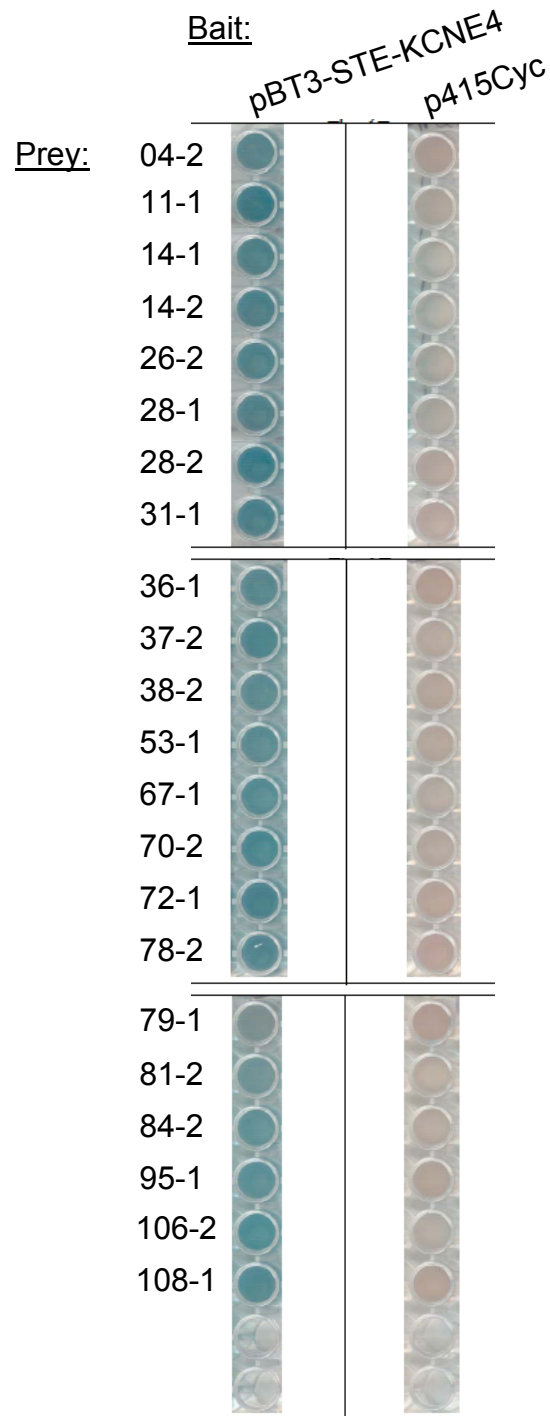
Figure 17. Repeat β-galactosidase assay for interaction between KCNE4 bait and 22 select prey clones. Accumulation of blue color reflects activation of MbYTH reporter gene *lacZ* in yeast co-transformed with each prey plus KCNE4 bait (versus empty bait control p415Cyc).

Table 3. Results of BLAST analysis revealing identity of 21 prey clones that yielded reproducible signs of interaction with KCNE4 bait.

prey ID	accession #	gene symbol	gene name	% Identity	length of hit (bp)
04-2	NM_198261.2	RSRC2	arginine/serine-rich coiled-coil 2	97	1080
11-1	NM_001154.2	ANXA5	annexin A5	98	1105
14-1	NM_001025101.1	MBP	myelin basic protein	98	1047
14-2	NM_000320.1	QDPR	quinoid dihydropteridine reductase	97	1018
26-2	NM_004522	KIF5C	kinesin family member 5C	98	1107
28-1	NM_001860.2	SLC31A2	solute carrier family 31 (copper transporters), member 2	98	1062
28-2	NM_01434.1	MTCH1	mitochondrial carrier homolog 1	97	699
31-1	NM_002567.2	PEBP1	phosphatidylethanolamine binding protein 1	100	823
36-1	NM_016484.3	PDZD11	PDZ domain containing 11	99	951
37-2	NM_005760.2	CEBPZ	CCAAT/enhancer binding protein zeta	98	1102
38-2	NM_182935.2	MOBP	myelin-associated oligodendrocyte basic protein	100	810
53-1	NM_005471.3	GNPDA1	glucosamine-6-phosphate deaminase 1	98	1069
67-1	NM_000365.4	TPI1	triosephosphate isomerase 1	98	1006
70-2	NM_030593.1	SIRT2	sirtuin 2	99	989
72-1	NM_032823.3	C9orf3	chromosome 9 open reading frame 3	98	1032
78-2	NM_001428.2	ENO1	enolase 1	98	1087
81-2	NM_001517.4	GTF2H4	general transcription factor IIH, polypeptide 4	98	890
84-2	AC104791.3	---	BAC clone RP11-181K12 from 4	99	985
95-1	NM_001743.3	CALM2	calmodulin 2	97	1078
106-2	NM_014235.2	UBL4A	ubiquitin-like 4A	100	520
108-1	NM_006070.4	TFG	TRK-fused gene	98	795

SLC31A2), 11 cytoplasmic proteins (KIF5C, QDPR, TFG, PEBP1, ENO1, TPI1, MTCH1, MOBP, GNPDA1, C9orf3, UBL4A), 3 nuclear proteins (GTF2H4, SIRT2, CEBPZ), and 1 protein of unknown localization (RSRC4). Table 4 includes a brief description of known functional characteristics for each protein.

Discussion

We successfully employed MbYTH to identify 21 putative interacting partners of KCNE4. The set of interacting proteins identified did not include any K_V channels as we had hoped, in order to identify novel targets of modulation by KCNE4. The lack of K_V channels among the screening hits carries a number of potential implications for our understanding of the function of KCNE4, including the possibility that 1) KCNE4 doesn't function as a K_V channel modulator in brain, or that 2) KCNE4 doesn't modulate K_V channels via direct interaction with the channel α subunit, and instead exerts its effect on channels via intermediate proteins.

Fortunately, identification of non-K_V channel protein interacting partners can provide useful leads toward understanding other aspects of the function of KCNE4 – for example, its trafficking, its regulation, and potential cellular functions beyond direct modulation of channel activity. Based on their known functions, a number of the hits have more obvious potential for intersection with KCNE4. For example, calmodulin is a known modulator of voltage-gated ion channels including KCNQ1[27,28,126-129]. The interaction between KCNQ1 and calmodulin has so far been studied without considering implications for K_V channel accessory subunits. To begin investigating a potential interaction between KCNE4 and calmodulin, we can use previous characterizations of the

Table 4. Functional characteristics of putative KCNE4 interacting partners identified in MbYTH screen.

gene symbol	gene name	protein type	remarks
RSRC2	arginine/serine-rich coiled-coil 2	uknown	unknown function
ANXA5	annexin A5	channel-like	phospholipase A2 and protein kinase C inhibitory protein with calcium channel activity
MBP	myelin basic protein	secreted protein	major constituent of the myelin sheath in oligodendrocytes and Schwann cells; also expressed in bone marrow and immune system
QDPR	quinoid dihydropteridine reductase	enzyme	catalyzes NADH-mediated reduction of quinonoid dihydrobiopterin. Essential component of the pterin-dependent aromatic amino acid hydroxylating systems
KIF5C	kinesin family member 5C	motor protein	member of kinesin 1 family of motor proteins which transport specific cargoes along the microtubules; substrate of protein kinase CK2
SLC31A2 *or* CTR2	solute carrier family 31 (copper transporters), member 2 *or* copper transporter 2	transporter	copper transporter
MTCH1 *or* PSAP	mitochondrial carrier homolog 1 *or* presenilin 1-associated protein	integral mitochondrial membrane	integral mitochondrial outer membrane protein; interacts with presenilin 1; induces apoptosis when overexpressed in cultured cells
PEBP1 *or* RKIP	phosphatidylethanolamine binding protein 1 *or* Raf-1 kinase inhibitor protein	kinase inhibitor	modulates signaling in the MAP kinase cascade; metastasis suppressor
PDZD11 *or* PISP	PDZ domain containing 11 *or* plasma membrane calcium ATPase-interacting single PDZ protein	modulator of membrane transporters	ubiquitously expressed; previously shown to modulate Ca-ATPase and Menkes copper ATPase
CEBPZ *or* CBF	CCAAT/enhancer binding protein zeta *or* CCAAT binding protein	DNA binding	transcriptional regulator
MOBP	myelin-associated oligodendrocyte basic protein	structural	soluble cytoplasmic protein which is important for stabilization of compact myelin
GNPDA1	glucosamine-6-phosphate deaminase 1	enzyme	catalyzes the reversible conversion of glucosamine-6-phosphate into D fructose-6-phosphate (Fru6P) and ammonium
TPI1	triosephosphate isomerase 1	enzyme	catalyzes the isomerization of glyceraldehydes 3-phosphate (G3P) and dihydroxy-acetone phosphate (DHAP) in glycolysis and gluconeogenesis
SIRT2	sirtuin 2	DNA binding	class III histone deacetylase implicated in control of mitotic exit
C9orf3	chromosome 9 open reading frame 3	enzyme	member of the M1 zinc aminopeptidase family; catalyzes the removal of an amino acid from the amino terminus of a protein or peptide
ENO1 *or* MBP-1	enolase 1 *or* c-myc promoter binding protein 1	enzyme	glycolytic enzyme; short form (MBP-1) exhibits transcriptional repressor activity
GTF2H4	general transcription factor IIH, polypeptide 4	DNA binding	general transcription factor, component of the preinitiation complex
---	BAC clone RP11-181K12 from 4	---	---
CALM2	calmodulin 2	calcium sensor	member of the EF-hand calcium-binding protein family
UBL4A	ubiquitin-like 4A	chaperone	part of protein complex that facilitates targeting of tail-anchored proteins to the TRC40 insertion pathway
TFG	TRK-fused gene	fusion protein	member of NF-kappaB pathway; target of translocations in lymphoma and thyroid tumors; normal cellular role is unclear

functional interaction between calmodulin and KCNQ1 as a starting point for formulating hypotheses. Experiments designed to characterize the biochemical and functional interaction between KCNE4 and calmodulin are discussed in Chapter III.

Similarly, we can speculate about the relevance of a potential interaction between KCNE4 and any of the other MbYTH hits based on their known functions, though the degree to which an apparent connection to KCNE4 already exists varies considerably among them. The appearance of several transcription factors among the hits is interesting in light of a previous study which described the ability of a C-terminal fragment of the voltage-gated calcium channel $Ca_V1.2$ to translocate to the nucleus and regulate expression of a number of genes through its interaction with other nuclear proteins[130]. A similar function is conceivable for KCNE4, especially since it has a long C terminus (unique among the KCNE proteins), the importance of which is not known. Alternatively, this long C terminus could promote the interaction of KCNE4 with any of the cytoplasmic proteins among the MbYTH hits, whether implicated in enzymatic reactions, signaling cascades, or other cellular functions.

A number of experimental limitations must be considered in our application of the MbYTH screen to identify novel KCNE4 protein interacting partners and learn more about its native physiologic function. MbYTH screening is most greatly limited by the inability to create a truly comprehensive, functional library of cDNA prey fused to NubG. When constructing the library, only one-third of the inserted cDNAs will be in-frame at their 3' end with NubG, and only a fraction of those in-frame cDNAs will be full-length. Additionally, in our MbYTH screen, which used a "NubG-*x*" prey library, we were unable to identify type I integral membrane proteins (with extracellular N-termini, such

as other KCNE proteins) that might interact with KCNE4. We may wish to eventually screen *x*- NubG cDNA libraries to expand our coverage to include type I integral membrane proteins, but these libraries present separate technical challenges. Together, these factors limit the sensitivity of the MbYTH screen at picking up all KCNE4 interacting partners.

Additionally, this screen can be assumed to carry a high rate of false positives, due to the possibility of self-activating bait or prey clones, or non-specific aggregation of bait and prey that allows reconstitution of split ubiquitin. Finally, it is important to consider that not all protein-protein interactions that occur in transformed yeast will reflect important protein-protein interactions that take place endogenously in mammalian cells.

Despite these limitations, the screen was a useful tool for identifying putative protein interacting partners of KCNE4, and has provided us with many new leads for investigating the native physiologic function of KCNE4. To pursue any of the interaction partners further, important next steps include validating the biochemical interaction then assessing its functional importance. We pursued further characterization of the interaction between KCNE4 and calmodulin by applying these steps, and our findings are described in Chapter III.

KCNE4 JUXTAMEMBRANE REGION IS REQUIRED FOR INTERACTION WITH
CALMODULIN AND FOR FUNCTIONAL SUPPRESSION OF KCNQ1

Regulation of many voltage-gated potassium (K_V) channels occurs through a variety of intracellular second messengers and by interactions with accessory subunits. Several K_V channels, including KCNQ1 ($K_V7.1$), are modulated by accessory subunits belonging to the KCNE family of single-transmembrane domain proteins[70,131,132]. KCNE1 associates with KCNQ1 to form the channel complex responsible for generating the slow component of the cardiac delayed rectifier current (I_{Ks}). I_{Ks} is a repolarizing K^+ current critical during later phases of the cardiac action potential[2,3] that is impaired in various genetic or acquired cardiac arrhythmia syndromes[42,133-137] arising from mutations in the genes encoding either KCNQ1 or KCNE1.

In some circumstances, accessory subunits are required for transducing intracellular signaling events into physiologically relevant changes in K_V channel activity. For example, in the heart KCNQ1 is modulated by β-adrenergic signaling through cAMP-mediated channel phosphorylation. However, this effect results in physiological changes in potassium current only when certain KCNE subunits are also expressed[138,139]. Elucidating other functional and biochemical events that accompany KCNE modulation of K_V channels is important for understanding the physiological importance of this accessory subunit family.

A comprehensive understanding of KCNQ1 regulation by KCNE proteins may require that we consider properties of these interactions in the context of the relevant

intracellular milieu such as the cycling of internal Ca^{2+} concentration that occurs in cardiac myocytes. Each ionic component of the cardiac action potential including I_{Ks} is a potential target for feedback regulation by intracellular Ca^{2+}. Indeed, calmodulin (CaM), the ubiquitous Ca^{2+}-transducing protein[28,140], is recognized to bind and confer Ca^{2+} sensitivity to the biophysical properties of several cardiac ion channels including KCNQ1[27,28,141-144]. Of note, KCNQ1 interacts biochemically with CaM through a domain in the channel carboxyl-terminus, and pharmacological disruption of the KCNQ1-CaM interaction causes complete suppression of KCNQ1 current, suggesting that CaM is required for KCNQ1 activity[27,28]. In this study, we asked whether certain KCNE accessory subunits might interact biochemically or functionally with CaM. Specifically, because the dramatic inhibitory modulation of KCNQ1 by KCNE4 resembles the effect of disrupting the binding of CaM to KCNQ1, we hypothesized that an interaction between KCNE4 and CaM could be involved in the modulation of KCNQ1 by KCNE4. This hypothesis is supported by work described in Chapter II.

Our results demonstrate that KCNE4, but not KCNE1, can biochemically interact with CaM and that this interaction requires a tetra-leucine motif in the juxtamembrane region of the KCNE4 carboxyl-terminus. Further, mutation of this tetra-leucine motif abolishes CaM association with KCNE4 and impairs functional interactions of KCNE4 with KCNQ1. Our findings have potential relevance to KCNQ1 regulation by an important and ubiquitous intracellular signaling molecule.

Methods

cDNA constructs

Full-length KCNQ1 was expressed from the pIRES2-DsRed vector, whereas KCNE1 and KCNE4 were subcloned into pIRES2-EGFP (Clontech), as described previously[70]. A triple HA epitope (YPYDVPDYAGYPYDV PDYAGSYPYDVPDYA) was introduced into the KCNE4 vector, and a triple FLAG epitope (DYKDHDGDYKDHDIDYKDDDDK) into the KCNE1 cDNA, immediately upstream of the stop codon. HA sequence was PCR amplified from a plasmid provided by Sabina Kupershmidt (Vanderbilt University, Nashville, TN, USA); FLAG sequence was PCR amplified from p3XFLAG-CMV™-13 (Sigma-Aldrich). Addition of the epitope tags did not affect the modulatory properties of KCNE4 or KCNE1, as previously reported[52]. Point mutations were engineered using QuikChange Mutagenesis (Stratagene). All constructs were verified by complete sequencing of the open reading frames.

Cell culture and transfection

Chinese hamster ovary cells (CHO-K1, American Type Culture Collection) were grown at 37°C with 5% CO_2 in F-12 nutrient mixture medium supplemented with 10% fetal bovine serum (FBS, Atlanta Biologicals), penicillin (50 units ml^{-1})–streptomycin (50 μg ml^{-1}) and L-glutamine (2 mM). CHO cells stably expressing KCNQ1 or KCNQ1 plus KCNE1 were generated using transposon-mediated gene transfer[145]. Stable clones were identified by G418 resistance and tested by patch-clamp recording, and maintained at 37°C with 5% CO_2 in CHO cell medium plus 600 μg/ml G418. Unless otherwise

stated, all tissue culture media were obtained from Invitrogen. CHO cells were transiently transfected using FuGENE-6 (Roche Applied Science). For electrophysiology studies shown in Figure 25, cells were transfected with a 2:1 ratio of KCNQ1 to E4-HA, L[69-72]A-HA, or empty vector DNA.

Protein isolation

Forty-eight hours post-transfection, CHO cells were lysed for recovery of protein as previously described[52]. Briefly, one 100 mm dish of cells for each transfected construct was washed twice with ice-cold phosphate buffered saline (PBS) (137 mM NaCl, 2.7 mM KCl, 10 mM Na_2HPO_4, 2 mM KH_2PO_4, pH 7.4), then lysed with NP-40 lysis buffer (1% NP-40, 150 mM NaCl, 50 mM Tris, pH 8.0) supplemented with Complete mini protease inhibitor tablet (Roche Applied Science). Lysates were rocked for 30 min at 4°C then centrifuged twice at 14,000 x g for 10 min to remove insoluble debris. Total protein concentration was quantified using a Bradford reagent (Bio-Rad Laboratories).

Peptides

CaM-inhibitory peptides CaMKII-P, LKKFNARRKLKGAILTTMLA (Enzo Life Sciences) and MLCK-P, RRKWQKTGHAVRAIGRL, and control peptide CTRL-P, RRKEQKTGHAVRAIGRE (CalBiochem) were used in biochemical and functional experiments in Figures 18, 19 and 22. In a previous characterization of MLCK-P ("Trp peptide"), the K_d of calmodulin and MLCK-P was calculated to be 6 pM from assay of MLCK inhibition, yielding the conclusion that the peptide inhibits MLCK by trapping calmodulin and leaving free calmodulin concentration very low[146]. Similarly, prior

characterization of CaMKII-P ("peptide 290-309") determined that CaMKII-P inhibits CaMKII and CaM-dependent phosphodiesterase activity by peptide interaction with CaM and not by a direct effect on the enzyme [147]. Our experiments in Figures 18, 19 and 22 make use of the ability of these peptides to bind CaM and induce its dissociation from KCNQ1 or KCNE4. CTRL-P is an analog of MLCK-P with two amino acid substitutions that disrupt its interaction with CaM[146].

CaM-agarose pull-down

Cellular lysate (100 μg) was added to 50 μL CaM-agarose beads slurry (Sigma-Aldrich) in 1.7 ml microcentrifuge tubes, and volume was brought to 0.5 ml with wash buffer consisting of NP-40 lysis buffer with protease inhibitors and either 2 mM $CaCl_2$ or 2 mM EGTA + 2 mM EDTA. Protein was incubated with beads for 2 h at 4°C with rocking, in the presence or absence of CaM-inhibitory peptides CaMKII-P, MLCK-P, or CTRL-P. Beads were pelleted and supernatant was reserved as unbound fraction. Beads were washed six times in 1 ml $CaCl_2$ or EGTA + EDTA wash buffer, then resuspended in 25 μl 2x SDS-PAGE sample buffer (100 mM Tris pH 7.5, 20% glycerol, 4% Na dodecyl sulfate, 0.008% bromophenol blue, 5% β-mercaptoethanol, 5 M urea). Proteins were eluted from beads by heating for 5 min at 95°C.

Preparation of cross-linked antibody

As previously described [52], 10 μg of antibody were combined with 750 μl of borate buffer (200 mM sodium tetraborate decahydrate, pH 9.0), and 50 μl of Protein-G Sepharose™ 4 Fast Flow (GE Healthcare) and rocked at room temperature for 1 h. The

beads were washed with borate buffer supplemented with 20 mM dimethyl pimelimidate dihydro-chloride, and rocked for 30 min at room temperature. The cross-linking reaction was quenched by 1 h incubation with 200 mM ethanolamine, pH 8.0. Beads were washed in PBS and stored at 4°C until use.

Co-immunoprecipitation

Cellular lysates were pre-cleared with Protein-G Sepharose™ 4 Fast Flow then incubated for 1 h at 4°C with 50 μl cross-linked antibody. Beads were washed three times in ice-cold lysis buffer plus protease inhibitors, then proteins were eluted with 2X SDS-PAGE sample buffer for 5 min at 55 °C.

Cell-surface biotinylation

Forty-eight hours after transfection, CHO cells were bathed in 1.5 mg·ml^{-1} sulfo-NHS-biotin (Pierce Chemical Company) in PBS for 1 h on ice. The biotinylation reaction was quenched with 100 mM glycine in PBS, then cellular lysates were prepared as described above, in ice-cold RIPA buffer (150 mm NaCl, 50 mm Tris-Base, pH 7.5, 1% NP-40, 0.5% sodium deoxycholate, 0.1% SDS, supplemented with a Complete mini-protease inhibitor tablet). Lysates were incubated with ImmunoPure Immobilized Streptavidin beads (Pierce Chemical Co.) overnight at 4°C. Beads were pelleted and the supernatant was reserved as the non-biotinylated fraction. Beads were washed three times then biotinylated proteins were eluted in 2x SDS-PAGE sample buffer for 30 min at room temperature.

SDS-PAGE and Western blotting

Protein samples were subjected to electrophoresis on pre-cast 4-20% Tris-HCl gels, then transferred to Immun-Blot™ PVDF membranes (Bio-Rad Laboratories). Membranes were blocked for one hour with 10% non-fat dry milk in TBS-T before applying the appropriate primary antibody in 4% non-fat dry milk in TBS-T: 1:5000 mouse monoclonal anti-HA (Covance), 1:200 goat polyclonal anti-KCNQ1 (Santa Cruz Biotechnology), 1:2000 mouse monoclonal anti-calmodulin (Millipore Corporation), or 1:1000 rabbit polyclonal anti-calnexin (Sigma). Membranes were washed in TBS-T then probed with the appropriate secondary antibody in 4% non-fat dry milk in TBS-T: 1:5000 goat anti-mouse IgG-HRP, rabbit anti-goat IgG-HRP, or goat anti-rabbit IgG-HRP (Santa Cruz). Membranes were washed in TBS-T and HRP signal was detected using ECL Plus (GE Healthcare Life Sciences) and Kodak BioMax MS film (Kodak). For E4-HA pull-down by CaM-agarose in the presence of CaM-inhibitory peptides, protein band densitometry was performed on scanned films using ImageJ software (National Institutes of Health). Differences among groups were determined by one-way ANOVA, with Tukey post-test for pairwise comparison.

Electrophysiology

Currents were measured in CHO cells using the broken-patch, whole-cell configuration of the patch clamp technique[148]. For experiments using transiently co-transfected cells, only yellow fluorescent cells (positive for both dsRed-MST and EGFP fluorescence) were recorded. Whole cell currents were recorded at room temperature (20–23°C) using Axopatch 200 and 200B amplifiers (MDS Analytical Technologies).

Pulses were generated using Clampex 8.1 (MDS Analytical Technologies), and whole cell currents were filtered at 1 kHz and acquired at 5 kHz. The access resistance and apparent membrane capacitance were estimated as previously described[149]. Whole-cell currents were not leak subtracted. Unless otherwise indicated, whole-cell currents were measured during a series of 2-s voltage steps from a holding potential of −80 mV to test potentials ranging from −80 to +60 mV (in 10-mV increments) followed by a 1-s step to −30 mV to record tail currents. The extracellular solution contained (in mM): 132 NaCl, 4.8 KCl, 1.2 $MgCl_2$, 1 $CaCl_2$, 5 glucose, and 10 HEPES, pH 7.4. The standard intracellular solution contained (in mM): 110 K^+ aspartate, 1 $CaCl_2$, 10 HEPES, 11 EGTA, 1 $MgCl_2$, and 5 K_2ATP, pH 7.35. Pipette solution was diluted 5–10% to prevent activation of swelling-activated currents. For experiments using CaM-inhibitory peptides, 50 μM peptide was added to the diluted pipette solution. For experiments using varying concentrations of intracellular free Ca^{2+} (Figures 20 and 26), see Table 5 for composition of intracellular solution. We also tested the effects of including EDTA along with EGTA to the 30 nM $[Ca^{+2}]_i$ pipette solution (Figure 20) to control for non-specific effects of EDTA. Patch pipettes were pulled from thick-wall borosilicate glass (World Precision Instruments, Inc.) with a multistage P-97 Flaming-Brown micropipette puller (Sutter Instrument Co.) and heat polished with a Micro Forge MF 830 (Narashige). After heat polishing, the resistance of the patch pipettes was 2–5 MΩ in the standard solutions. As a reference electrode, a 2% agar bridge with composition similar to the control bath solution was used. Junction potentials were zeroed with the filled pipette in the bath solution. Unless otherwise stated, all chemicals were obtained from Sigma-Aldrich. Data were collected for each experimental condition from at least three distinct transient

Table 5. CaCl$_2$ and chelator composition of pipette solutions for varying [Ca^{2+}]$_i$

free [Ca^{2+}] (nM)	CaCl$_2$ (mM)	EDTA (mM)	EGTA (mM)
3	0.42	11	0
10	1	0	11
30	2.67	0	11
30 (EGTA + EDTA)	2.67	11	11
100	5.67	0	11

transfections and analyzed using a combination of Clampfit (MDS Analytical Technologies), OriginPro 7 (OriginLab Corporation) and SigmaPlot 2000 (Systat Software, Inc.). Steady-state current at each test potential was measured 1.9 s following the voltage step, and current density was obtained by normalizing steady-state current to cell capacitance. Voltage-dependence of activation was determined by normalizing peak tail current for each test potential to the maximal value for each cell, and plotting normalized peak tail current versus voltage. Activation curves were fitted with a Boltzmann function to determine the voltage for half-maximal activation ($V_{1/2}$) and slope (k). To analyze kinetics of activation, the current recorded between 0.075 s and 0.475 s after the voltage step to +60 mV was fitted with a single exponential function to determine the time constant, tau (τ). Statistical analyses were performed using SigmaStat 2.03 (Systat Software, Inc.).

Results

KCNQ1 interacts biochemically and functionally with CaM

To demonstrate that KCNQ1 interacts biochemically with CaM in our experimental system (i.e., heterologous expression in CHO cells), we used CaM-agarose beads to pull down KCNQ1 in the presence of either $CaCl_2$ or the Ca^{2+} chelators EGTA and EDTA. KCNQ1 was immunodetected robustly in eluate from beads incubated in the presence of $CaCl_2$ but less was detectable when the incubation was performed in the presence of Ca^{2+} chelators (Figure 18A). To examine the specificity of this finding, we performed pull-down assays in the presence of $CaCl_2$ plus either of two CaM-inhibitory peptides,
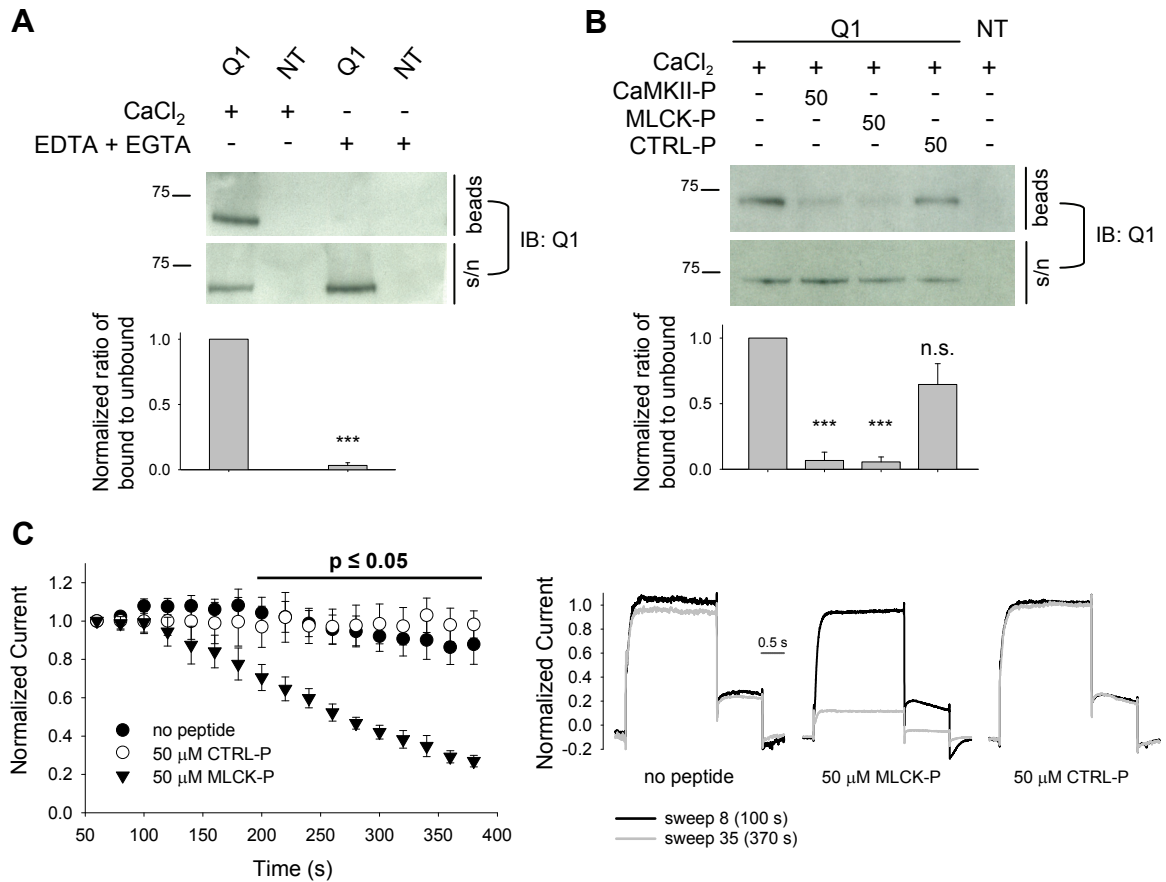
Figure 18. Biochemical and functional interaction between KCNQ1 and CaM. *A*, Representative immunoblot (IB) following CaM-agarose pull-down using lysates from CHO cells transiently transfected with full-length KCNQ1 (Q1) or non-transfected cells (NT), performed in duplicate in the presence of 2 mM $CaCl_2$ or 2 mM EDTA + 2 mM EGTA. Bound (beads) and unbound (supernatant, s/n) fractions were each probed for KCNQ1 using anti-KCNQ1. Bars below each lane indicate average bound-to-unbound signal ratio, normalized to $CaCl_2$ condition from same experimental replicate. Mean ± SEM for normalized ratios: EDTA + EGTA, 0.03 ± 0.02, n = 3; ***, $p < 0.001$ versus $CaCl_2$ by t-test. *B*, Representative immunoblot following CaM-agarose pull-down of KCNQ1 in the presence of 2 mM $CaCl_2$ and CaMKII-P, MLCK-P, or CTRL-P at indicated concentrations in μM. Bars below each lane indicate average bound-to-unbound signal ratio, normalized to no peptide condition from same experimental replicate. Mean ± SEM for normalized ratios: CaMKII-P, 0.07 ± 0.06, n = 2; MLCK-P, 0.06 ± 0.04, n = 3; CTRL-P, 0.65 ± 0.16, n = 3; ***, $p < 0.001$ by Tukey post-test pairwise comparisons to no peptide following one-way ANOVA ($p < 0.001$). *C*, Decay of steady-state whole-cell current over time recorded in CHO cells expressing KCNQ1 in the presence of 50 mM CTRL-P, 50 mM MLCK-P or no peptide in the pipette solution. Left, average (± SEM) steady-state current for each sweep during 0.1 Hz-train of 2-s depolarizations to +60 mV from holding potential −80 mV, each normalized to current recorded in same cell 60 s after obtaining whole-cell configuration; n = 4; $p \leq 0.05$ for one-way ANOVA and Tukey post-test pairwise comparison of MLCK-P versus CTRL-P and MLCK-P versus no peptide. Right, representative current traces recorded at 100 s and 370 s, normalized to steady-state current recorded at 60 s.

70

CaMKII-P and MLCK-P (named according to the binding regions of calmodulin-dependent kinase II and myosin light chain kinase, respectively), or a control peptide, CTRL-P. Compared to the peptide-free condition, both CaM-inhibitory peptides impeded pull-down of KCNQ1 by CaM-agarose, whereas CTRL peptide did not diminish the interaction (Figure 18B).

We next examined the functional significance of the interaction between KCNQ1 and CaM in CHO cells. We recorded whole-cell currents in CHO cells transiently transfected with KCNQ1, using the MLCK inhibitory peptide in the pipette solution to disrupt the biochemical interaction between KCNQ1 and CaM. In the presence of 50 μM MLCK peptide, steady-state current amplitude decayed rapidly over time whereas cells dialyzed with 50 μM CTRL or with no peptide showed minimal decay (Figure 18C). We also studied whether the CaM-inhibitory peptide has a functional effect on I_{Ks}, by recording whole-cell currents in CHO cells stably expressing KCNQ1 + KCNE1. Again, in the presence of 50 μM MLCK peptide, steady-state current amplitude decayed rapidly over time whereas cells dialyzed with 50 μM CTRL or with no peptide showed minimal decay (Figure 19).

We also observed that KCNQ1 function is Ca^{2+}-sensitive. Specifically, we observed no effect of varying $[Ca^{2+}]_i$ on current density, but a shift toward more depolarized voltage-dependence of activation was observed at lower intracellular Ca^{2+} concentrations (Figure 20). Overall, our results demonstrate a Ca^{2+}-dependent interaction of KCNQ1 with CaM that is necessary for channel activity.
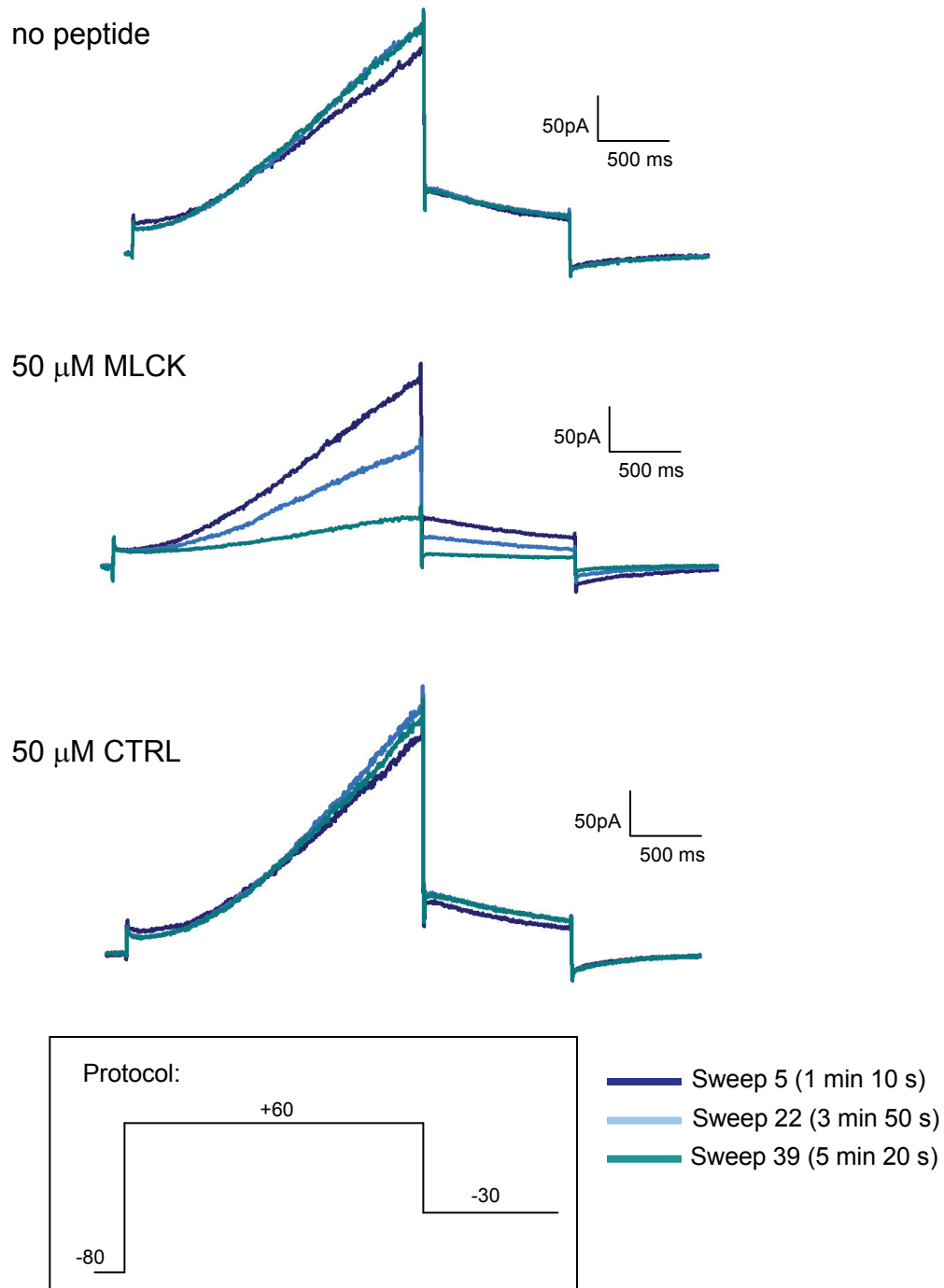
Figure 19. I$_{Ks}$ is sensitive to CaM availability. Representative whole-cell currents recorded from CHO cells stably expressing I$_{Ks}$ in the presence or absence of CaM-inhibitory peptide in the pipette solution. Traces reflect currents at time intervals indicated following membrane rupture
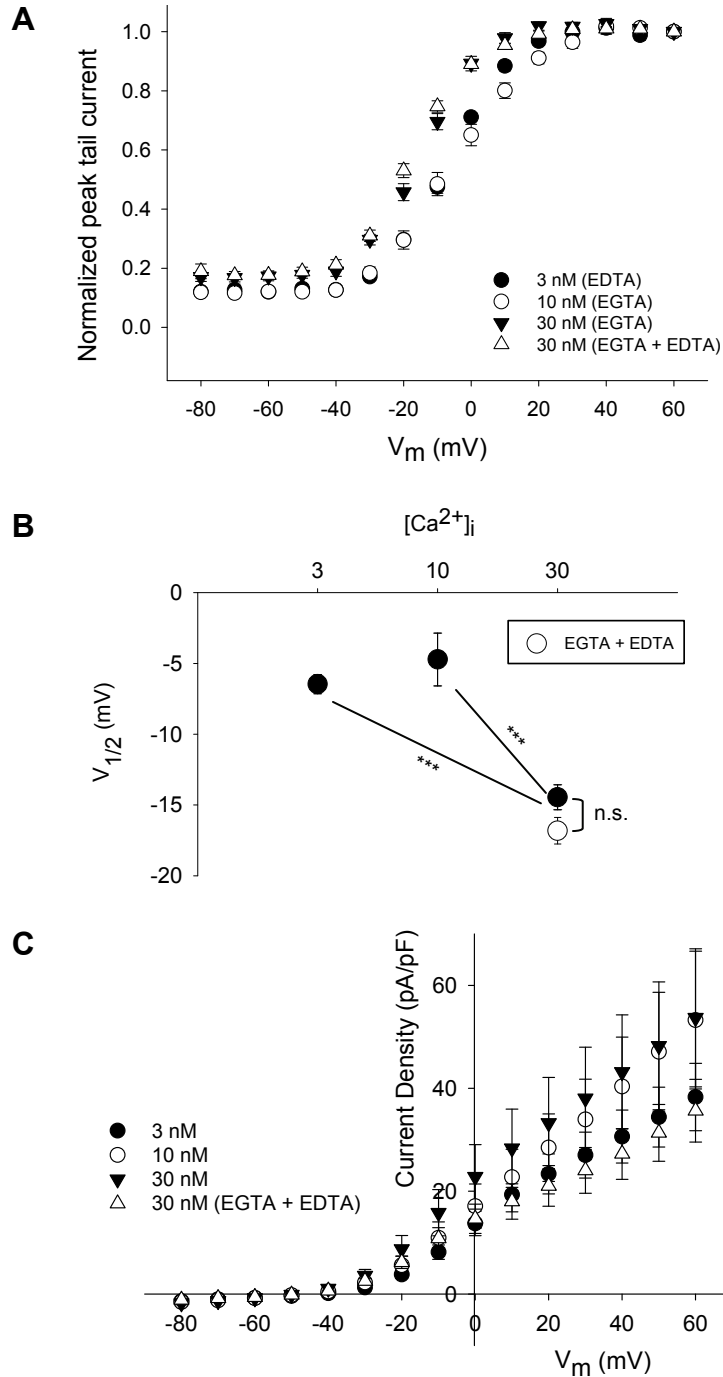
Figure 20. Q1 voltage-dependence of activation is modulated by low intracellular free calcium concentrations. A, Activation curves for CHO cells stably expressing Q1 recorded in the presence of 3 nM, 10 nM, or 30 nM $[Ca^{2+}]_i$ buffered with chelators as indicated (n = 8). B, $V_{1/2}$ measured in CHO cells stably expressing Q1 recorded with 3 nM, 10 nM, 30 nM, and 100 nM $[Ca^{2+}]_i$, plotted against $[Ca^{2+}]_i$. Mean $V_{1/2} \pm$ SEM: 3 nM -6.5 $\pm$ 0.7 mV, n = 8; 10 nM -4.7 $\pm$ 1.9 mV, n = 8; 30 nM -14.5 $\pm$ 0.9 mV, n = 8; 30 nM (EGTA + EDTA) -16.8 $\pm$ 0.9, n = 8; p<0.001 by ANOVA and ***, p<0.001 for Tukey post-test pairwise comparison. C, Mean $\pm$ SEM current density versus voltage recorded in CHO cells stably expressing Q1 measured in the presence of 3 nM, 10 nM, 30 nM and 30 nM (EGTA + EDTA) $[Ca^{2+}]_i$. No trend in current density is observed with varying $[Ca^{2+}]_i$ (n = 8).

73

Ca²⁺-dependent interaction of KCNE4 with CaM

The suppression of KCNQ1 current resulting from CaM inhibition closely resembles the effects of KCNE4 co-expression with the channel. We hypothesized that the mechanism of KCNQ1 inhibition by KCNE4 may involve the ability of KCNE4 to mimic a CaM inhibitory peptide. To test this hypothesis, we first sought to demonstrate interaction between KCNE4 and CaM.

We used multiple biochemical approaches to assess whether KCNE4 can interact with CaM. First, CaM-agarose pull-down assays using lysates from CHO cells transiently transfected with epitope-tagged KCNE4 (KCNE4-HA) revealed that KCNE4-HA interacts with CaM in a Ca^{2+}-dependent manner (Figure 21A). Next, we validated the biochemical interaction between KCNE4-HA and CaM by co-immunoprecipitation using an anti-CaM primary antibody. KCNE4-HA was detected following immunoprecipitation performed in the presence of $CaCl_2$ but not Ca^{2+} chelators, whereas CaM was detectable in the immunoprecipitate regardless of Ca^{2+} availability (Figure 21B). Finally, we demonstrated that the interaction of KCNE4-HA with CaM could be significantly disrupted by CaM-inhibitory peptides but not by the control peptide (Figure 22). These data indicate that KCNE4-HA and CaM biochemically interact in CHO cells.

We also tested whether another KCNE subunit can interact biochemically with CaM by CaM-agarose pull-down using CHO cells transiently transfected with FLAG epitope-tagged KCNE1. No signal was detected in the bound fraction, regardless of whether the pull-down was performed in the presence of $CaCl_2$ or Ca^{2+} chelators (Figure 23). These results suggest that CaM interaction is not a universal property of all KCNE subunits.
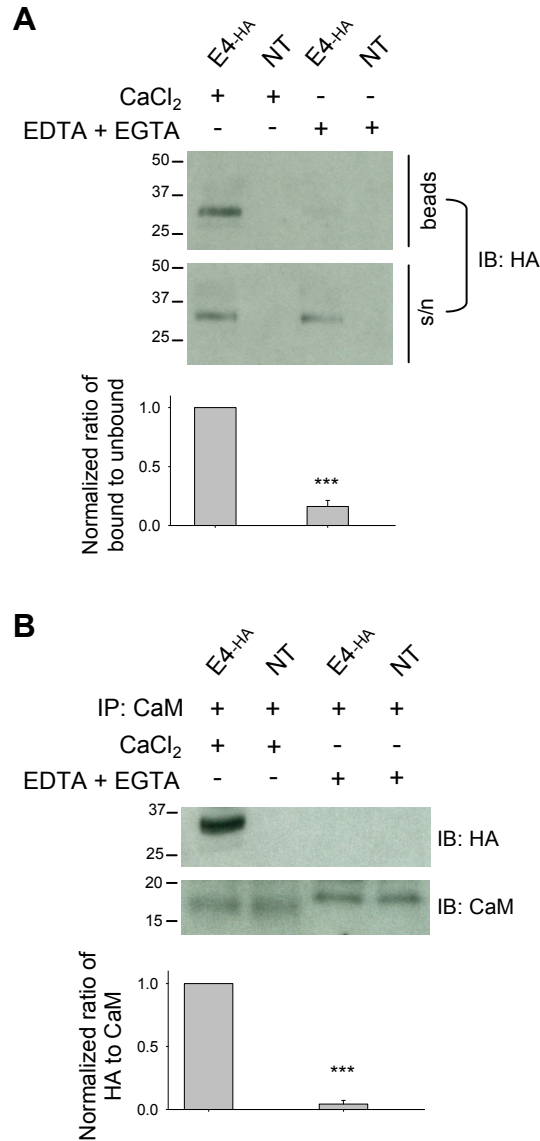
Figure 21. Biochemical interaction between KCNE4 and CaM. *A*, Representative immunoblot following CaM-agarose pull-down using lysates from CHO cells transiently transfected with E4-HA or non-transfected cells (NT), performed in duplicate in the presence of 2 mM $CaCl_2$ or 2 mM EDTA + 2 mM EGTA. Bound (beads) and unbound (s/n) fractions were each probed for KCNE4 using monoclonal HA antibody. Bars below each lane indicate average bound-to-unbound signal ratio, normalized to $CaCl_2$ condition from same experimental replicate. Mean ± SEM for normalized ratios: EDTA + EGTA, 0.16 ± 0.09, n = 3; ***, p < 0.001 versus $CaCl_2$ by t-test. *B*, Representative immunoblot following co-immunoprecipitation with anti-CaM in the presence of 2 mM $CaCl_2$ or 2 mM EDTA + 2 mM EGTA. The apparent higher molecular weight of apo-CaM versus holo-CaM following SDS-PAGE is consistent with previous findings[20] and is attributable to conformational changes that allow CaM to adopt a more compact form upon binding Ca^{2+} [38]. Bars below each lane indicate average HA-to-CaM signal ratio, normalized to $CaCl_2$ condition from same experimental replicate. Mean ± SEM for normalized ratios: EDTA + EGTA, 0.04 ± 0.06, n = 4; ***, p < 0.001 versus $CaCl_2$ by t-test.
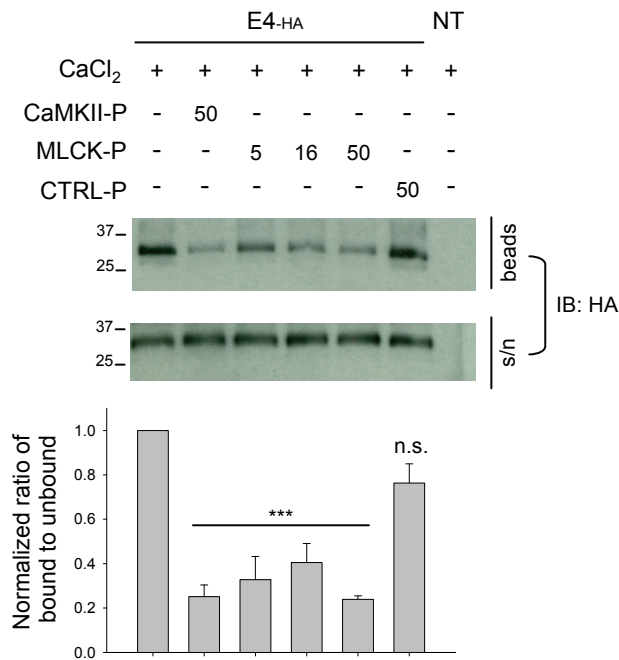
Figure 22. CaM-inhibitory peptides disrupt KCNE4-CaM interaction.
Representative immunoblot following CaM-agarose pull-down of E4-HA in the
presence of CaMKII-P, MLCK-P, or CTRL-P at indicated concentrations in μM.
Pull-down performed in the presence of 2mM $CaCl_2$. Bound (beads) and unbound
(supernatant, s/n) fractions were each probed for KCNE4 using monoclonal anti-
HA. Bars below each lane indicate average bound-to-unbound signal ratio,
normalized to no peptide condition. Mean ± SEM for normalized ratios: 50 μM
CaMKII-P, 0.25 ± 0.05, n = 4; 5 μM MLCK-P, 0.33 ± 0.11, n = 3; 16 μM MLCK-P,
0.41 ± 0.09, n = 3; 50 μM MLCK-P, 0.24 ± 0.02, n = 4; 50 μM CTRL-P, 0.76 ± 0.09,
n = 4; ***, p < 0.01 for Tukey pairwise comparison to no peptide following one-way
ANOVA (p = 0.001).

	E1-FLAG		NT		E1-FLAG		NT	
CaCl$_2$	+	+	+	+	-	-	-	-
EDTA + EGTA	-	-	-	-	+	+	+	+
	B	s/n	B	s/n	B	s/n	B	s/n

IB: FLAG
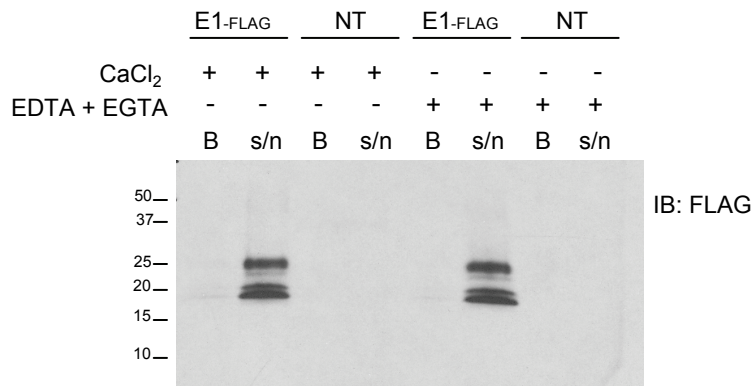
Figure 23. KCNE1 does not interact biochemically with CaM. Representative anti-FLAG immunoblot following CaM-agarose pull-down using lysates from cells expressing KCNE1-flag or non-transfected cells, performed in duplicate in the presence of 2 mM CaCl$_2$ or 2 mM EDTA + 2 mM EGTA.

Juxtamembrane tetra-leucine motif is critical for KCNE4-CaM interaction

To survey where CaM might interact with KCNE4 we examined the full-length KCNE4 amino acid sequence using an online CaM binding site prediction algorithm (http://calcium.uhnres.utoronto.ca). Based upon various peptide properties including hydropathy, α-helical propensity, residue weight, side chain charge, and helical class, we identified one potential CaM interaction site located between KCNE4 residues 44 and 73. This candidate interaction site spans part of the transmembrane domain plus 15 residues of the adjacent intracellular juxtamembrane region of the KCNE4 carboxyl terminus (Figure 24A). Because critical binding energy in protein-protein interactions involving CaM is often provided by bulky hydrophobic amino acids[150], we targeted a tetra-leucine motif (residues 69-72) within the candidate binding site for disruption of the interaction between KCNE4 and CaM. Specifically, we mutated the four leucine residues to alanines (designated L[69-72]A-HA), then performed CaM pull-down assays to determine effects on the protein-protein interaction. CaM-agarose assays comparing pull-down of wild-type KCNE4-HA to L[69-72]A-HA demonstrated that this juxtamembrane tetra-leucine motif is required for the biochemical interaction of KCNE4 with CaM (Figure 24B) most likely because this sequence is part of a CaM binding site. Importantly, this tetraleucine motif is conserved in KCNE4 orthologues across mammals, birds, and amphibians. Similar motifs are absent in the other KCNE subunits and this is consistent with the observed lack of KCNE1 biochemical interaction with CaM (Figure 23).

We also assessed CaM-agarose pull-down of E4-HA constructs engineered with charge reversals in the same region, R[62-63]E-HA and K[65-66]E-HA, and found that these mutations did not disrupt the biochemical interaction between KCNE4 and CaM

A

NH₂- **M L K M E P L N S T H P G T A A S S S P L E S R A A G G**

G S G N G N E `Y F Y I L V V M S F Y G I F L I G I M L G Y M` **K S**

K R R E K K S S L L L L **Y K D E E R L W G E A M K P L P V V**

S G L R S V Q V P L M L N M L Q E S V A P A L S C T L C S M

E G D S V S S E S S S P D V H L T I Q E E G A D E E L E E T S

E T P L N E S S E G S S E N I H Q N S -COOH
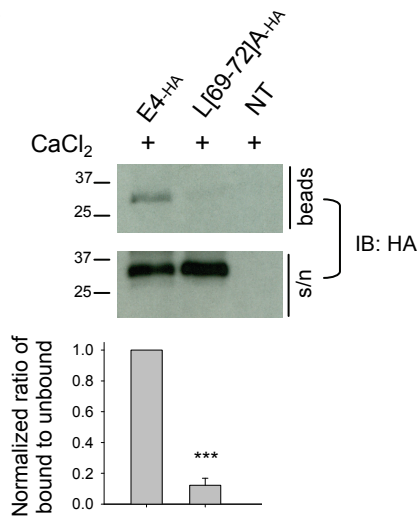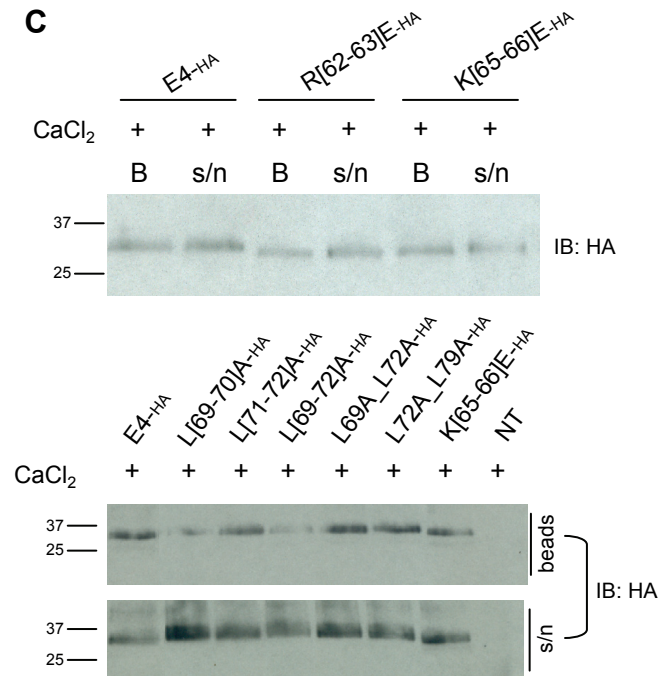
Figure 24. KCNE4 juxtamembrane tetra-leucine motif is critical for biochemical interaction with CaM. A, Amino acid sequence of human KCNE4. Box encloses predicted transmembrane domain, underline denotes region identified by online prediction tool (http://calcium.uhnres.utoronto.ca) as most likely to contain putative CaM binding site. B, Representative immunoblot following CaM-agarose pull-down comparing lysates from CHO cells transiently transfected with wild-type E4-HA, L[69-72]A-HA, or non-transfected cells (NT). Pull-down performed in the presence of 2 mM CaCl₂. Bound (beads) and unbound (s/n) fractions each probed for KCNE4 using monoclonal anti-HA. Bars below each lane indicate average bound-to-unbound signal ratio, normalized to wild-type E4-HA from same experimental replicate. Mean ± SEM for normalized ratios: L[69-72]A-HA, 0.12 ± 0.08, n = 3; ***, p < 0.001 versus wild-type by t-test. C, Representative immunoblots following CaM-agarose pull-down comparing lysates from CHO cells transiently transfected with wild-type E4-HA, R[62-63]A-HA, K[65-66]E-HA, L[69-70]A-HA, L[71-72]A-HA, L[69-72]A-HA, L69A_L72A-HA, and L72A_L79A-HA.

79

(Figure 24C). Additionally, we generated E4- HA constructs with *pairs* of leucine-to-alanine substitutions in the following combinations: L[69-70]A, L[71-72]A, L69A_L72A, and L72A_L79A. By CaM-agarose pull-down, it appears that none of these pairs of substitutions (except possibly L[69-70]A) is as effective at disrupting the KCNE4-CaM interaction as is substituting all four leucines in positions 69-72 with alanines (Figure 24C).

Altered KCNQ1 modulation by L[69-72]A- HA

To test whether disruption of the biochemical interaction between KCNE4 and CaM is accompanied by any functional consequences, we compared whole-cell currents recorded from CHO cells expressing KCNQ1 alone, KCNQ1 co-expressed with wild-type KCNE4- HA, and KCNQ1 co-expressed with L[69-72]A- HA. Representative current traces and a current density-voltage plot illustrate that the dramatic KCNQ1 suppression normally exerted by wild-type KCNE4 is not evident with L[69-72]A- HA (Figure 25A & 25B). The degree of KCNQ1 suppression was significantly less for L[69-72]A- HA than for wild-type KCNE4. Interestingly, L[69-72]A- HA exerts other modulatory effects on KCNQ1 including a significant shift in the voltage-dependence of activation curve to more depolarized potentials (Figure 25C; Table 6) and a significant slowing of the kinetics of activation (Figure 25D).

It is important to note that cell-surface biotinylation assays revealed that L[69-72]A- HA is detectable at the cell surface (Figure 25E), albeit at a reduced level. However, the modulatory effects of L[69-72]- HA on KCNQ1 described in Figure 25C and 25D imply that mutant KCNE4 subunits still associate with KCNQ1 at the plasma membrane
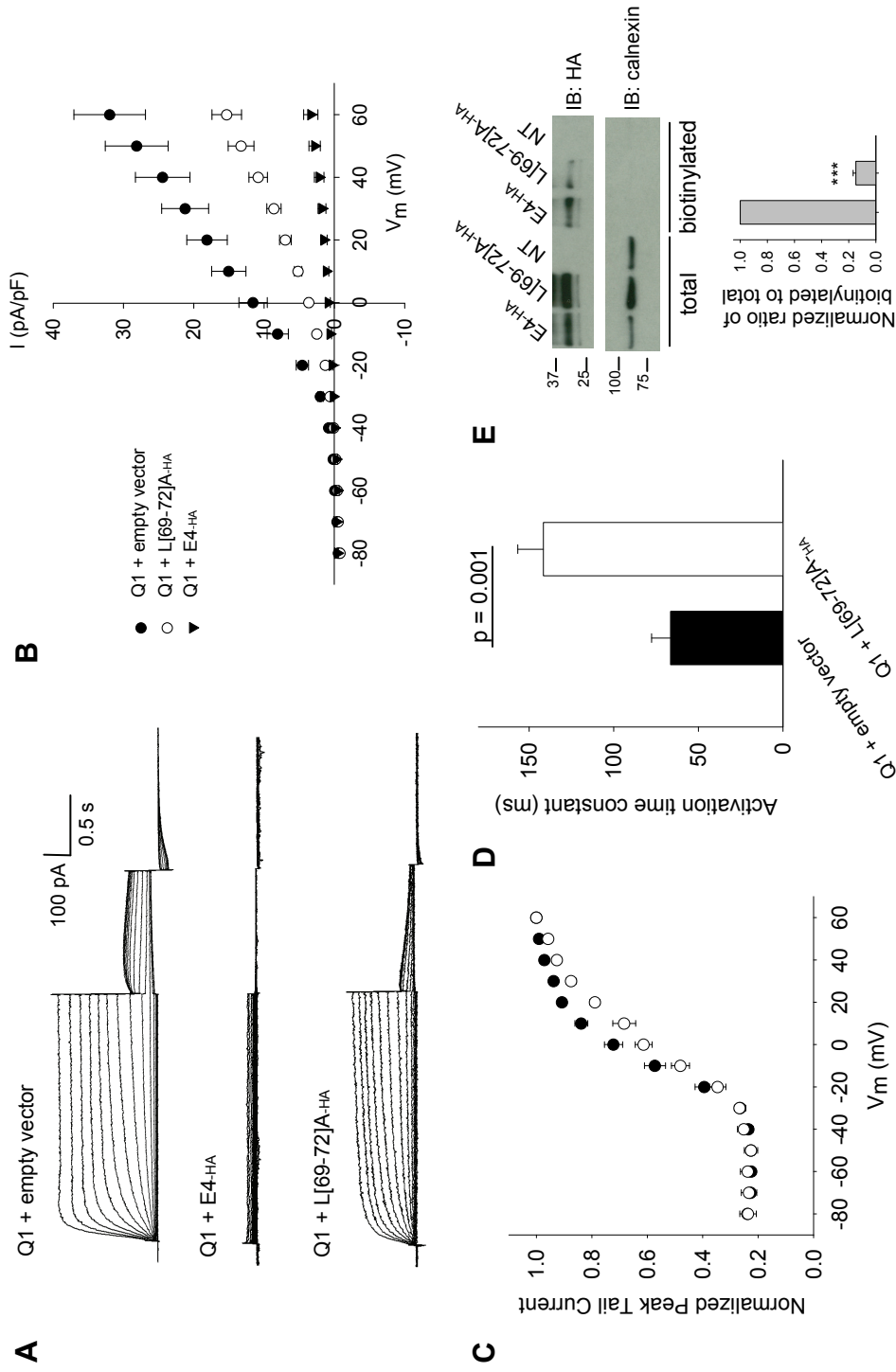
Figure 25. L[69-72]A-HA modulation of KCNQ1. A, Representative whole-cell currents from CHO cells transfected with Q1 plus empty vector, Q1 plus E4-HA, or Q1 plus L[69-72]A-HA. B, Mean (± SEM) current density versus voltage plot. At all test potentials > -40 mV, p < 0.05 for comparison of Q1 + L[69-72]A-HA to each Q1 + empty vector and Q1 + E4-HA by t-test. C, Voltage-dependence of activation for Q1 plus empty vector versus Q1 plus L(69-72)A-HA. D, Mean ± SEM for time-constant of activation for +60 mV current recorded between 0.075 s and 0.475 s after voltage step. E, Representative immunoblot following cell-surface biotinylation using CHO cells transfected with E4-HA, L(69-72)A-HA, or non-transfected cells (NT); probed with anti-HA to detect KCNE4 and with anti-calnexin to assess stringency of the biotinylation. Bars below each lane indicate average biotinylated-to-total protein signal ratio, normalized to wild-type E4-HA from same experimental replicate. Mean ± SEM for normalized ratios: L[69-72]A-HA, 0.15 ± 0.03, n = 3; ***, p < 0.001 versus wild-type by t-test.

81

Table 6. Electrophysiological parameters characterizing the modulation of Q1 by L[69-72]A-HA in comparison to Q1 alone and Q1 modulation by E4-HA. p-values reported for t-test comparison to Q1 + L[69-72]A-HA.

	n	current density, +60 mV (pA/pF) mean ± SEM	p	$V_{1/2}$ (mV) mean ± SEM	p	k (mV) mean ± SEM	p	τ (ms) mean ± SEM	p
Q1 + empty vector	8	32.0 ± 5.1	0.02	-7.0 ± 1.9	0.005	10.4 ± 0.5	0.004	66.4 ± 11.2	0.001
Q1 + L[69-72]A-HA	6	15.3 ± 2.1	N/A	2.4 ± 2.0	N/A	15.6 ± 1.5	N/A	141.6 ± 15.1	N/A
Q1 + E4-HA	7	3.3 ± 1.0	0.001	---	---	---	---	---	---

to a significant extent. Overall, these findings demonstrate that disrupting KCNE4-CaM interaction hinders the inhibition of KCNQ1 by KCNE4 and suggests possible mechanisms for the regulation of KCNQ1 function.

KCNE4 inhibition of KCNQ1 is Ca^{2+}-sensitive

To assess whether KCNE4 inhibition of KCNQ1 is sensitive to $[Ca^{2+}]_i$, we compared whole-cell currents recorded from CHO cells stably expressing KCNQ1 and transiently transfected with KCNE4 or empty vector, measured using a pipette solution that contained either 10 nM or 3 nM free $[Ca^{2+}]$. Representative current traces and a current density versus voltage plot (Figure 26) illustrate that KCNE4 fails to completely inhibit KCNQ1 current when $[Ca^{2+}]_i$ is chelated acutely. CHO cells expressing KCNE4 in the absence of KCNQ1 generated no current when recorded using 3 nM $[Ca^{2+}]$ pipette solution, suggesting that the recorded currents illustrated in Figure 26 are not from endogenous channels activated by low $[Ca^{2+}]_i$ (data not shown). These findings are consistent with the Ca^{2+} sensitivity of the biochemical interaction between KCNE4 and CaM (Figure 21A) and the impaired KCNQ1 inhibition by KCNE4 upon disrupting interactions between KCNE4 and CaM by mutagenesis. Importantly, the impairment of KCNE4 inhibition of KCNQ1 upon acutely chelating $[Ca^{2+}]_i$ is unlikely explained by an acute decrease in KCNE4 cell-surface expression, favoring the interpretation that the KCNE4 function is directly affected by disrupting its interaction with CaM.
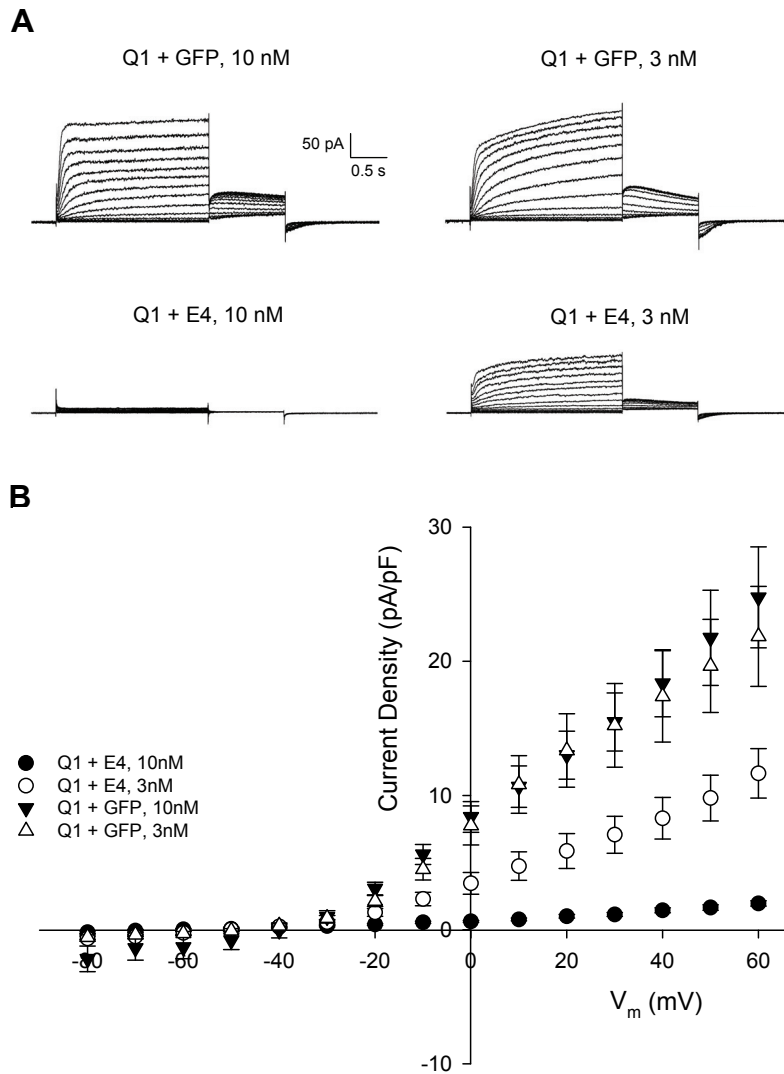
Figure 26. KCNE4 inhibition of KCNQ1 is impaired upon reducing [Ca^{2+}]$_i$.
A, Representative whole-cell currents from CHO cells stably expressing Q1 and transiently transfected with empty vector or E4, recorded in the presence of 10 nM or 3 nM free [Ca^{2+}]. B, Mean (± SEM) current density versus voltage plot (n = 8). At all test potentials more positive than -20 mV, p < 0.05 for Q1 + GFP, 3 nM (△) versus Q1 + E4, 3 nM (○) and p < 0.01 for Q1 + E4, 10 nM (●) versus Q1 + E4, 3 nM (○) by t-test.

Discussion

Regulation of KCNQ1 is physiologically important especially in heart where this protein constitutes the pore-forming subunit required to generate I_{Ks}, an essential repolarizing current. KCNQ1 is part of a macromolecular complex containing accessory subunits and regulatory proteins such as yotiao[21], phosphodiesterase PDE4D3[151] and CaM[27,28]. In addition to regulation by multiple intracellular second messengers including cAMP, PIP_2[23,24], and Ca^{2+}[27,28,141,143,144], KCNQ1 is modulated by KCNE proteins, some of which can exert dramatic effects on the channel[70,131].

Interactions between accessory subunits (e.g., KCNE) and other regulatory proteins associated with the macromolecular I_{Ks} complex are emerging as another layer of complexity in regulating KCNQ1 function[138]. In this study, we uncovered a new and intriguing example of an interaction between a KCNE subunit and another important KCNQ1 regulatory protein. Specifically, we identified an interaction between KCNE4 and CaM that is linked to the robust inhibitory effect of this accessory protein on KCNQ1. The observation that pharmacological inhibition of CaM dramatically blunts KCNQ1 activity[27,28], which resembles the modulatory effect of KCNE4 on KCNQ1, prompted our hypothesis that KCNQ1 inhibition by KCNE4 could involve CaM.

Our demonstration of a Ca^{2+}-dependent biochemical interaction between KCNE4 and CaM, and that KCNQ1 functional modulation by KCNE4 is impaired both upon mutation of a candidate CaM-interaction site in the juxtamembrane region of KCNE4 and by acutely chelating $[Ca^{2+}]_i$ to displace CaM from KCNE4, suggests a connection between the mechanism of KCNQ1 inhibition by KCNE4 and the effect of CaM on the channel. We previously assumed that the inhibition of KCNQ1 by KCNE4 is caused by a

direct effect of KCNE4 on the channel[48,152]. In demonstrating that the interaction between CaM and KCNE4 is critical for the inhibitory effect of KCNE4, the data presented here introduce the new possibility that KCNE4 inhibits KCNQ1 by disrupting CaM-mediated KCNQ1 activation.

The KCNE4 region we identified to be critical for its biochemical interaction with CaM lacks typical motifs shared by many (but not all) CaM-interacting proteins, such as an IQ domain or a 1-5-10 motif[150]. However, there are other examples of membrane proteins known to interact with CaM at an intracellular juxtamembrane region (as we demonstrated for KCNE4), including the epidermal growth factor receptor[153-155]. We previously demonstrated that the cytoplasmic domain of KCNE4 is necessary for its inhibition of KCNQ1, and is sufficient to confer inhibitory function to a chimera consisting of the N-terminus and transmembrane domain of KCNE1 but the C-terminus of KCNE4[48]. This overlap between the CaM-binding site and the KCNE4 domain necessary for inhibition of KCNQ1 activity supports our hypothesis that KCNQ1 inhibition by KCNE4 may involve its ability to interact with CaM.

The primary structure of KCNE4 is distinct from the other four KCNE proteins at the juxtamembrane site identified here as a CaM-binding region. Specifically, the region containing four sequential hydrophobic leucine residues in KCNE4 is occupied by polar residues in the other four KCNE proteins, which would likely not support interactions with CaM. As we demonstrated in this study, KCNE1 does not interact with CaM when expressed alone (Figure 23).

The identification of critical residues for CaM binding also allowed us to study the functional consequences of disrupting the KCNE4-CaM interaction. We demonstrated

that KCNE4 L[69-72]A subunits fail to robustly inhibit KCNQ1. However, expression of this KCNE4 mutant does modulate the kinetics and voltage-dependence of KCNQ1 activation and changes kinetic properties of tail currents consistent with removal of inactivation (Figure 25). Overall these findings indicate that the mutant KCNE4 with impaired biochemical interaction with CaM also exhibits impaired ability to inhibit KCNQ1, whereas its ability to function as a modulatory subunit to KCNQ1 is not lost. We speculate that these residual functional effects of KCNE4 L[69-72]A on KCNQ1 could be mediated through interactions between the pore-forming subunit and the KCNE4 transmembrane domain. In support of this notion, there are similarities in KCNQ1 modulation evoked by KCNE4 L[69-72]A and a chimera consisting of the N- and C-termini of KCNE1 coupled to the transmembrane domain of KCNE4[48].

The physiological implications of the observations presented here may be significant, but are difficult to assign because of the primary lack of understanding of the physiological contributions of KCNE4. In heart, where KCNE4 could modulate repolarizing currents such as I_{Ks}, and where local free Ca^{2+} concentrations cycle dramatically, the Ca^{2+}-CaM sensitivity described here for KCNE4 may enable Ca^{2+}-dependent regulation of repolarization time. Because repolarization time is critical for action potential duration as well as Ca^{2+} release and contractility[156], CaM-KCNE4 interactions might constitute part of a feedback loop for regulating intracellular Ca^{2+}. Further characterization of KCNE4 L[69-72]A in native cardiac myocytes will be valuable toward establishing the physiologic consequences of disrupting the interaction between KCNE4 and CaM.

The novel protein-protein interaction we demonstrated in this study reinforces the notion that K_V channels function as dynamic protein complexes subject to regulation by both accessory subunits and intracellular signaling molecules, which may themselves interact to impact channel function.

CHAPTER IV

INVESTIGATING THE PHYSIOLOGIC FUNCTION OF KCNE4

Each of the five KCNE proteins modulates potassium channel function in a distinct manner, allowing specific transformation of the biophysical properties of a channel depending on which accessory subunit(s) is (are) present in the channel complex. Given that the KCNE proteins can exert potent and diverse modulatory effects and may potentially participate in a large variety of channel complexes, a compelling question emerges: what is the native physiologic role of each *KCNE* gene?

The answer is partly revealed by the association of mutations in *KCNE* genes with inherited human diseases. Specifically, mutations in *KCNE1* have been associated with congenital long QT syndrome (LQTS)[72,86,157], while *KCNE2* variants have been identified in cases of sporadic and drug-induced LQTS[72,84,87,88]. Periodic paralysis, a skeletal muscle disorder, has been associated with mutations in *KCNE3*[65,158]. Finally, deletion of a genomic region (Xq22.3) containing *KCNE5* results in a syndrome featuring Alport syndrome, mental retardation, midface hypoplasia, and elliptocytosis[55].

These disease associations provide strong focus points for elucidating the physiologic roles of *KCNE1*, *KCNE2*, *KCNE3*, and *KCNE5*. In the case of *KCNE4*, other than a single report[159] that the minor allele of a SNP (1057 G/T) leading to a conservative amino acid substitution (145 E/D) is found slightly more frequently in patients with idiopathic atrial fibrillation than controls in a Chinese population (34.0% versus 27.1%, respectively), no human inherited disease has been associated with a mutation in *KCNE4*.

Considering the particularly dramatic modulatory effects imparted by *KCNE4* on critical channel complexes and the broad expression of *KCNE4* by human tissues, it is likely that *KCNE4* plays an important role in one or more physiologic systems, but we are left to investigate that role without the natural focus point arising from phenotypic characterization of native mutation carriers.

An alternative approach to an investigation into the physiologic function of KCNE4 is to first consider which tissues express KCNE4. The mRNA expression pattern of *KCNE4* (Figure 6, Chapter I) reveals that many tissues express *KCNE4*. This set of tissues includes those whose functions are directly dependent on their ability to conduct electricity (such as heart, skeletal muscle, and brain) and some that are non-excitable (such as kidney, testes, and colon).

K_V channel complexes (including those comprised of KCNQ1 and KCNE subunits) have previously been implicated in critical physiologic functions in many of the tissues that express KCNE4. As one example in a non-excitable cell type, data suggest that KCNQ1-KCNE3 channel complexes provide the basolateral K^+ recycling in colonic crypt cells required to maintain the electrochemical driving forces behind lumenal Cl^- secretion through CFTR at the apical membrane[160]. This lead and the other studies cited in Chapter I establish a precedent for the importance of K_V channels and KCNE modulatory subunits in the physiology of non-excitable tissues. Because our data demonstrate that KCNE4 is expressed in a number of non-excitable tissues, any effort toward determining the native function of KCNE4 would be incomplete without considering potential roles in these systems.

On the other hand, K_V channels are primarily studied for their contributions to the physiology of excitable cells, such as myocytes or neurons. The electrical excitability of these cells stems directly from the capacity of their plasma membranes to respond to changes in voltage and to propagate an electrical signal; voltage-gated ion channels provide both of these functions. Thus, in addition to considering potential roles for KCNE4 in non-excitable tissues as described above, it is critical to investigate its possible contributions to the physiology of excitable tissues.

In vitro observations of the functional properties of KCNE4 and studies of its expression in human heart provide us with strong, specific leads in cardiac physiology. In heterologous expression systems, KCNE4 dramatically inhibits I_{Ks}[70], a critical repolarizing current in the human cardiac action potential (Figure 5, Chapter I). Further, expression of KCNE4 is robust in all regions of adult heart as well as in fetal heart[70] (Figure 9, Chapter I). These findings as well as the physiologic functions in cardiac physiology already established for other members of the KCNE family lead us to believe that *KCNE4* may be an endogenous regulator of I_{Ks} and contribute to fine-tuning of the cardiac action potential, with implications for heart rhythm and contractility.

Because a primary focus of our lab is on the function of KCNE subunits in the context of cardiac electrophysiology and because of the compelling preliminary data identifying KCNE4 as a potential modulator of I_{Ks}, our initial effort in characterizing the function of KCNE4 has been directed to its potential role in cardiac physiology. Our studies have been motivated by the hypothesis that KCNE4 is an endogenous negative regulator of I_{Ks} and/or other repolarizing K^+ currents in the human cardiac action potential. In this role, KCNE4 could serve to reduce repolarizing currents in cardiac

myocytes, thereby lengthening the QT interval, which may in turn have effects on excitation-contraction coupling and contractility.

Kcne4-null mouse model

Our primary approach to studying the function of KCNE4 in cardiac physiology was to characterize the cardiac phenotype of a *Kcne4*-null mouse. As a model organism, the mouse offers many appealing traits: it is a mammal, has a short breeding cycle, is relatively easy to manipulate in many experimental systems, has a fully sequenced genome of approximately the same size as the human genome, and has been the target of many advanced gene transfer technologies.

For the specific needs of this project, the mouse also presents considerable limitations. Most critically, the cardiac electrophysiology of a mouse does not closely resemble human cardiac electrophysiology. As shown in Figure 27, the mouse and human ventricular action potentials have distinct morphological differences owing to unique sets of underlying currents. Of particular relevance, the currents responsible for repolarization (which we hypothesize may be critical targets of KCNE4 modulation) are not conserved between the two species. In humans, the delayed rectifier potassium currents I_{Ks} and I_{Kr} contribute to an elongated repolarization phase characterized by its plateau. By contrast, adult mouse ventricular cells express a different cohort of potassium channels with distinct time- and voltage-dependent properties. These channels give rise to unique delayed rectifier currents ($I_{K,slow1}$, $I_{K,slow2}$, and I_{SS}) which contribute to a much abbreviated repolarization phase in the mouse compared to human[161].
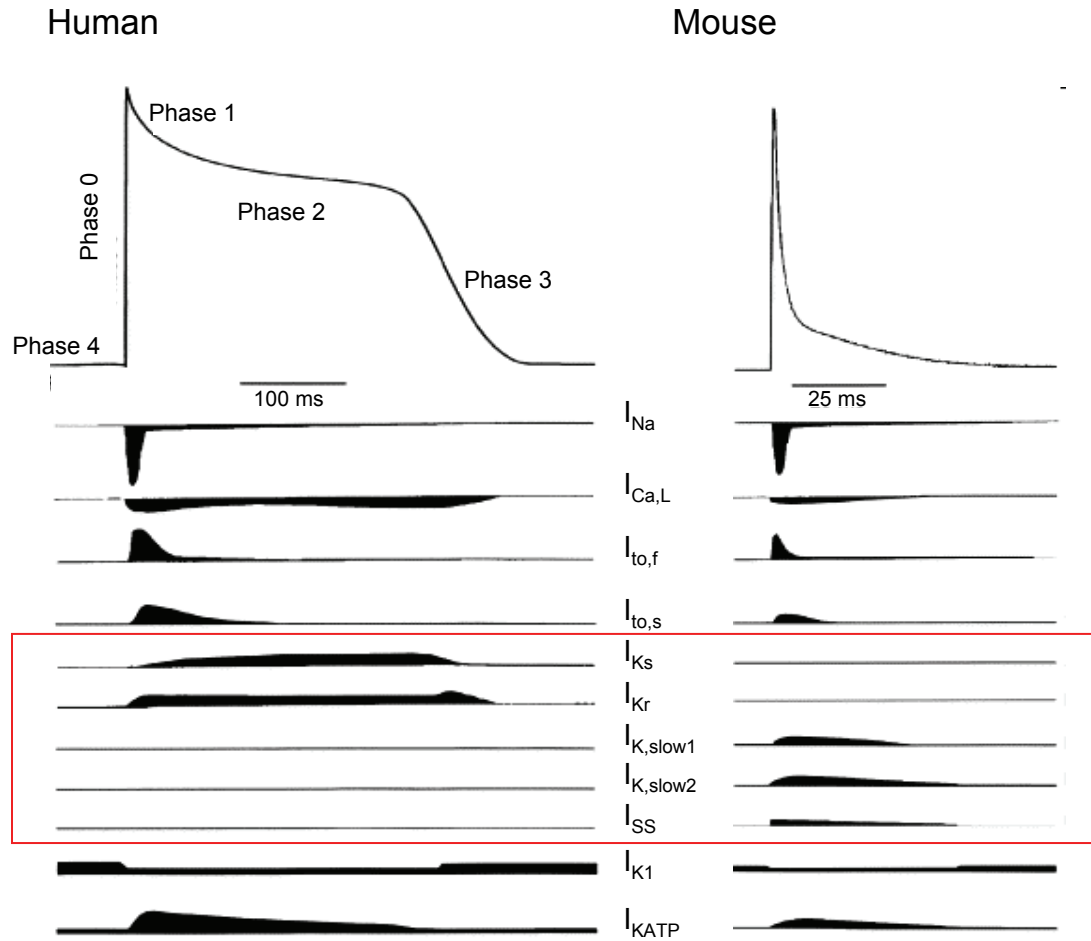
Figure 27. Human versus mouse ventricular cardiac action potentials. Potassium currents contributing to repolarization differ markedly between the two species (red box). In humans, I_{to} accounts for transient repolarization (phase 1) followed by a plateau (phase 2) attributable to K^+ efflux via I_{Ks} and I_{Kr} balanced against Ca^{2+} influx via $I_{Ca,L}$. As Ca^{2+} channels inactivate and K^+ currents predominate, the cell rapidly repolarizes (phase 3) back to the resting potential. By contrast, mouse ventricular cells do not prominently express I_{Ks} or I_{Kr}, but their unique repolarizing K^+ currents $I_{K,slow1}$, $I_{K,slow2}$, and I_{SS} drive rapid repolarization with no plateau phase. Adapted from Nerbonne JM *Trends Cardiovasc Med* **14**, 83-93 (2004).

Despite these limitations, phenotypic characterization of mouse models following genetic manipulation of various K^+ channels has provided much insight into molecular mechanisms underlying normal and pathological cardiac physiology[94,162-171]. Thus we decided that a *Kcne4*-null mouse line could ultimately provide us the best opportunity to observe the effects of knocking out *Kcne4* on cardiac electrophysiology *in vivo*. In the studies described here, we acknowledge that our findings must be interpreted in the specific context of mouse physiology and our ability to generalize to human physiology is limited. With these considerations, we hypothesized that if *Kcne4* is an important negative regulator of repolarizing currents in the mouse cardiac action potential, the phenotype of *Kcne4*-null animals might include a shortened QT interval, possible enhanced susceptibility to or protection against cardiac arrhythmias, and possible contractile defects.

Methods

Breeding and marker-assisted selection to establish isogenic lines of Kcne4$^{-/-}$ mice

Kcne4 knockout

We obtained four *Kcne4*$^{+/-}$ founder mice from Lexicon Pharmaceuticals Inc., which were generated by homologous recombination in embryonic stem cells of the129/SvEv mouse strain, with a lacZ-containing Neo cassette replacing the entire coding region of *Kcne4*. Recombinant cells were injected into early-stage host embryos of the C57BL/6 albino strain and implanted into the uterus of a female C57BL/6 mouse. Pups were bred

with selection for animals with the transgene in the germ cell line, and we received *Kcne4*^{+/-} animals on a hybrid C57BL/6-129/SvEv background strain.

Speed Congenics

Because the C57BL/6 and 129/SvEv strains exhibit significant differences in cardiac physiology[172] (Table 7) which could confound phenotypic findings, our first priority was to separately enrich each background strain and move our transgene to two isogenic lines. To do this efficiently, we implemented a marker-assisted selection protocol while performing a series of backcrosses with pure C57BL/6 or 129S6/SvEv female mice to enrich that strain. At each generation, the genomes of male *Kcne4*^{+/-} pups were screened using 70 microsatellite markers that span the genome and can discriminate between the two strains, to deduce the percentage of C57BL/6 versus 129S6/SvEv background in each. The most enriched male *Kcne4*^{+/-} mouse was selected as the founder for the next generation, and so on. This process allowed us to generate congenic litters of *Kcne4*^{+/+}, *Kcne4*^{+/-}, and *Kcne4*^{-/-} mice within 4-5 generations. Once congeneity was attained, we used Vanderbilt's Transgenic / Embryonic Stem Cell Shared Resource Core to cryopreserve 632 *Kcne4*^{-/-} embryos on the C57BL/6 background. Of these, 45 embryos (from two separate vials) were thawed to test viability, which yielded six live pups whose genotypes were confirmed as *Kcne4*^{-/-}. The Core continues to store the remaining 587 frozen embryos in 24 vials, for future repopulation of the mouse colony if necessary.

Table 7. Electrocardiographic parameters in male and female 129/Sv and C57BL/6 conscious mice. Values are mean ± SEM. HR var, heart rate variability; p, p-value following student t-test comparing strains. Adapted from Chu V et al., BMC Physiol. 2001; 1:6.

	Males			Females		
	129/S6 (n = 10)	**C57BL/6** (n = 10)	p	**129/S6** (n = 10)	**C57BL/6** (n = 10)	p
Heart Rate (bpm)	571 ± 13	692 ± 5	<0.001	689 ± 12	741 ± 2***	<0.001
HR var (bpm)	15 ± 4	12 ± 3	0.850	20 ± 4	15 ± 3	0.331
PR (ms)	31.9 ± 1.3	26.0 ± 0.8	0.001	28.3 ± 0.6	24.4 ± 0.7	<0.001
QRS (ms)	9.6 ± 0.3	8.1 ± 0.2	<0.001	8.5 ± 0.1	7.5 ± 0.2	<0.001
QT (ms)	70.2 ± 1.8	55.4 ± 0.8	<0.001	54.7 ± 2.0	53.8 ± 0.6	0.672
QT_c (ms)	66.7 ± 1.9	59.0 ± 0.8	0.002	58.4 ± 1.6	58.7 ± 0.3	0.856

Genotyping

We employed a simple PCR assay that discriminates wild-type from transgenic alleles, using genomic DNA isolated from ear punches collected when pups were 3 weeks old. Importantly, during this breeding process we observed that crosses exhibited a Mendelian ratio of $Kcne4^{+/+}$, $Kcne4^{+/-}$, and $Kcne4^{-/-}$ animals and all three genotypes are viable.

Consequences of Kcne4 knockout on cardiac physiology at the whole-animal level

Electrocardiography

Adult mice were examined under isoflurane anesthesia for cardiac electrophysiological and arrhythmia phenotypes using high-resolution surface electrocardiography (ECG) recording. Anesthesia was induced with 3% inhaled isoflurane and maintained at 1.5-2%. Following induction of anesthesia, an electrode was placed subcutaneously in each limb. Four-lead ECGs were recorded and digitized at 2 kHz using a data-acquisition board and custom-built software available in the laboratory of our collaborator, Dr. Bjorn Knollman. ECGs were recorded continuously for at least five minutes, then electrodes were removed, isoflurane was withdrawn, and mice were allowed to recover under a warm lamp. Comparisons of resting heart rate, PR, QT, and QRS duration were made from signal-averaged recordings among $Kcne4^{+/+}$, $Kcne4^{+/-}$, and $Kcne4^{-/-}$ littermates. Rate-corrected QT interval, denoted QTc, was calculated using the Mitchell equation for mice QTc = QT/sqrt(RR/100). Data were examined for evidence of conduction disturbances (eg. prolonged PR, increased QRS

97

duration) and abnormal rhythm, specifically for evidence of atrial and ventricular arrhythmias. All measurements were performed off-line and blinded to genotype. Statistical significance for differences in the above parameters among groups was assessed using ANOVA followed by an appropriate post-test. Separate analyses were performed for male and female animals.

Echocardiography

We evaluated myocardial contractile function in conscious $Kcne4^{+/+}$, $Kcne4^{+/-}$, and $Kcne4^{-/-}$ littermates using transthoracic echocardiography. These studies were performed by an established core laboratory in the Division of Cardiovascular Medicine, which is equipped with a 15-MHz high-frequency transducer. Measurements of left ventricular (LV) end-diastolic and end-systolic diameter, LV fractional shortening, and estimated LV ejection fraction were obtained from 2D guided M-mode images acquired at 100 frames per second. Images were read off-line using short-axis and parasternal long-axis views by two independent investigators blinded to genotype. Statistical significance for differences in the above parameters among groups was assessed using ANOVA with an appropriate post-test. All studies were performed at two different ages (8 and 30 weeks) to investigate the age-dependence of the phenotype. Separate analysis was performed for male and female mice.

Isolation of adult cardiac myocytes

Isolation of adult mouse ventricular myocytes was performed following heparin injection (0.1 mL 5000 USP U/mL) under isoflurane anesthesia with rapid excision of the heart. The aorta was cannulated and the heart perfused in retro-aortic fashion with Modified Tyrode solution (mM: NaCl 130, NaH$_2$PO$_4$ 1.2, glucose 10.0, KCl 5.4, MgCl$_2$ 1.2, pH 7.2) for 3 min at 33.8-34.0 $^{\circ}$C measured at the apex of the heart. Type II collagenase (Worthington) at 0.5 mg/mL and type XIV protease at 0.05 mg/mL were added to the perfusate and the myocardium was perfused for 4-6 minutes, until fluid resistance in the tubing dropped by 50 % and the tissue began to turn pale in color. The heart was then removed from the cannula, and the atria and ventricles were separated. Myocytes were dispersed by gentle agitation through a Pasteur pipette in a solution consisting of Modified Tyrode plus 1 mg/mL BSA, 1.0 mM MgCl$_2$, 0.5 mM EDTA, and 0.2 mM CaCl$_2$ (pH 7.2). Cells were washed twice in this solution (pelleting by gravity) then plated on coverslips for acute electrophysiological recordings.

Electrophysiology

All recordings were performed using the ruptured-patch technique at room temperature. Recordings and subsequent analyses were performed blinded to the genotype of the cells. Statistical comparisons were made between groups from *Kcne4$^{+/+}$, Kcne4$^{+/-}$,* and *Kcne4$^{-/-}$* littermates by one-way ANOVA with an appropriate post-test.

Current-clamp recordings -- Recordings were performed in normal Tyrode solution without blockers. Action potentials were elicited with 2 ms square wave pulses (1-2 nA, or approximately 1.25 times threshold) at 1 or 0.3 Hz stimulation frequency. Cells were paced at 1 Hz for 4 minutes, and sweeps 181-183 were averaged for analysis. Action potential duration at 50 % (APD_{50}) and 90 % (APD_{90}) repolarization were determined as well as resting membrane potential and overshoot (peak membrane potential).

Voltage-clamp recordings -- Examination of adult ventricular myocytes allowed for analysis of I_{to}, I_{K1} and I_{sus} (comprised of $I_{Kslow,1}$ and $I_{Kslow,2}$). Recordings were performed under conditions that suppress activation of Na^+ and Ca^{2+} channels. We recorded currents evoked by 4.5 s voltage pulses ranging from –40 to +40 mV (holding potential – 80 mV) in 10 mV increments. Distinct potassium currents were differentiated on the basis of their time dependence. Current density normalized to cell capacitance was deduced for the individual currents.

Results

Consequences of Kcne4 knockout on general animal health

We observed that *Kcne4*^{-/-} mice of both background strains appear healthy, grow at the same rate as their *Kcne4*^{+/+} littermates, and can live in the research facility to at least 18 months of age.

We acquired multi-system phenotyping data from Lexicon Pharmaceuticals, who generated the transgenic mouse line. Among pertinent findings from their studies of F2 mice on a hybrid C57BL/6-129/SvEv background are the following:

- *Kcne4$^{-/-}$* mice have significantly reduced conscious heart rate compared to *Kcne4$^{+/+}$* littermates (age 15 weeks): 558.6 ± 21.0 (n = 32) versus 635.2 ± 31.6 bpm (n = 12); p = 0.05 for comparison of genotypes after allowing for effects of sex (two-way ANOVA)

- No difference in mean systolic blood pressure (age 15 weeks) following measurements ten times daily by tail cuff for four days

- *Kcne4$^{-/-}$* mice have significantly reduced body temperature (measured rectally) compared to *Kcne4$^{+/+}$* littermates (age 12 weeks): 36.1 ± 0.24 (n = 8) versus 37.2 ± 0.34 °C (n = 4); p = 0.04 for comparison of genotypes after allowing for effects of sex (two-way ANOVA)

- *Kcne4$^{-/-}$* have significantly elevated blood phosphorous levels compared to *Kcne4$^{+/+}$* littermates (age 16 weeks): 6.1 ± 0.2 (n = 8) versus 4.8 ± 0.2 mg/dL (n = 4); p = 0.001 for comparison of genotypes after allowing for effects of sex (two-way ANOVA)

- *Kcne4$^{-/-}$* mice have significantly elevated blood calcium levels compared to *Kcne4$^{+/+}$* littermates (age 16 weeks): 9.6 ± 0.09 (n = 8) versus 9.3 ± 0.1 mg/dL (n = 4); p = 0.05 for comparison of genotypes after allowing for effects of sex (two-way ANOVA)

- *Kcne4*^{-/-} mice have a trend toward reduced blood glucose compared to *Kcne4*^{+/+} littermates (age 16 weeks): 80.1 ± 5.5 (n = 8) versus 100.8 ± 7.7 mg/dL (n = 4); p = 0.07 for comparison of genotypes after allowing for effects of sex (two-way ANOVA)

- *Kcne4*^{-/-} mice have a trend toward elevated blood cholesterol levels compared to *Kcne4*^{+/+} littermates (age 16 weeks): 122.3 ± 7.9 (n = 8) versus 95.0 ± 11.2 mg/dL (n = 4); p = 0.08 for comparison of genotypes after allowing for effects of sex (two-way ANOVA)

- No difference in blood levels of albumin, alkaline phosphatase, alanine aminotransferase, blood urea nitrogen, creatinine, triglycerides, or uric acid (age 16 weeks)

- No difference in glucose tolerance nor blood insulin levels (age 15 weeks)

- No abnormalities upon urinalysis assessing: leukocytes, nitrites, urobilinogen, protein, pH, blood, specific gravity, ketones, bilirubin, glucose (age 15 weeks)

- No difference in body length at age 16 weeks, nor weight measured at 2-week intervals from age 2 weeks through 14 weeks

- No difference in acute phase response (TNFα, MCP-1, or IL-6 blood levels) following sublethal intraperitoneal LPS injection (age 18 weeks)

- No difference in peripheral blood mononuclear cell profile assessing counts of: CD4$^+$ cells, CD8$^+$ cells, NK cells, B cells, monocytes (age 16 weeks)

- No difference in hematology profile assessing: red cell count, white blood cell count, lymphocytes, neutrophils, eosinophils, basophils, monocytes, hemoglobin, hematocrit, mean corpuscular volume, mean corpuscular hemoglobin, mean

corpuscular hemoglobin concentration, red cell distribution weidth, platelet count, mean platelet volume (age 16 weeks)

- No difference in ability to produce IgG1 or IgG2 antibodies following antigen challenge (age 24 weeks)

- No abnormalities observed by CT scan in 1 male *Kcne4*^{-/-} mouse nor 1 female *Kcne4*^{-/-} mouse, sedated with 1.25% 2,2,2,-tribromoethanol (20 ml/kg body weight), each age 30 weeks. From report: "No abnormalities seen in gross skeleton, thorax, and abdomen. Liver, kidneys, and spleen appear normal in size, shape and position. The rate of excretion of contrast media by the kidneys is within normal limits, reflecting normal function."

- No differences in bone mineral density, percentage body fat, or lean body mass (age 15 weeks)

- No observed deficits in gross neurological function as measured by a functional observation battery of tests from the Irwin neurological screen (age 12 weeks)

- No observed deficits in nociception by hotplate test (latency to limb withdrawal on hotplate), age 12 weeks

- No observed deficits or enhancements in motor strength by inverted screen (age 12 weeks)

- No difference in proliferative capacity of skin fibroblasts grown in culture following biopsy (age 20 weeks)

- Pertinent findings from histological post-mortem studies in *Kcne4*^{-/-} mice include: multifocal minimal protein casts and minimal focal regeneration of renal tubule (one of two mice); mild (2+) multifocal endometrial hyperplasia (one of one female mice); moderate (3+) chronic diffuse inflammation of pancreatic duct (one

of two mice); mild (2+) focal spermatocoele (one of one male mice); mild (2+) splenic hyperplasia (one of two mice)

Consequences of Kcne4 knockout on cardiac physiology at the whole-animal level

Shortened QT interval

We recorded electrocardiograms in adult mice under isoflurane anesthesia in both strains, and in the C57BL/6 strain at two different ages (8-11 weeks and 30 weeks). While no difference in spontaneous arrhythmia susceptibility was noted among genotypes for any of the experimental groups, some changes in a number of ECG parameters were detected. As shown in Figure 28 and Table 8, $Kcne4^{-/-}$ mice in all three experimental groups exhibited a trend toward shorter QT and QTc intervals versus $Kcne4^{+/+}$ littermates, and in two of the experimental groups (C57BL/6 age 30 weeks and 129S6/SvEv age 8 weeks) the difference in QTc was statistically significant. Further, in the 129S6/SvEv strain, all other ECG parameters (RR, PR, QRS, QT) were significantly shortened in $Kcne4^{-/-}$ versus $Kcne4^{+/+}$ mice.

Left ventricular dilation and reduced fractional shortening

Echocardiography performed on conscious adult $Kcne4^{+/+}$, $Kcne4^{+/-}$, and $Kcne4^{-/-}$ mice of each strain (and at two ages in the C57BL/6 strain, 8 weeks and 30 weeks) allowed us to assess whether *Kcne4* knockout has any consequences for cardiac chamber dimensions or contractility. As shown in Figures 29 and Table 9, C57BL/6 $Kcne4^{-/-}$ mice at age 8 weeks exhibit a significantly dilated left ventricular internal diameter during both
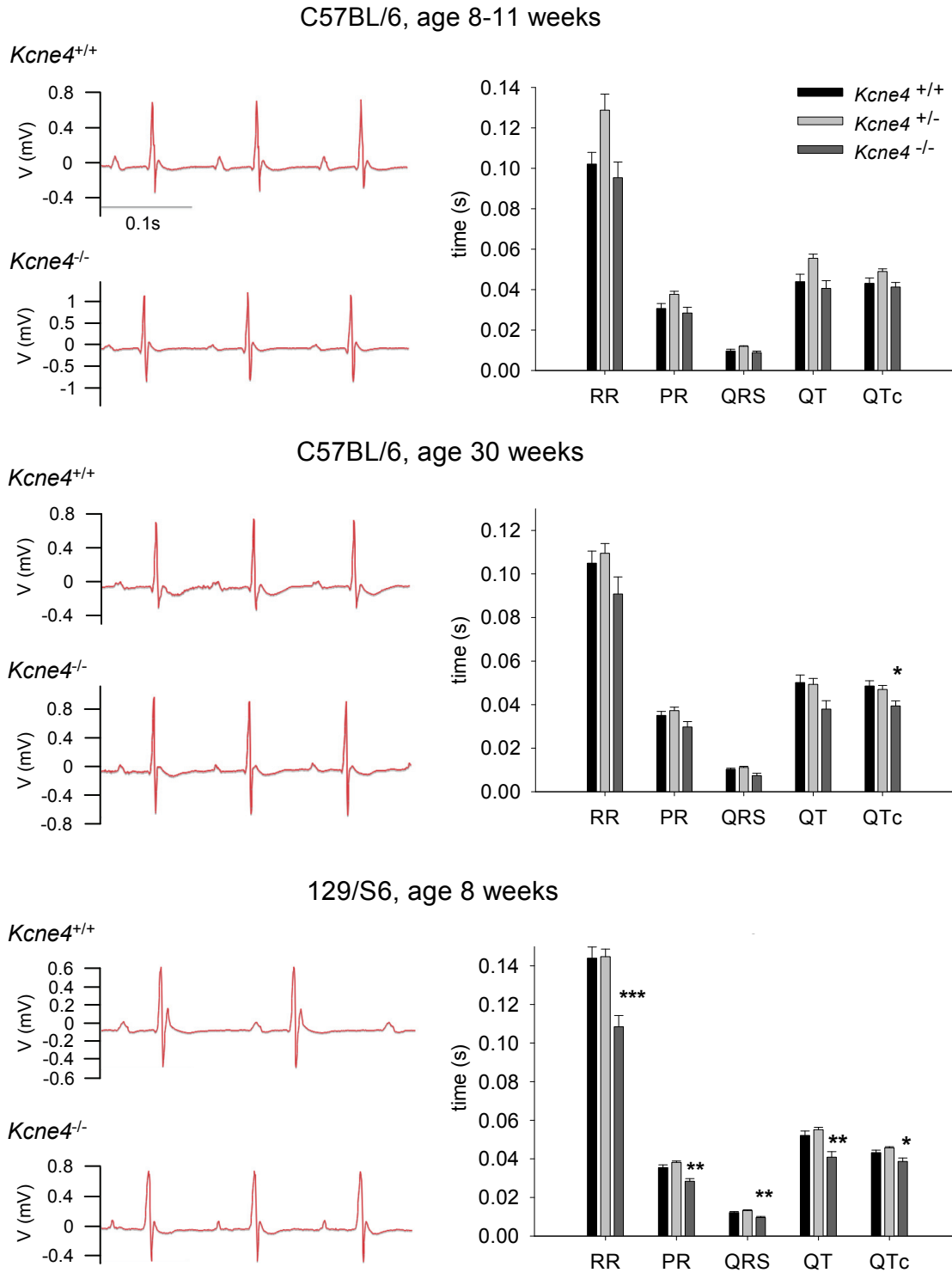
Figure 28. Electrocardiography in *Kcne4⁻ᐟ⁻* mice. Left, representative recordings from wild-type and *Kcne4*-null animals from each experimental group. Right, bar charts display mean ± SEM for each interval. *, $p < 0.05$; **, $p < 0.01$; ***, $p < 0.001$ for Tukey pariwise comparison to wild-type following two-way ANOVA ($p < 0.05$) comparing genotypes after allowing for the effects of differences in sex.

Table 8. Mean ± SEM for major EKG intervals, plus p-value for two-way ANOVA comparing genotypes after allowing for the effects of difference in sex.

	C57BL/6, 8-11 weeks				C57BL/6, 30 weeks				129/S6, 8 weeks			
	+/+	+/-	-/-	Two-Way ANOVA	+/+	+/-	-/-	Two-Way ANOVA	+/+	+/-	-/-	Two-Way ANOVA
	n = 10 (6 M + 4 F)	n = 4 (1 M + 3 F)	n = 6 (3 M + 3 F)	p	n = 12 (9 M + 3 F)	n = 13 (8 M + 5 F)	n = 9 (5 M + 4 F)	p	n = 25 (14 M + 11 F)	n = 13 (9 M + 4 F)	n = 18 (7 M + 11 F)	p
RR (s)	0.102 ± 0.006	0.122 ± 0.011	0.095 ± 0.008	0.175	0.104 ± 0.007	0.109 ± 0.006	0.091 ± 0.007	0.118	0.144 ± 0.005	0.146 ± 0.008	0.107 ± 0.006	<0.001
PR (s)	0.031 ± 0.002	0.038 ± 0.004	0.028 ± 0.003	0.235	0.034 ± 0.002	0.037 ± 0.002	0.030 ± 0.002	0.059	0.036 ± 0.001	0.039 ± 0.002	0.028 ± 0.001	<0.001
QRS (s)	0.010 ± 0.001	0.012 ± 0.001	0.009 ± 0.001	0.943	0.010 ± 0.001	0.011 ± 0.001	0.008 ± 0.001	0.010	0.012 ± 0.001	0.013 ± 0.001	0.009 ± 0.001	<0.001
QT (s)	0.044 ± 0.004	0.054 ± 0.006	0.041 ± 0.004	0.273	0.051 ± 0.004	0.050 ± 0.003	0.039 ± 0.004	0.054	0.052 ± 0.002	0.055 ± 0.003	0.040 ± 0.003	<0.001
QTc (s)	0.043 ± 0.002	0.049 ± 0.004	0.041 ± 0.003	0.403	0.049 ± 0.002	0.047 ± 0.002	0.040 ± 0.002	0.036	0.043 ± 0.001	0.046 ± 0.002	0.038 ± 0.002	0.009

Figure 29. Echocardiography results from conscious C57BL/6, 8-week-old mice. A, Representative dynamic M-mode images from wild-type and *Kcne4*-null mice. B, Cardiac dimensions and working parameters calculated from M-mode recordings. n = 6 male + 6 female mice per group; *, $p < 0.05$; **, $p < 0.01$; ***, $p < 0.001$ for Tukey pairwise comparison to wild-type following two-way ANOVA comparing genotypes after allowing for effects of sex. LVID, left ventricular internal diameter; FS, fractional shortening; EF, ejection fraction; HR, heart rate.

Table 9. Mean ± SEM for major echo parameters, plus p-value for two-way ANOVA comparing genotypes after allowing for the effects of difference in sex.

	C57BL/6, 8-11 weeks				C57BL/6, 30 weeks				129/S6, 8 weeks			
	+/+	+/-	-/-	p	+/+	+/-	-/-	p	+/+	+/-	-/-	p
	n = 12 (6 M + 6 F)	n = 12 (6 M + 6 F)	n = 12 (6 M + 6 F)		n = 12 (6 M + 6 F)	n = 12 (6 M + 6 F)	n = 9 (5 M + 4 F)		n = 12 (6 M + 6 F)	n = 12 (6 M + 6 F)	n = 12 (6 M + 6 F)	
LVIDD/BW (cm/g)	0.0129 ±.0005	0.0138 ±.0004	0.0150 ±.0005	<0.001	0.0110 ±.0003	0.0103 ±.0003	0.0110 ±.0004	0.218	0.0153 ±.0004	0.0147 ±.0004	0.0148 ±.0004	0.406
LVIDS/BW (cm/g)	0.0068 ±.0003	0.0079 ±.0003	0.0089 ±.0003	<0.001	0.0057 ±.0002	0.0055 ±.0002	0.0059 ±.0002	0.293	0.0083 ±.0003	0.0076 ±.0003	0.0077 ±.0003	0.164
FS (%)	47.0 ± 1.01	42.8 ± 0.6	40.4 ± 1.0	<0.001	48.3 ± 0.59	46.7 ± 0.57	46.2 ± 0.68	0.064	45.9 ± 1.3	48.7 ± 1.4	47.5 ± 1.5	0.365
EF	0.84 ±.0089	0.81 ±.0064	0.78 ±.010	<0.001	0.85 ±.0054	0.84 ±.0051	0.84 ±.0063	0.053	0.83 ±.0013	0.86 ±.0014	0.84 ±.0014	0.380
HR (bpm)	709.2 ± 5.3	704.2 ± 7.6	710.8 ± 7.8	0.799	666.7 ± 12.1	677.3 ± 11.6	681.5 ± 14.0	0.699	561.0 ± 27.2	601.7 ± 29.1	571.5 ± 30.5	0.584

diastole and systole, as well as reduced fractional shortening and ejection fraction compared to $Kcne4^{+/+}$ littermates. A similar trend toward reduced fractional shortening and ejection fraction was observed for C57BL/6 $Kcne4^{-/-}$ mice at age 30 weeks (Figure 30), though the differences were not statistically significant. No differences in left ventricular internal diameter nor fractional shortening or ejection fraction were observed in 129S6/SvEv mice (Figure 31), and no difference in heart rate was observed in any of the experimental groups. Importantly, the echocardiography studies also allowed us to monitor for arrhythmias in conscious mice, and none were detected in any of the experimental groups.

Consequences of Kcne4 knockout on cardiac physiology at the cellular level

Shortened action potential duration

We performed preliminary current-clamp experiments on ventricular myocytes isolated from adult C7BL/6 and 129/S6 $Kcne4^{+/+}$ and $Kcne4^{-/-}$ mice, including two age groups for the C57BL/6 strain (6-7 weeks and 13-15 weeks). Figure 32 and Table 10 illustrate our findings for action potential duration, resting membrane potential, and peak membrane potential for each experimental group. A significant shortening of the action potential was observed for $Kcne4^{-/-}$ mice in the C57BL/6 age 13-15 week group, but not in the others.
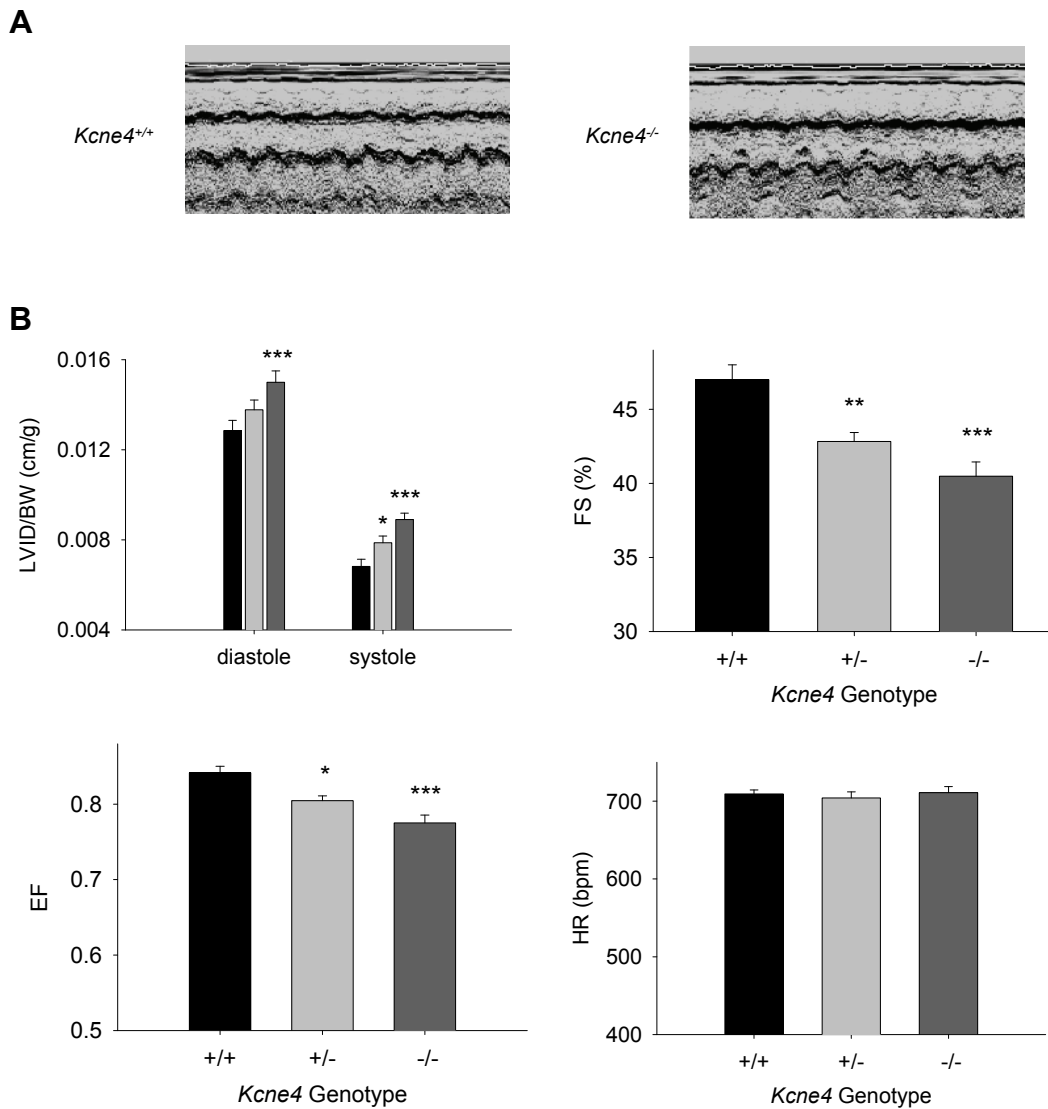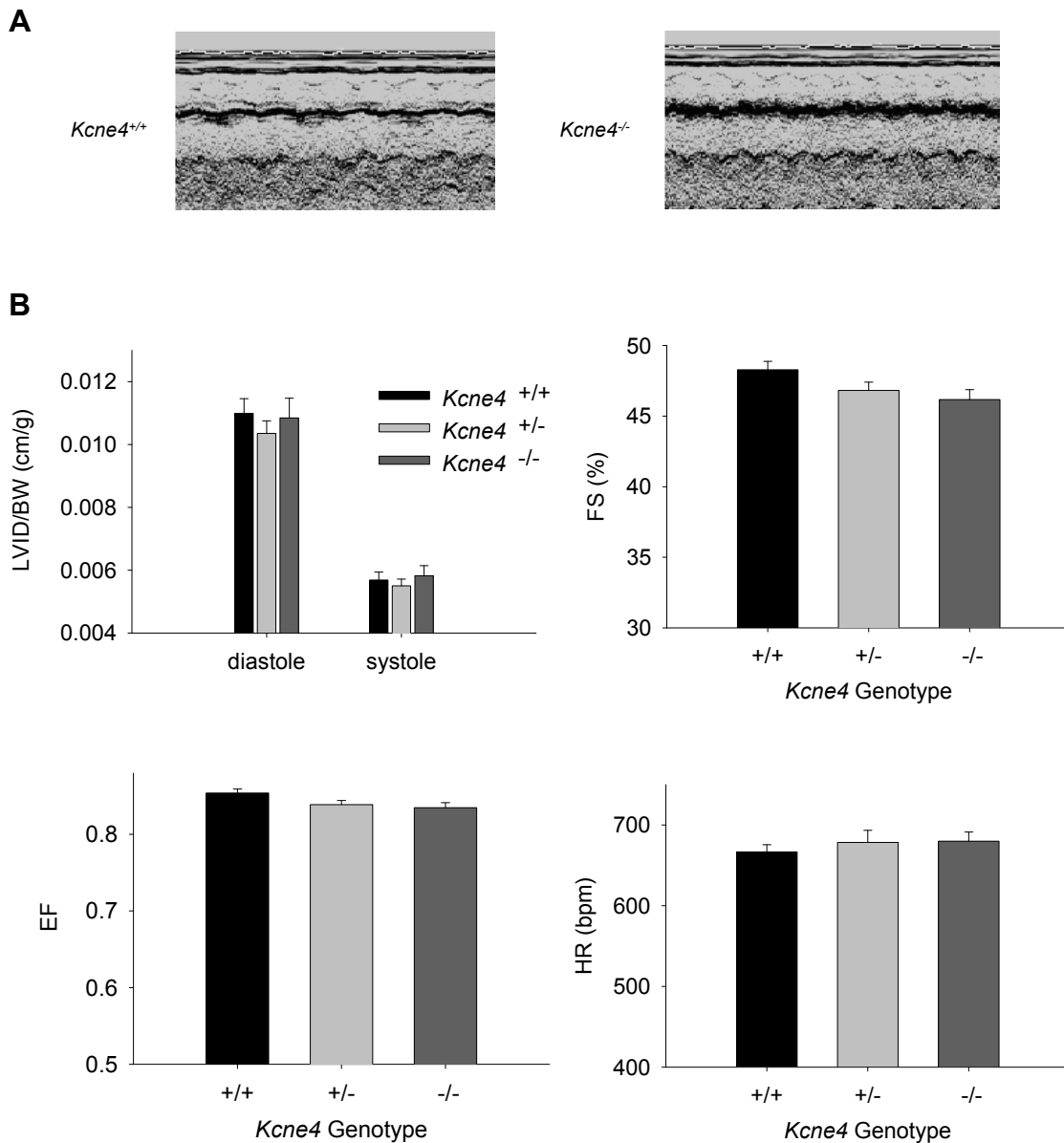
Figure 30. Echocardiography results from conscious C57BL/6, 30-week-old mice. A, Representative dynamic M-mode images from wild-type and *Kcne4*-null mice. B, Cardiac dimensions and working parameters calculated from M-mode recordings. *Kcne4*+/+ and *Kcne4*+/-, n = 6 male + 6 female mice per group; *Kcne4*-/-, n = 5 male + 4 female mice. LVID, left ventricular internal diameter; FS, fractional shortening; EF, ejection fraction; HR, heart rate.
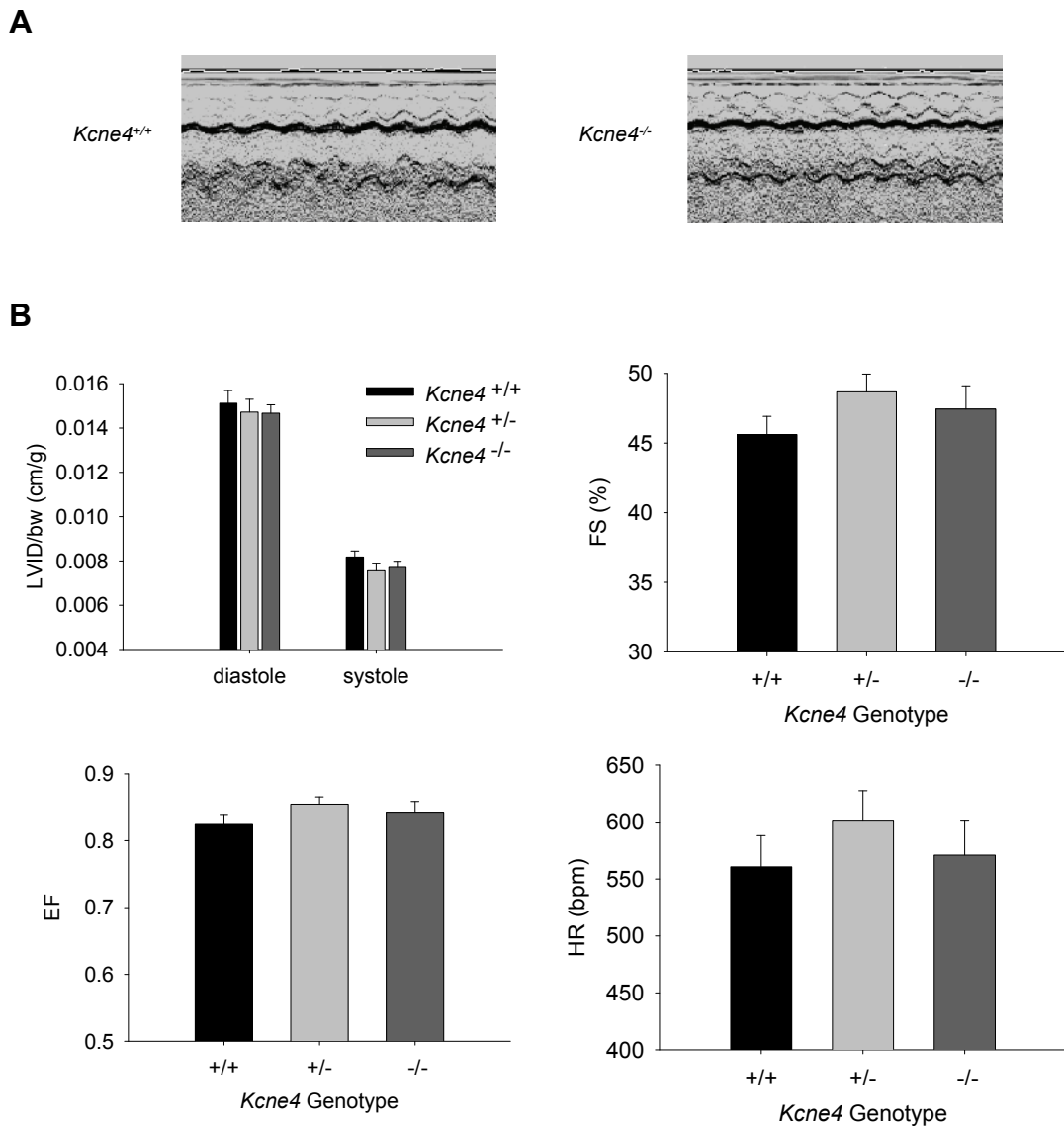
Figure 31. Echocardiography results from conscious 129S6/SvEv, 8-week-old mice. A, Representative dynamic M-mode images from wild-type and *Kcne4*-null mice. B, Cardiac dimensions and working parameters calculated from M-mode recordings. n = 6 male + 6 female mice per group. LVID, left ventricular internal diameter; FS, fractional shortening; EF, ejection fraction; HR, heart rate.
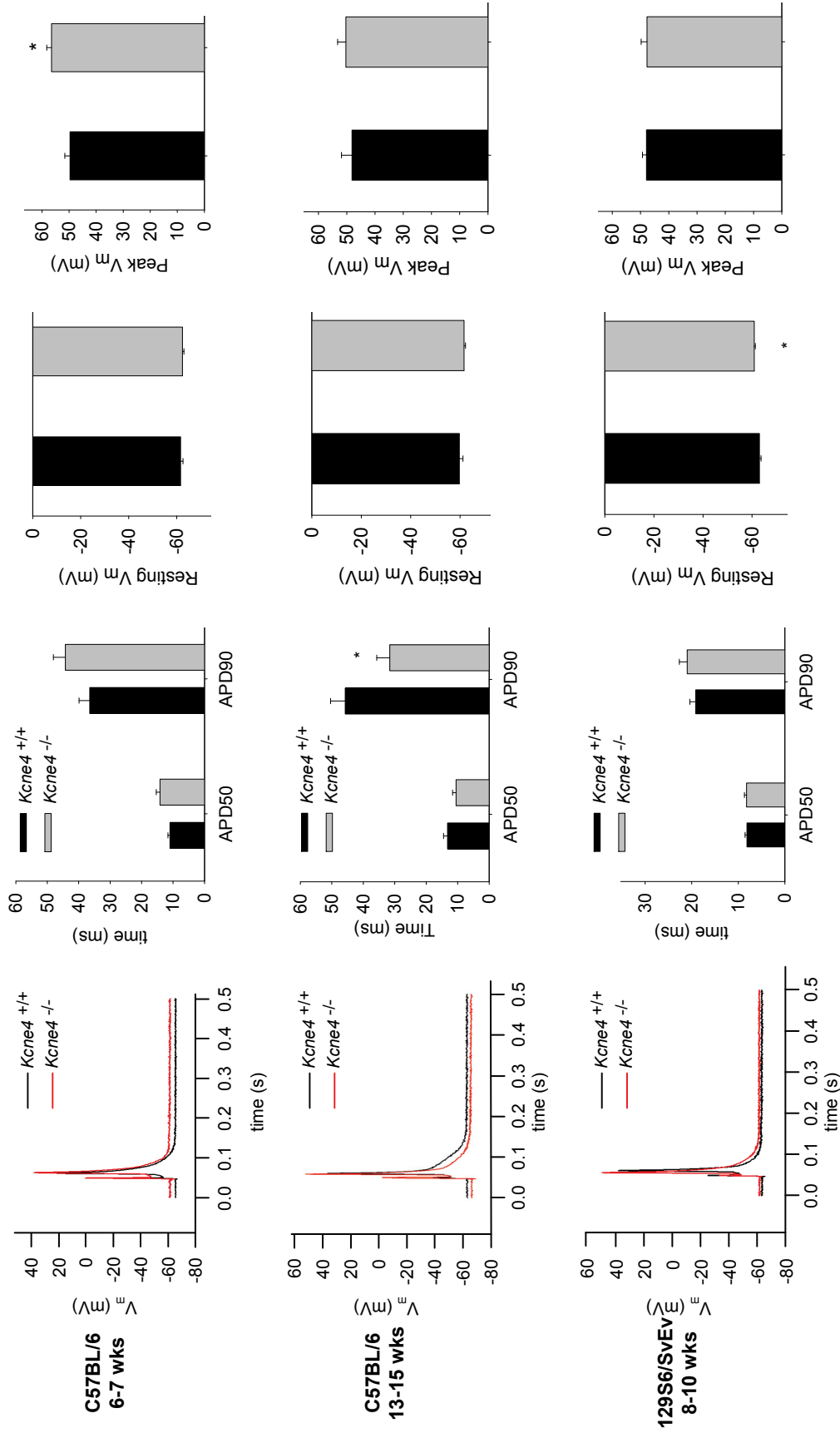
Figure 32. Action potentials recorded from adult mouse ventricular myocytes. Left, representative traces from wild-type and Kcne4-null animals. Bar charts display mean ± SEM for each parameter indicated. *, p < 0.05 versus *Kcne4*+/+ by student-t test.. C57BL/6, 6-7 weeks: n = 12 cells from 2 mice (*Kcne4*+/+), n = 15 cells from 2 mice (*Kcne4*-/-). C57BL/6, 13-15 weeks: n = 9 cells from 2 mice (*Kcne4*+/+), n = 11 cells from 3 mice (*Kcne4*-/-). 129S6/SvEv, 8-10 weeks: n = 23 cells from 3 mice (*Kcne4*+/+), n = 18 cells from 3 mice (*Kcne4*-/-).

Table 10. Mean ± SEM for action potential parameters in ventricular myocytes from adult mice, plus p-values for student-t test comparing genotypes.

	C57BL/6, 6-7 weeks			C57BL/6, 13-15 weeks			129/S6, 8-10 weeks		
	+/+	-/-	t-test	+/+	-/-	t-test	+/+	-/-	t-test
	n = 12 (2 mice)	n = 15 (2 mice)	p	n = 9 (2 mice)	n = 11 (3 mice)	p	n = 23 (3 mice)	n = 18 (3 mice)	p
APD$_{50}$ (ms)	11.0 ± 0.62	14.1 ± 1.21	0.064	13.1 ± 1.11	10.5 ± 1.12	0.122	8.14 ± 0.38	8.23 ± 0.46	0.885
APD$_{90}$ (ms)	36.5 ± 3.39	44.2 ± 3.82	0.152	45.7 ± 4.65	31.6 ± 4.14	0.035	19.2 ± 1.26	21.0 ± 1.69	0.380
Resting V$_m$ (mV)	-61.7 ± 1.01	-62.4 ± 0.57	0.485	-59.7 ± 1.46	-61.6 ± 0.68	0.231	-63.0 ± 0.64	-60.9 ± 0.44	0.013
Peak V$_m$ (mV)	49.7 ± 1.92	56.4 ± 1.79	0.016	48.1 ± 3.69	49.4 ± 3.04	0.788	47.9 ± 1.37	47.7 ± 2.07	0.926

No change in I_{to}, I_{sus}, or I_{K1}

We performed preliminary voltage-clamp experiments on ventricular myocytes isolated from adult C57BL/6 $Kcne4^{+/+}$ and $Kcne4^{-/-}$ mice. Figure 33 illustrates our findings for I_{to}, I_{sus}, and I_{K1}. No significant differences in current density were observed at any test potential for any of the potassium currents.

Discussion

An important basic observation from these studies is that $Kcne4$-null mice can live a normal lifespan with no major gross deficits. However, the collection of findings from focused phenotyping studies point to possible physiologic functions for $Kcne4$ in the mouse and help us assess our hypothesis that $Kcne4$ may be an endogenous negative regulator of repolarizing currents in the cardiac action potential.

The broad set of data we acquired from Lexicon is useful as a preliminary screen of a number of physiological systems, but these data must be interpreted in the context of a major limitation: that the studies were performed on F2 mice on a hybrid background. Given that significant physiological differences exist among the C57BL/6 and 129S6/SvEv strains, variability in genetic background among mice in the F2 generation makes it difficult to attribute any differences observed among groups of mice specifically to their $Kcne4$ genotype. With this limitation in mind, specific findings that are worth follow-up studies in congenic strains include decreased body temperature and resting heart rate, elevated blood phosphorous and calcium levels, and reduced blood glucose levels in $Kcne4^{-/-}$ mice. Collectively, these findings point toward potential metabolic disorders, which could involve impaired thyroid, parathyroid, or kidney function.
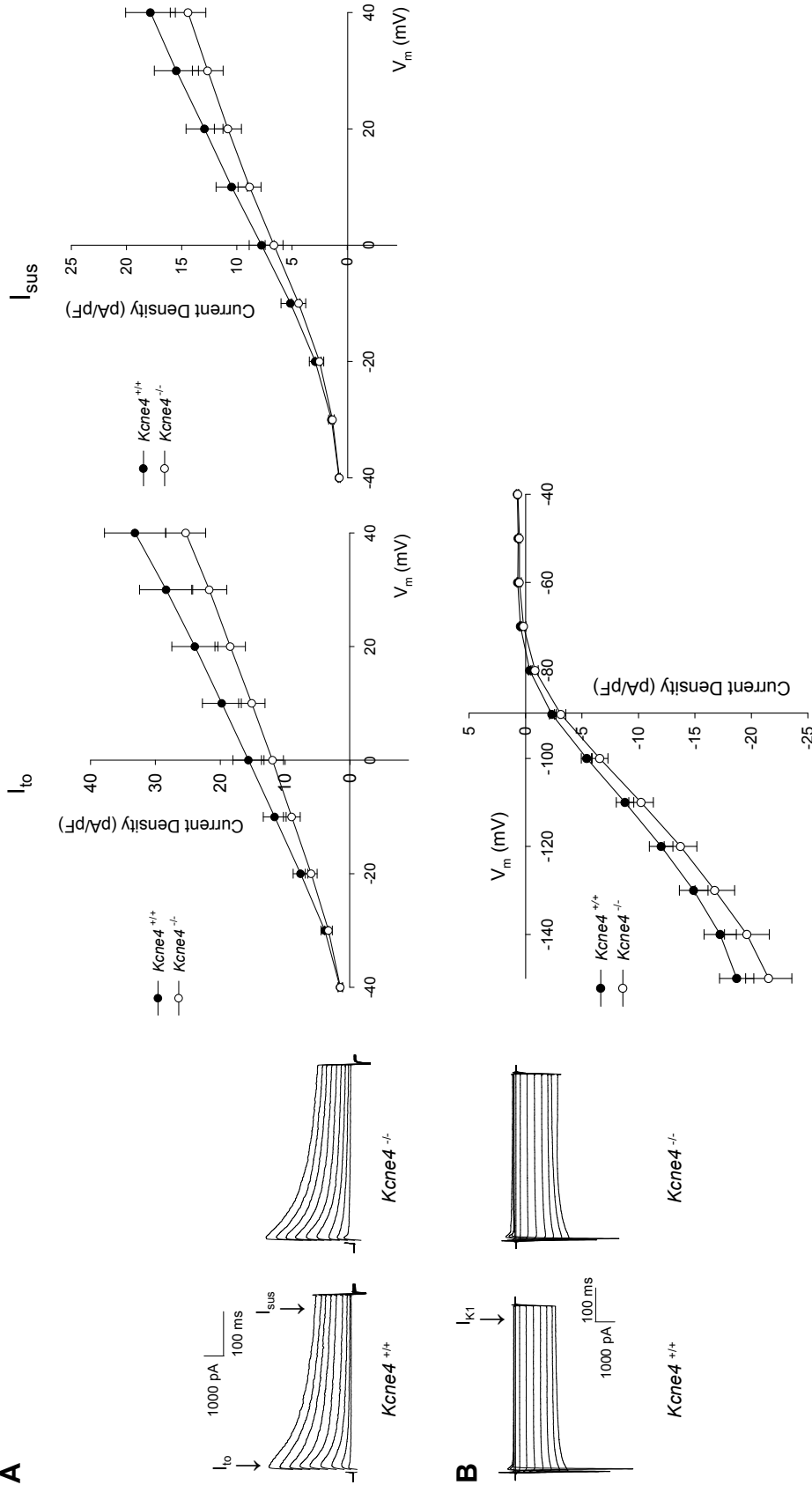
Figure 33. Whole-cell currents recorded from ventricular myocytes from adult C57BL/6 *Kcne4*+/+ and *Kcne4*-/- mice. A, Representative traces and average current density versus voltage plots for I_{to} and I_{sus}, recorded by step depolarizations from -40 mV to +40 mV at 10 mV intervals from a holding potential of -80 mV. I_{to}, peak current; I_{sus}, current recorded 400 ms after depolarization. No significant difference among genotypes at any test potential for either current. B, Representative traces and average current density versus voltage plot for I_{K1}, recorded by step depolarizations from -150 mV to -40 mV at 10 mV intervals from a holding potential of -80 mV. I_{K1} amplitude recorded 500 ms after depolarization. No significant difference among genotypes at any test potential. *Kcne4*+/+, n = 17 cells from 3 animals aged 7-16 weeks. *Kcne4*-/-, n = 10 cells from 3 animals aged 7-16 weeks.

In considering specifically the effect of *Kcne4* knockout on cardiac electrophysiology, the preliminary studies reported here provide some evidence to support our hypothesis that *Kcne4* is an endogenous negative regulator of repolarizing currents in the mouse cardiac action potential. The observation of a shortened QTc (rate-corrected QT) interval by ECG in *Kcne4*^{-/-} mice of both strains under isoflurane anesthesia (Figure 28) is consistent with that hypothesis: shortened repolarization time could be attributable to the absence of an inhibitor of repolarizing currents.

The finding of a shortened QTc interval in *Kcne4*^{-/-} mice by ECG is further supported by the observation of a shortened APD_{90} in isolated ventricular myocytes from C57BL/6 *Kcne4*^{-/-} mice at age 13-15 weeks (Figure 32). It is difficult to explain why shortening of the action potential was not also observed in 129S6/SvEv *Kcne4*^{-/-} mice (given the observation of a shortened QTc interval in these mice), though a number of experimental limitations may play a role. The data in Figure 32 reflect recordings made from cells that were isolated from just two or three mice per group. A small sample size may magnify any effects attributable to variability in cell quality and/or cell origin (eg. epicardium versus endocardium), which cannot be ruled out given the challenging nature of the myocyte isolation procedure.

These experimental limitations (small n, variable cell populations, imperfect recording techniques) may also explain why we did not observe any differences in K^+ currents recorded in ventricular myocytes from adult C57BL/6 *Kcne4*^{+/+} versus *Kcne4*^{-/-} mice (Figure 33), despite having observed a shortened action potential in *Kcne4*^{-/-} mice. Alternatively, it is possible that *Kcne4* knockout has no effect on ventricular K^+ currents,

and the findings of shortened repolarization time by action potential and ECG recordings were merely artifacts. Further studies are needed to resolve these inconsistencies and secure a complete set of reliable data.

There were a number of findings from our cardiac phenotyping studies that we did not anticipate. One example is the ECG finding of a shortened RR interval in *Kcne4*$^{-/-}$ mice in the 129S6/SvEv strain, with concurrent shortening of the PR and QRS intervals. These findings may indicate that pacemaker cells are firing at a higher frequency in *Kcne4*$^{-/-}$ mice, or that conduction from the sinus node through the AV node is occurring at a faster rate. It should be noted that calculating the rate-corrected QTc interval allows for assessing the *relative* length of the QT interval compared to the overall RR length. Whereas the finding of shortened PR and QRS intervals can be attributed to shortening of the entire cardiac electrical cycle, the finding of a shortened QTc implies that other factors are at play to specifically shorten ventricular repolarization.

The finding of a shortened RR interval in 129S6/SvEv *Kcne4*$^{-/-}$ mice is inconsistent with the report from Lexicon that *Kcne4*$^{-/-}$ mice have a lower resting heart rate, and also with our own findings from echocardiography studies (Figures 29, 30, 31) that there are no differences in resting heart rate among *Kcne4* genotypes in either strain. One interpretation that can reconcile these three conflicting findings is as follows: the results from the echocardiograms may be considered the 'true' or most meaningful data reflecting resting heart rate, since these experiments were performed in conscious mice from congenic backgrounds, whereas the Lexicon studies used mice from hybrid backgrounds, and our ECG finding of increased heart rate in *Kcne4*$^{-/-}$ mice may reflect a

117

difference in response to isoflurane anesthesia rather than resting heart rate. Alternatively, the dramatic inconsistency among these three studies of heart rate may reflect major limitations inherent in one or all of our experimental approaches.

We also observed unexpectedly that *Kcne4* knockout mice exhibit impaired myocardial contractility by 8 weeks of age. Cardiac chamber dimensions of conscious mice measured via echocardiography suggest that C57BL/6 *Kcne4*$^{+/-}$ and *Kcne4*$^{-/-}$ mice have increased LV internal diameter during diastole and systole (LVIDD, LVIDS, respectively) and decreased LV fractional shortening (FS) and ejection fraction (EF) compared to wild-type (*Kcne4*$^{+/+}$) littermates (Figures 29, 30, 31). While we did not anticipate this finding, we hypothesize that impaired myocardial contractility could be an additional functional consequence of enhanced repolarizing currents (such as I$_{to}$) in *Kcne4*$^{-/-}$ mice caused by dampened intracellular calcium transients and impaired excitation-contraction coupling, consistent with the relationship between I$_{to}$ and Ca^{2+} signaling in rodents described by others[156,173-176]. Further discussion of this hypothesis and a description of future studies that could be performed to test it directly can be found in Chapter V.

Overall, we cannot draw many final conclusions but are presented with a number of interesting leads from the work reported here following initial characterization of the *Kcne4* knockout mouse. Important future directions not already mentioned include studying the electrophysiology of neonatal cardiac myocytes, which, compared to adult cells, express a different cohort of K$^+$ channels and rely on a unique set of currents for repolarization (including I$_{Ks}$). It is possible that *Kcne4* is an important modulator of

118

neonatal K$^+$ currents and that electrophysiological findings in *Kcne4$^{-/-}$* mice may be more pronounced in this setting. Other important considerations when interpreting any phenotyping data from the *Kcne4$^{-/-}$* mouse include the possibility that the expression of other *Kcne* genes may change in compensation for the lack of *Kcne4*, as well as the important limitations described previously related to the imperfect parallels between human and mouse cardiac electrophysiology.

CHAPTER V

SUMMARY AND FUTURE DIRECTIONS

Summary

KCNE1-KCNE5 comprise a family of K_V channel modulating proteins that evoke diverse functional effects, are expressed by a broad range of human tissues, and in some cases are known to contribute to cellular functions that are required for normal physiology. Though KCNE4 demonstrates a remarkable ability to extinguish distinct K^+ currents in heterologous expression systems, we lack a clear understanding of both its mechanism for doing so and its physiologic significance. This project sought evidence that could improve our understanding of the physiological functions of KCNE4, through identification of its protein interacting partners and an assessment of the consequences of *Kcne4* knockout in mouse cardiac physiology.

A membrane-based yeast two-hybrid (MbYTH) screen for protein interacting partners of KCNE4 using a cDNA library from adult human brain yielded 98 clones that were positive for an interaction with KCNE4 based on both a primary growth assay and a secondary lacZ expression assay. Among those 98 clones we pursued follow-up analysis for 20, and ultimately identified their parent genes. These putative KCNE4 interacting partners include five membrane-associated proteins, eleven cytoplasmic proteins, three nuclear proteins, and one protein of unknown localization (Table 4). The set of interacting proteins did not include any K_V channels as we had hoped, in order to identify

novel channel targets of modulation by KCNE4. However, identification of non-K_V channel protein interacting partners did provide useful leads toward understanding other aspects of the function of KCNE4 – for example, its trafficking, its regulation, and potential cellular functions beyond direct modulation of channel activity.

The MbYTH 'hit' with the most obvious potential for intersection with KCNE4 was calmodulin (CaM), which is a known modulator of voltage-gated ion channels including KCNQ1. Interactions between accessory subunits (e.g., KCNE) and other regulatory proteins associated with macromolecular channel complexes such as I_{Ks} are emerging as another layer of complexity in regulating channel function. We demonstrated a Ca^{2+}-dependent biochemical interaction between KCNE4 and CaM (Figure 21) and that KCNQ1 functional modulation by KCNE4 is impaired both upon mutation of a candidate CaM-interaction site (L[69-72]A) in the juxtamembrane region of KCNE4 (Figure 24) and by acutely chelating $[Ca^{2+}]_i$ to displace CaM from KCNE4 (Figure 26). These findings suggest a connection between the mechanism of KCNQ1 inhibition by KCNE4 and the activating effect of CaM on the channel. Whereas we had previously assumed that the inhibition of KCNQ1 by KCNE4 is caused by a direct effect of KCNE4 on the channel, the data in this study introduce the new possibility that KCNE4 inhibits KCNQ1 by disrupting CaM-mediated activation.

Analysis of a $Kcne4^{-/-}$ mouse constituted our other approach to uncovering the physiologic significance of KCNE4. We hypothesized that Kcne4 may be an endogenous negative regulator of repolarizing currents in the cardiac action potential, and that $Kcne4$-

null mice might display a shortened QT interval, with possible implications for arrhythmia susceptibility or excitation-contraction coupling. Although the *Kcne4*-null mice did not display an increased susceptibility to arrhythmia versus their wild-type littermates, ECG analysis revealed that *Kcne4*-null mice of both the C5BL/6 and 129S6/SvEv strains have a shortened QTc interval compared with wild-type mice under isoflurane anesthesia (Figure 28). Our hypothesis was also supported by the observation of a shortened APD_{90} in isolated ventricular myocytes from C57BL/6 *Kcne4*-null mice at age 13-15 weeks (Figure 32), though this finding was not consistent across both mouse strains.

Unexpectedly, we also observed that C57BL/6 *Kcne4*-null mice have impaired myocardial contractility by eight weeks of age (Figure 29). Cardiac chamber dimensions of conscious mice measured by echocardiography suggest that C57BL/6 $Kcne4^{+/-}$ and $Kcne4^{-/-}$ mice have increased left ventricular (LV) internal diameter during diastole and systole and decreased LV fractional shortening (FS) and ejection fraction (EF) compared to wild-type littermates.

Unanswered questions that remain or have been generated by this work include: What can we learn about KCNE4 in human cardiac electrophysiology from the *Kcne4* knockout mouse? What is the molecular etiology of left ventricular dilation and reduced fractional shortening in *Kcne4* knockout mice? What are the non-cardiac phenotypes of the *Kcne4* knockout mouse? How do KCNE4, KCNQ1, and CaM interact to yield the functional findings in Chapter III? What is the physiologic significance of the Ca^{2+}-

sensitivity of KCNQ1 inhibition by KCNE4 and the KCNE4-CaM interaction? What is the functional significance of the other 19 KCNE4 MbYTH hits?

Future Directions

Biochemical and Functional Validation of KCNE4 interaction with MbYTH 'hits'

The degree to which an apparent connection between KCNE4 and the other 19 MbYTH hits exists varies considerably among the putative interaction partners. The appearance of several DNA-binding proteins among the 'hits' is particularly interesting in light of a previous study which described the ability of a C-terminal fragment of the voltage-gated calcium channel Ca$_V$1.2 to translocate to the nucleus and regulate expression of a number of genes through its interaction with other nuclear proteins[130]. A similar function is conceivable for KCNE4, especially because it has a long C terminus (unique among the KCNE proteins), the importance of which is not known. Because demonstration of an interaction with transcription factors has the potential to revolutionize our understanding of the function of KCNE4, studies are proposed here to pursue biochemical and functional validation of the interactions between KCNE4 and DNA-binding proteins SIRT2, GTF2H4, and CEBPZ.

We can begin by validating the biochemical interaction between KCNE4 and each of the putative nuclear interaction partners by coimmunoprecipitation studies. The specificity of each interaction can be checked against the other KCNE proteins, which will also help elucidate which structural domains of KCNE4 are necessary for interaction with each nuclear protein. Subsequently, we can generate KCNE4 truncation constructs

by incremental removal of N- and C-terminal sequences and assess their interaction with the nuclear protein to define a minimal KCNE4 peptide sequence that is required for its biochemical interaction with the nuclear protein.

If interaction between KCNE4 and any of the nuclear proteins is confirmed, then we can assess whether a KCNE4 cleavage product (including the minimal KCNE4 sequence identified above) is detectable in native cells. Several different approaches can be used to this end: we can probe nuclear extracts from native cells using an antibody against the appropriate portion of KCNE4 and look for full-length KCNE4 plus the cleavage product by Western blot; alternatively, we can study localization of KCNE4 in intact cells by immunofluorescence to determine if KCNE4 localizes to the nucleus.

If nuclear localization of a KCNE4 cleavage product is observed, then we can seek to identify genes it might regulate. As an initial approach, we can use microarray analysis to compare gene expression in cells transfected with full-length KCNE4 versus a truncation mutant that demonstrates deficient interaction with the DNA binding protein, and also versus cells transfected with empty vector. Any gene that is found to be significantly up- or down-regulated in the presence of KCNE4 can be further validated as a target of transcriptional regulation by KCNE4 using quantitative RT-PCR analysis or a reporter assay using the firefly-luciferase gene fused to the promoter/enhancer region of the target gene to assess relative expression in the presence versus absence of KCNE4.

Anticipated Results: If we can demonstrate a biochemical interaction between KCNE4 and any of the DNA-binding proteins that were identified in the MbYTH screen as putative interacting partners, then we will have an intriguing lead toward a new role for KCNE4 as a potential transcriptional regulator. We expect that an interaction between

KCNE4 and a nuclear protein could only take place if a cleavage event liberated a portion of KCNE4 to translocate from the membrane to the nucleus. Identification of up- or down-regulated genes following KCNE4 expression may provide direct evidence linking KCNE4 to new cellular functions, which may or may not be related to any of the phenotypes observed in the *Kcne4$^{-/-}$* mouse.

Experimental Limitations: Proteolytic cleavage of the KCNE4 C-terminus to allow translocation to the nucleus and transcriptional regulation may only occur under certain cellular conditions. It may thus be difficult to determine and apply the conditions (eg. stimulation by a specific agonist, or free $[Ca^{2+}]$ within a certain range) needed to detect an interaction between KCNE4 and the candidate nuclear proteins or to elicit changes in the expression profile of a target gene, and negative results will be difficult to interpret.

Further characterization of KCNE4-CaM interaction

1. What molecular mechanism links KCNQ1, CaM and KCNE4?

Our demonstration of a Ca^{2+}-dependent biochemical interaction between KCNE4 and CaM, and that KCNQ1 functional modulation by KCNE4 is impaired both upon mutation of a candidate CaM-interaction site in the juxtamembrane region of KCNE4 and by acutely chelating $[Ca^{2+}]_i$ to displace CaM from KCNE4, suggests a connection between the mechanism of KCNQ1 inhibition by KCNE4 and the activating effect of CaM on the channel. Clearly delineating any link between these findings as it pertains to the mechanism of KCNE4 inhibition of KCNQ1 is the most important next step for this

work. An enticing hypothesis that could tie these observations together is that KCNE4 inhibits KCNQ1 by disrupting CaM-mediated KCNQ1 activation.

Biochemical demonstration of disruption of the CaM-KCNQ1 interaction in the presence of KCNE4 would constitute strong evidence in support of our hypothesis, but this is difficult to achieve experimentally and there are likely to be multiple confounding interpretations of such experiments. For example, biochemical assays such as CaM-agarose pull-down or co-immunoprecipitation require complete displacement of CaM from KCNQ1 in the presence of KCNE4 to yield an observable effect, whereas KCNE4 may cause a conformational change that is sufficient to prevent transduction of the activating signal CaM provides to KCNQ1 without fully disrupting CaM and KCNQ1 interactions. Further, we do not know the KCNQ1-KCNE4-CaM stoichiometry in functional channel complexes. The presence of KCNE4 may displace some but not all CaM molecules from a given KCNQ1 channel complex -- enough to affect channel function but perhaps leaving enough KCNQ1-CaM complexes intact to produce no observable change in a biochemical assay. Finally, a given cell may express mixed populations of KCNQ1 channel complexes – some that include KCNE4 as well as some that do not, leaving the possibility that even when KCNE4 is coexpressed some KCNQ1-CaM complexes will be intact, yielding a positive interaction by biochemical assay.

Instead, a structural approach will probably be needed to address the question of whether the KCNQ1-CaM interaction is disrupted in the presence of KCNE4, and given the limitations described previously for solving structures composed of KCNQ1 and KCNE subunits, acquiring those data may depend on application of innovative methods for structural analysis. In the meantime, we can address the question indirectly by making

use of the KCNE1-KCNE4 chimeras we generated for a previous investigation into which domains of KCNE4 are required for its inhibitory effect on KCNQ1[48], and exploiting our observation that KCNE1 does not interact biochemically with CaM. By studying functional and biochemical properties of each of the chimeric proteins, we can assess whether the ability to inhibit KCNQ1 segregates with an ability to interact biochemically with CaM.

Anticipated Findings: If our hypothesis is correct and the mechanism for KCNQ1 inhibition by KCNE4 involves KCNE4 disruption of the CaM-mediated KCNQ1 activation, then we expect to find that KCNQ1 inhibitory properties are conferred only to those KCNE1-KCNE4 chimeras that can interact biochemically with CaM. Ultimately, we can learn from structural studies how CaM mediates its activating effect on KCNQ1, and seek evidence that supports our hypothesis that in the presence of KCNE4 that effect is disrupted.

2. What is the physiologic significance of the KCNE4-CaM interaction?

The physiological implications of the interaction between KCNE4 and CaM may be significant, but are difficult to assign because of the primary lack of understanding of the physiological contributions of KCNE4. In heart, where KCNE4 could modulate repolarizing currents such as I_{Ks}, and where local free Ca^{2+} concentrations cycle dramatically, the Ca^{2+}-CaM sensitivity described for KCNE4 may enable Ca^{2+}-dependent regulation of repolarization time. Because repolarization time is critical for action potential duration as well as Ca^{2+} release and contractility, CaM-KCNE4 interactions might constitute part of a feedback loop for regulating intracellular Ca^{2+}.

To investigate the physiologic significance of the KCNE4-CaM interaction, we can study guinea pig or rabbit myocytes expressing the CaM-insensitive KCNE4 mutant L[69-72]A. After applying overexpression techniques described below (biolistics or viral delivery of wild-type versus mutant KCNE4 cDNA), we can assess the effects of disrupting the interaction between KCNE4 and CaM on myocyte K^+ currents, action potential duration and morphology, Ca^{2+} transients, and cell shortening.

Anticipated Findings: If KCNE4 is an endogenous inhibitor of I_{Ks} in guinea pig or rabbit cardiac myocytes, then we expect that the CaM-insensitive KCNE4 mutant will exhibit impaired I_{Ks} inhibition, and we will record enhanced I_{Ks} and shortened action potentials in myocytes expressing L[69-72]A. Concurrently, we may observe altered Ca^{2+} transients and myocyte contractility due to effects of repolarization time on excitation-contraction coupling.

Experimental Limitations: Unless the L[69-72]A mutant exerts a dominant-negative effect, we may have to knock down endogenous *Kcne4* in conjunction with expression of exogenous L[69-72]A in order to uncover its effects on native K^+ currents. Lentiviral delivery of anti-Kcne4 shRNA sequences can be used to achieve this goal, as described below. Additionally, we may have to apply an adrenergic agonist or other factor that can upregulate CaM signaling in order to unmask any effects of the CaM-insensitive KCNE4 mutant on native cardiac myocyte electrophysiology.

Further characterization of the Kcne4-knockout mouse

1. What are the implications of shortened repolarization time in *Kcne4*-null mice for human cardiac electrophysiology?

Given the differences between the human and mouse ventricular cardiac action potentials (most notably in repolarizing K^+ currents, see Figure 27), it is important not to over-interpret findings in the *Kcne4* knockout mouse when considering how KCNE4 might contribute to human cardiac physiology. A valuable next step in testing how our mouse findings translate to more human-like cardiac electrophysiology is to assess the effects of KCNE4 silencing and overexpression in ventricular myocytes with a human-like electrophysiological profile, for example those from guinea pig or rabbit.

Guinea pig and rabbit ventricular myocytes are known to express similar repolarizing currents to those in humans[177,178], and they can be cultured and genetically manipulated following isolation. We are currently optimizing protocols for several methods of gene silencing and overexpression in rabbit and guinea pig myocytes. Overexpression will be achieved either by biolistics or viral delivery of human KCNE4 cDNA (plus a fluorescent marker to enable selection of cells expressing the exogenous subunit). Gene silencing will be achieved using lentiviral delivery of shRNAs targeting endogenous *Kcne4*; infected cells will also express a fluorescent marker and an antibiotic resistance gene for selection, and we will confirm *Kcne4* knockdown with analysis of Kcne4 protein expression by Western blot, and/or of *Kcne4* transcripts by quantitative real-time RT-PCR.

Following *KCNE4* overexpression or silencing of endogenous *Kcne4*, we will perform voltage-clamp and current-clamp experiments in order to record K^+ currents and

action potentials, respectively, using methods described in Chapter IV for experiments on isolated mouse myocytes. By comparing K^+ currents and action potential duration and morphology in cells overexpressing *KCNE4* versus empty vector, or in cells following *Kcne4* silencing with targeted shRNA sequences versus scrambled controls, we can directly assess the contributions of KCNE4 to the electrophysiology of ventricular myocytes in a cellular model with an electrophysiologic profile that closely resembles that of human cardiac myocytes.

Anticipated Results: If KCNE4 is an endogenous inhibitor of repolarizing currents in these species (consistent with our hypothesis and with our findings in mice), we anticipate observing reduced K^+ currents and increased action potential duration in *KCNE4* overexpression studies, and enhanced K^+ currents and reduced action potential duration in *Kcne4* silencing studies.

Experimental Limitations: As with any cells that have been cultured outside of their native environment, cardiac myocytes will be imperfect physiologic models by the time we record K^+ currents and action potentials from them. Nonetheless, we expect these studies will provide valuable insight into the contributions of KCNE4 to cardiac electrophysiology.

2. What is the etiology of impaired cardiac contractility in *Kcne4*-null mice?

Our unexpected observation of left ventricular dilation and reduced fractional shortening in *Kcne4*$^{-/-}$ mice by 8 weeks of age warrants investigation into the connection between *Kcne4* and myocardial contractility. Given our preliminary observations suggesting that *Kcne4* is an endogenous negative regulator of cardiac repolarization, we

hypothesize that impaired myocardial contractility is a functional consequence of enhanced I_{to} in *Kcne4*^{-/-} mice caused by dampened intracellular calcium transients and impaired excitation-contraction coupling, consistent with the relationship between I_{to} and Ca^{2+} signaling in rodents described by others[156,173-176] and reviewed by Sah et al[179].

I_{to} is responsible for early phase repolarization during the cardiac action potential, and is closely linked to downstream excitation-contraction coupling. The transient rise in intracellular free calcium $[Ca^{2+}]_i$ that triggers cardiac myocyte contraction is generated primarily by Ca^{2+} influx from the sarcoplasmic reticulum (SR) through ryanodine-sensitive Ca^{2+} release channels (RyR2). In turn, RyR2 channels are gated by local increases in $[Ca^{2+}]_i$ that occur with opening of sarcolemmal L-type Ca^{2+} channels (LTCC) in response to membrane depolarization[179-182]. The tight regulation of LTCC by membrane voltage makes the amplitude, frequency, and time course of calcium transients (and by extension, myocyte contractility) susceptible to modulation by the action potential profile[156,173,174,183]. The early repolarization phase of the cardiac action potential is particularly influential in regulating the open probability of LTCC and the efficiency of downstream excitation-contraction coupling (ECC)[156,173,174,184]. Thus, factors that modulate the biophysical properties of I_{to} can regulate calcium transients and myocyte contractility[179].

Factors that decrease I_{to} and prolong early repolarization *in rodents* ultimately increase Ca^{2+} transients and potentiate contractile strength, as has been demonstrated in several settings: rat myocytes following administration of the I_{to} blocker 4-aminopyridine (4-AP)[173], rat myocytes with decreased I_{to} following myocardial infarction[174], and myocytes from transgenic mice overexpressing dominant-negative I_{to} subunits[176]. This

effect is opposite that which is observed in larger mammals (including rabbits, dogs, and humans), in which I_{to} inhibition decreases Ca^{2+} transients and impairs ECC and myocyte contractility[184]. This dichotomy is highlighted by work from the Backx laboratory[179].

There is considerable evidence suggesting that I_{to} is generated by channel complexes consisting of $K_V4.2$ and/or $K_V4.3$ pore-forming subunits, including extensive functional data from heterologously expressed candidate K_V subunits[185-187], observations of K_V channel expression in native cardiac tissue[188,189], results from mRNA knockdown and adenoviral gene transfer studies in native cardiac myocytes[183,190-192], plus observations in transgenic animal models[163,166,193,194]. However, I_{to} exhibits high variability in its biophysical properties among species and within cardiac regions of a given species[91,92,194-197].

Understanding of the regulation and molecular determinants of I_{to} is incomplete. Recent studies have examined whether the KCNE proteins may contribute to modulation of I_{to}, and electrophysiological data from CHO cells heterologously co-expressing $K_V4.3$ plus KChIP (a probable accessory subunit in the endogenous I_{to} channel complex) in addition to individual KCNE proteins indicates that each KCNE subunit is capable of modulating the biophysical properties of this reconstituted I_{to}-like current[98]. KCNE4 has been observed to modulate $K_V4.2$-ChIP2 channels (specifically by slowing activation and shifting voltage-dependence of activation toward more positive potentials). KCNE4 was also found to co-localize with $K_V4.2$ to transverse tubules of rat cardiac myocytes, and it was co-immunoprecipitated with $K_V4.2$ and KChIP2 following heterologous expression in tsA201 cells[97]. Our preliminary mouse studies did not indicate that I_{to} is enhanced in cardiac myocytes from *Kcne4*-null mice, but a number of experimental limitations

(described in Chapter IV) could account for the negative results and further study is necessary.

If we demonstrate that I_{to} is enhanced in *Kcne4*-null mice, we will pursue our hypothesis that *Kcne4*$^{+/-}$ and *Kcne4*$^{-/-}$ mice exhibit LV dilation and reduced FS and EF because of a functional effect: loss of I_{to} suppression by KCNE4, accentuated early phase repolarization and blunted intracellular calcium transients. As a consequence, we predict that cardiac myocytes from *Kcne4*$^{-/-}$ mice will display blunted calcium transients and reduced cell shortening as compared to wild-type animals in response to electrical stimulation. Further, we predict that blocking I_{to} pharmacologically will restore normal contractility and correct aberrations in calcium signaling. Our *Kcne4* knockout mouse line enables us to directly test this hypothesis, using the following set of experiments.

A. Further phenotypic characterization

Because impaired contractility can arise from structural defects of the heart[198] including myocardial fibrosis, we first plan to perform post-mortem analysis of cardiac chamber morphology and histology to investigate this possibility. We can analyze major morphological features (including myocardium, valves, coronary arteries, and the great vessels) by dissection and gross examination. Separately, we can study tissue sections stained with hematoxylin and eosin for histological analysis by standard light microscopy and Sirius red for quantification of fibrosis. We will quantify right and left ventricle chamber size, and evaluate the extent of ventricular fibrosis.

Additionally, to investigate whether there is age-dependence of impaired contractility, we can perform echocardiograms on conscious *Kcne4*$^{+/+}$, *Kcne4*$^{+/-}$, and

Kcne4^{-/-} mice at age 30 weeks and compare these findings stratified by sex and genotype with our data obtained on 8 week old mice. Further, we can assess whether *Kcne4* knockout mice exhibit physiological and pathological signs associated with heart failure, by measurement of systemic blood pressure at ages 8 and 30 weeks, and by gross and histologic analysis of pulmonary morphology to look for signs of edema.

Anticipated Results: We predict that gross and histological analysis of cardiac morphology will demonstrate that the hearts of *Kcne4^{+/-}* and *Kcne4^{-/-}* mice are free of any structural defects (such as valvular disease, coronary artery disease, aortic stenosis, or fibrosis) that could account for the observed impaired myocardiac contractility. This prediction is consistent with our preliminary inspection of the animals over several generations that suggest that general health does not deteriorate with advancing age. Further, we predict that 30-week-old *Kcne4^{+/-}* and *Kcne4^{-/-}* mice will display a similar degree of LV dilation and FS impairment as 8-week-old mice. It is also conceivable that as the mice age their hearts engage compensatory mechanisms to restore adequate contractile strength and cardiac output. If this is the case, then we can elucidate those mechanisms through electrophysiological recordings and measurements of calcium transients in cardiac myocytes using approaches outlined below. Similarly, we do not anticipate that *Kcne4^{+/-}* and *Kcne4^{-/-}* mice will exhibit overt clinical signs of heart failure but we need to systematically examine the animals for the potential pathophysiological consequences of impaired myocardial contractility to document the full spectrum of the phenotype.

B. Assessment of Ca^{2+} signaling and myocyte shortening

We hypothesize that $Kcne4^{-/-}$ mice have impaired contractility due to diminished amplitude of intracellular calcium transients as a consequence of enhanced I_{to}. We can test this hypothesis by comparing calcium transients and cell shortening in ventricular cardiac myocytes from $Kcne4^{+/+}$ and $Kcne4^{-/-}$ mice. We will perform these studies using dual-beam excitation fluorescence photometry and the IonOptix system for measuring calcium transients and cell shortening in cardiac myocytes.

After isolating individual ventricular myocytes from excised hearts of 8-week-old $Kcne4^{+/+}$ and $Kcne4^{-/-}$ mice we will load the cells with the fluorescent calcium ratiometric indicator fura-2 acetoxymethyl ester (fura-2) and begin field stimulation with 1Hz pacing. After 5 minutes of steady-state pacing, we will obtain 10-second records of calcium transients and myocyte shortening, using excitation wavelengths of 360 and 380nm to monitor the fluorescence signals of Ca^{2+}-bound and Ca^{2+}-free fura-2. Subsequently, we will expose the myocytes to 10 mM caffeine and record caffeine-induced Ca^{2+} transients to estimate total SR content. After subtracting background and cellular autofluorescence, $[Ca^{2+}]$ will be deduced from the fluorescence ratio (F_{ratio}) at 360nm and 280nm excitation[199].

Ca^{2+} transients and ventricular myocyte shortening will be analyzed using specialized data analysis software, allowing us to compare the following parameters between $Kcne4^{-/-}$ and $Kcne4^{+/+}$ cells: diastolic calcium F_{ratio}, peak F_{ratio} of Ca^{2+} transient, time-to-peak, time to 50% peak, time constant of Ca^{2+} transient decay, time to 90% relaxation, SR Ca^{2+} content, fractional SR Ca^{2+} release, diastolic myocyte segment length, % fractional shortening, time to peak cell shortening, time to 50% peak cell

shortening, time to 90% peak cell shortening. If we observe abnormal Ca^{2+} transients and/or impaired cell shortening in $Kcne4^{-/-}$ cells, then we can test whether pharmacological I_{to} blocking agents such as 4-AP and *Heteropoda* toxin-3 (HpTx-3)[194,200,201] can normalize these cellular phenomena.

Anticipated Results: We predict that ventricular myocytes from $Kcne4^{-/-}$ mice will exhibit a lower peak F_{ratio} corresponding to field-stimulated Ca^{2+} transients, indicating smaller rises in intracellular calcium concentration in these cells as compared with myocytes from $Kcne4^{+/+}$ mice. Further, we predict that cell shortening will be attenuated in $Kcne4^{-/-}$ myocytes. Time-to-peak F_{ratio} and cell shortening may also be reduced if accentuated early repolarization in $Kcne4^{-/-}$ cells promotes shorter open-times for SR and plasma membrane Ca^{2+} channels. We further anticipate that pharmacological I_{to} blockers will normalize these defects and this would provide evidence for a link between this repolarizing current and contractile force.

Experimental limitations: The proposed experiments are based on our observation that $Kcne4$-null mice have shortened action potential duration and our prediction that $Kcne4$ knockout is associated with increased I_{to} in ventricular myocytes. This association may occur because of a direct influence of KCNE4 on potassium channels responsible for I_{to} or alternatively because of an indirect effect, but our studies are not designed to differentiate between these two molecular mechanisms.

For experiments with I_{to} blockers, we are severely limited by the lack of highly specific agents. It may be useful to test whether wild-type mice treated with a pharmacological I_{to} *activator* exhibit impaired contractility. We are aware of one such compound (NS5806 from NeuroSearch), and could potentially use this agent to test

whether I_{to} augmentation is a plausible mechanism underlying impaired contractility in mice.

We recognize that impaired contractility in *Kcne4* knockout mice could have an extra-cardiac (neural, humoral, etc) etiology. To rule out this possibility we could engineer a mouse line with cardiac-specific *Kcne4* knockout with Cre/lox recombination technology and assess whether the contracile phenotype disappears despite normal Kcne4 expression in extra-cardiac tissues.

Finally, as addressed above, it is critical to assess any cardiac findings from the *Kcne4*-null mouse in a model that more closely resembles human cardiac electrophysiology. If I_{to} is a target of *Kcne4* modulation in mice and its modulation has implications for Ca^{2+} signaling and myocyte contractility, then it is difficult to predict what the implications are for human cardiac physiology, for a number of reasons. As previously noted, different K^+ currents account for repolarization in mouse versus human myocytes; additionally, the relationship between repolarization time and contractility is dichotomous across rodents and humans. It will thus be critical to study early repolarization, Ca^{2+} signaling, and cell shortening in guinea pig or rabbit myocytes upon *Kcne4* overexpression or silencing to be able to apply findings in mice toward better understanding human physiology.

3. What is the etiology of non-cardiac phenotypes of the *Kcne4*-knockout mouse?

For this project we chose to focus on characterizing cardiac phenotypes of the *Kcne4*-null mouse, but recognize that there may be important consequences to *Kcne4* knockout beyond cardiac physiology. The broad expression of KCNE4 (observed most

prominently in kidney, skeletal muscle, testis, prostate, spleen, ovary, and uterus) suggests that it may contribute to important physiologic processes in a number of tissues. Further, other members of the KCNE family have previously been implicated in non-cardiac physiology – notably, KCNE1 in K^+ flux in hair cells of the inner ear that contributes to hearing[61], KCNE2 in K^+ flux that drives thyroid hormone synthesis[110] and acid secretion by the stomach[13], and KCNE3 in skeletal muscle excitability[65].

The data set generated by Lexicon's multi-system survey of $Kcne4^{-/-}$ mouse physiology provides us with several interesting leads, but these data must be interpreted in the context of a major limitation: that the studies were performed on F2 mice on a hybrid background. Given that significant physiological differences exist among the C57BL/6 and 129S6/SvEv strains, variability in genetic background among mice in the F2 generation makes it difficult to attribute any differences observed among groups of mice specifically to their $Kcne4$ genotype. Before proceeding with any proposed follow-up studies, the original findings comparing $Kcne4^{-/-}$ mice to wild-type mice should be confirmed in congenic strains.

The most striking of Lexicon's findings included: decreased body temperature and resting heart rate, and elevated blood phosphate (PO_4^{2-}) and free Ca^{2+} levels in $Kcne4^{-/-}$ versus wild-type mice. Collectively, these findings point toward potential metabolic disorders, which could signal impaired thyroid, parathyroid, or kidney function. The following experiments are proposed to pursue whether the absence of $Kcne4$ affects any of these physiologic systems.

A. Decreased body temperature and bradycardia

The findings of decreased body temperature and bradycardia are suggestive of hypothyroidism. Roepke *et al.*[110] recently demonstrated that K^+ flux through a channel complex comprised of KCNQ1 and KCNE2 subunits is necessary for I^- uptake by thyrocytes and normal thyroid hormone synthesis, which leads us to hypothesize that KCNE4 may be an endogenous modulator of this current, possibly causing impaired thyroid hormone synthesis in *Kcne4*^{-/-} mice. Further phenotypic characterization of *Kcne4*^{-/-} mice at both the whole-animal and molecular levels will allow us to test this hypothesis.

Assessment of thyroid function in *Kcne4*^{-/-} mice should include analysis of the gross morphology of the thyroid and histology of thyroid follicular epithelia. Further, plasma levels of T3, T4, and TSH can be measured by ELISA and compared among *Kcne4*^{-/-} and *Kcne4*^{+/+} littermates, along with I^- uptake by positron emission tomography (PET) imaging to detect specific deficiencies. Depending on the findings of these experiments, rescue experiments can be performed (e.g. administration of T4 in *Kcne4*^{-/-} mice if T4 levels are low) to further assess whether thyroid deficits are responsible for low body temperature and bradycardia in *Kcne4*^{-/-} mice.

If impaired thyroid function is confirmed in *Kcne4*^{-/-} mice, further experiments will be needed to uncover the molecular link between *Kcne4* and thyroid hormone production. The TSH-sensitive K^+ current generated by KCNQ1-KCNE2 channel complexes in thyrocytes may be a target of KCNE4 modulation and is the most obvious candidate linking KCNE4 to thyroid hormone production. To study this possibility it will be important to assess whether KCNE4 co-localizes or forms complexes with KCNQ1 and

KCNE2 in thyrocytes. Further, we can assess KCNE4 modulation of this current under basal and TSH-stimulated conditions using the rat thyroid-derived cell line FRTL5 and KCNE4 overexpression and gene silencing approaches described above for guinea pig and rabbit cardiac myocytes.

Anticipated Results: If low body temperature and bradycardia in $Kcne4^{-/-}$ mice are attributable to primary hypothyroidism, we would expect these studies to show reduced T3 and/or T4 levels, elevated TSH levels, and enlarged thyroid glands and/or abnormal gland architecture in $Kcne4^{-/-}$ mice. Further, we would expect to be able to normalize body temperature and heart rate upon administration of synthetic thyroid hormone. If KCNE4 contributes to thyroid hormone synthesis by modulation of thyrocyte KCNQ1-KCNE2 channels, we would expect to find co-localization of these subunits in native thyrocytes and altered biophysical properties of the current upon KCNE4 overexpression or silencing in FLTR5 cells.

Experimental Limitations: These studies consider primary hypothyroidism as a potential etiology for reduced body temperature and bradycardia, but related possibilities not addressed include pituitary dysfunction causing secondary hypothyroidism, or systemic defects in responsiveness to thyroid hormone. Because the thyrocyte KCNQ1-KCNE2 channel complex provides an obvious potential link to primary hypothyroidism, this etiology should be assessed first.

B. Impaired Ca^{2+} and PO_4^{2-} homeostasis

Parathyroid hormone (PTH) and calcitonin are two important regulators of plasma Ca^{2+} and PO_4^{2-} levels, and thus they capture our attention when considering findings of

elevated Ca^{2+} and PO_4^{2-} in *Kcne4^{-/-}* mice. The parathyroid releases PTH upon sensing low free Ca^{2+} in the blood, and the effects of PTH include: stimulating osteoclasts to release Ca^{2+} and PO_4^{2-} from bone into the blood, stimulating vitamin D production by the kidney, which in turn stimulates intestinal epithelial cells to synthesize a Ca^{2+}-binding protein to increase Ca^{2+} absorption from the gut, and stimulating the kidney to reabsorb more Ca^{2+} and excrete more phosphate in the urine. Conversely, calcitonin (produced by parafollicular cells in the thyroid) acts to reduce free Ca^{2+} levels in the blood by inhibiting release of Ca^{2+} and phosphate by osteoclasts and inhibiting tubular reabsorption of Ca^{2+} and phosphate in the kidney.

Although none of these processes has been directly linked to K^+ channel activity, we can speculate which points along the pathways might be affected by KCNE4 function, potentially contributing to a phenotype of increased Ca^{2+} and PO_4^{2-} in *Kcne4^{-/-}* mice. They include: impaired calcium sensing by the calcium-sensing receptor (CaR), which acts upstream of PTH and calcitonin release in the parathyroid and thyroid parafollicular cells; hyperactive PTH production; hypersensitive or constitutively active PTH receptors in osteoclasts or kidney; augmented vitamin D production by the kidney; impaired calcitonin production; or impaired responsiveness to calcitonin in osteoclasts or kidney.

The molecular mechanisms that regulate many of the processes described above are poorly understood, especially with respect to any dependence on K^+ flux. Thus we must begin with a very broad investigation of the etiology of increased Ca^{2+} and PO_4^{2-} in *Kcne4^{-/-}* mice, for example by comparing basal PTH, calcitonin, and vitamin D levels in *Kcne4^{-/-}* versus *Kcne4^{+/+}* mice. Additionally, we can assess gross morphology and histological features of the parathyroid and parafollicular cells of the thyroid from *Kcne4^-*

$^{/-}$ mice for evidence of pathology. Expression of KCNE4 in these tissues plus osteoclasts should also be surveyed, as no studies have yet reported on KCNE4 expression by these cell types. Finally, bone density and calcification should be examined in $Kcne4^{-/-}$ mice for signs of excessive PTH stimulation of osteoclasts.

Anticipated Findings: The experiments described here should help identify if PTH, calcitonin, or Vitamin D are implicated in the findings of elevated Ca^{2+} and P in $Kcne4^{-/-}$ mice. If one function of KCNE4 is to contribute to regulation of any of these factors, we might expect to see differences in their levels among $Kcne4^{+/+}$ and $Kcne4^{-/-}$ mice. If such differences are observed, rescue experiments where applicable (i.e., administering a hormone found to be deficient in $Kcne4^{-/-}$ mice) might be useful in corroborating the link to elevated blood levels of free Ca^{2+} and PO_4^{2-}.

Experimental Limitations: We are limited to a very broad assessment of potential pathways that $Kcne4$ may contribute to in Ca^{2+} and PO_4^{2-} homeostasis, due to limited existing data describing molecular mechanisms that underlie these processes in normal physiology. Whereas these studies might identify gross abnormalities (such as impaired hormone production), more subtle defects will be more difficult to detect. For example, if Kcne4 modulates a K^+ current that normally attenuates the intestinal epithelial response to vitamin D, the $Kcne4$-null mouse might have an augmented response to vitamin D (ie. excessive absorption of Ca^{2+}) without showing abnormal levels of vitamin D or PTH. Further, these studies likely will not provide satisfying answers as to how $Kcne4$ contributes to Ca^{2+} and PO_4^{2-} homeostasis at the molecular level, but the findings they generate can be used to guide further investigation.

REFERENCES

1. Anderson, P. A. & Greenberg, R. M. Phylogeny of ion channels: clues to structure and function. *Comp Biochem. Physiol B Biochem. Mol. Biol.* **129**, 17-28 (2001).

2. Barhanin, J. *et al.* K_vLQT1 and IsK (minK) proteins associate to form the I_{Ks} cardiac potassium current. *Nature* **384**, 78-80 (1996).

3. Sanguinetti, M. C. *et al.* Coassembly of K_vLQT1 and minK (IsK) proteins to form cardiac I_{Ks} potassium channel. *Nature* **384**, 80-83 (1996).

4. Kottgen, M. *et al.* Carbachol activates a K+ channel of very small conductance in the basolateral membrane of rat pancreatic acinar cells. *Pflugers Arch.* **438**, 597-603 (1999).

5. Kim, S. J. & Greger, R. Voltage-dependent, slowly activating K+ current (I(Ks)) and its augmentation by carbachol in rat pancreatic acini. *Pflugers Arch.* **438**, 604-611 (1999).

6. Arrighi, I. *et al.* Altered potassium balance and aldosterone secretion in a mouse model of human congenital long QT syndrome. *Proc. Natl. Acad. Sci. U. S. A* **98**, 8792-8797 (2001).

7. Vallon, V. *et al.* KCNQ1-dependent transport in renal and gastrointestinal epithelia. *Proc. Natl. Acad. Sci. U. S. A* **.**, (2005).

8. Jervell, A. & Lange-Nielsen, F. Congenital deaf-mutism, functional heart disease with prolongation of the Q-T interval and sudden death. *Am Heart J* **54**, 59-68 (1957).

9. Lee, M. P. *et al.* Targeted disruption of the Kvlqt1 gene causes deafness and gastric hyperplasia in mice. *J. Clin. Invest* **106**, 1447-1455 (2000).

10. Diener, M., Hug, F., Strabel, D. & Scharrer, E. Cyclic AMP-dependent regulation of K+ transport in the rat distal colon. *Br. J. Pharmacol.* **118**, 1477-1487 (1996).

11. Warth, R. *et al.* The cAMP-regulated and 293B-inhibited K+ conductance of rat colonic crypt base cells. *Pflugers Arch.* **432**, 81-88 (1996).

12. Dedek, K. & Waldegger, S. Colocalization of KCNQ1/KCNE channel subunits in the mouse gastrointestinal tract. *Pflugers Arch.* **442**, 896-902 (2001).

13. Roepke, T. K. *et al.* The KCNE2 potassium channel ancillary subunit is essential for gastric acid secretion. *J Biol. Chem.* **281**, 23740-23747 (2006).

14. Smith, J. A., Vanoye, C. G., Jr, A. L., Meiler, J. & Sanders, C. R. Structural Models for the KCNQ1 Voltage-Gated Potassium Channel. *Biochemistry. .,* (2007).

15. Hadley, J. K. *et al.* Stoichiometry of expressed KCNQ2/KCNQ3 potassium channels and subunit composition of native ganglionic M channels deduced from block by tetraethylammonium. *J Neurosci* **23**, 5012-5019 (2003).

16. Kubisch, C. *et al.* KCNQ4, a novel potassium channel expressed in sensory outer hair cells, is mutated in dominant deafness. *Cell* **96**, 437-446 (1999).

17. Schwake, M., Pusch, M., Kharkovets, T. & Jentsch, T. J. Surface expression and single channel properties of KCNQ2/KCNQ3, M-type K+ channels involved in epilepsy. *J Biol Chem.* **275**, 13343-13348 (2000).

18. Selyanko, A. A. *et al.* Inhibition of KCNQ1-4 potassium channels expressed in mammalian cells via M1 muscarinic acetylcholine receptors. *J Physiol (London)* **522 Pt 3**, 349-355 (2000).

19. Wang, H. S. *et al.* KCNQ2 and KCNQ3 potassium channel subunits: molecular correlates of the M-channel. *Science* **282**, 1890-1893 (1998).

20. Terrenoire, C., Clancy, C. E., Cormier, J. W., Sampson, K. J. & Kass, R. S. Autonomic Control of Cardiac Action Potentials. Role of Potassium Channel Kinetics in Response to Sympathetic Stimulation. *Circ. Res.* **96**, E25-E34 (2005).

21. Marx, S. O. *et al.* Requirement of a macromolecular signaling complex for beta adrenergic receptor modulation of the KCNQ1-KCNE1 potassium channel. *Science* **295**, 496-499 (2002).

22. Kurokawa, J., Motoike, H. K., Rao, J. & Kass, R. S. Regulatory actions of the A-kinase anchoring protein Yotiao on a heart potassium channel downstream of PKA phosphorylation. *Proc Natl Acad Sci U S A* **101**, 16374-16378 (2004).

23. Loussouarn, G. *et al.* Phosphatidylinositol-4,5-bisphosphate, PIP2, controls KCNQ1/KCNE1 voltage-gated potassium channels: a functional homology between voltage-gated and inward rectifier K+ channels. *EMBO J.* **22**, 5412-5421 (2003).

24. Park, K. H. *et al.* Impaired KCNQ1-KCNE1 and phosphatidylinositol-4,5-bisphosphate interaction underlies the long QT syndrome. *Circ. Res.* **96**, 730-739 (2005).

25. Grunnet, M. *et al.* KCNQ1 channels sense small changes in cell volume. *J. Physiol* **549**, 419-427 (2003).

26. Peretz, A., Schottelndreier, H., haron-Shamgar, L. B. & Attali, B. Modulation of homomeric and heteromeric KCNQ1 channels by external acidification. *J. Physiol* **545**, 751-766 (2002).

27. Shamgar, L. *et al.* Calmodulin is essential for cardiac IKS channel gating and assembly: impaired function in long-QT mutations. *Circ. Res.* **98**, 1055-1063 (2006).

28. Ghosh, S., Nunziato, D. A. & Pitt, G. S. KCNQ1 Assembly and Function Is Blocked by Long-QT Syndrome Mutations That Disrupt Interaction With Calmodulin. *Circ. Res.* **98**, 1048-1054 (2006).

29. Pourrier, M., Schram, G. & Nattel, S. Properties, expression and potential roles of cardiac K+ channel accessory subunits: MinK, MiRPs, KChIP, and KChAP. *J. Membr. Biol.* **194**, 141-152 (2003).

30. Pusch, M. Increase of the single-channel conductance of KvLQT1 potassium channels induced by the association with minK. *Pflugers Arch.* **437**, 172-174 (1998).

31. Tinel, N., Diochot, S., Borsotto, M., Lazdunski, M. & Barhanin, J. KCNE2 confers background current characteristics to the cardiac KCNQ1 potassium channel. *EMBO J* **19**, 6326-6330 (2000).

32. Schroeder, B. C. *et al.* A constitutively open potassium channel formed by KCNQ1 and KCNE3. *Nature* **403**, 196-199 (2000).

33. Mazhari, R., Nuss, H. B., Armoundas, A. A., Winslow, R. L. & Marban, E. Ectopic expression of KCNE3 accelerates cardiac repolarization and abbreviates the QT interval. *J Clin Invest* **109**, 1083-1090 (2002).

34. Bendahhou, S. *et al.* In vitro molecular interactions and distribution of KCNE family with KCNQ1 in the human heart. *Cardiovasc. Res.* **67**, 529-538 (2005).

35. Grunnet, M. *et al.* KCNE4 is an inhibitory subunit to the KCNQ1 channel. *J Physiol (London)* **542**, 119-130 (2002).

36. Chen, H., Kim, L. A., Rajan, S., Xu, S. & Goldstein, S. A. N. Charybdotoxin binding in the I_{Ks} pore demonstrates two MinK subunits in each channel complex. Neuron 40, 15-23. 2003.
    Ref Type: Journal (Full)

37. Morin, T. J. & Kobertz, W. R. Counting membrane-embedded KCNE beta-subunits in functioning K+ channel complexes. *Proc. Natl. Acad. Sci. U. S. A.* **105**, 1478-1482 (2008).

38. Wang, W., Xia, J. & Kass, R. S. MinK-KvLQT1 fusion proteins, evidence for multiple stoichiometries of the assembled IsK channel. *J. Biol. Chem.* **273**, 34069-34074 (1998).

39. Nakajo, K. & Kubo, Y. KCNE1 and KCNE3 stabilize and/or slow voltage sensing S4 segment of KCNQ1 channel. *J Gen. Physiol.* **130**, 269-281 (2007).

40. Kang, C. *et al.* Structure of KCNE1 and Implications for How It Modulates the KCNQ1 Potassium Channel. *Biochemistry* (2008).

41. Melman, Y. F., Domenech, A., de la, L. S. & Mcdonald, T. V. Structural determinants of KvLQT1 control by the KCNE family of proteins. *J Biol Chem.* **276**, 6439-6444 (2001).

42. Melman, Y. F., Krumerman, A. & Mcdonald, T. V. A single transmembrane site in the KCNE-encoded proteins controls the specificity of KvLQT1 channel gating. *J Biol Chem.* **277**, 25187-25194 (2002).

43. Panaghie, G., Tai, K. K. & Abbott, G. W. Interaction of KCNE subunits with the KCNQ1 K+ channel pore. *J. Physiol* **570**, 455-467 (2006).

44. Chen, Y. H. *et al.* KCNQ1 gain-of-function mutation in familial atrial fibrillation. *Science* **299**, 251-254 (2003).

45. Arnestad, M. *et al.* Prevalence of long-QT syndrome gene variants in sudden infant death syndrome. *Circulation.* **115**, 361-367 (2007).

46. Bianchi, L. *et al.* Mechanisms of I(Ks) suppression in LQT1 mutants. *Am. J Physiol Heart Circ. Physiol* **279**, H3003-H3011 (2000).

47. Hong, K. *et al.* De novo KCNQ1 mutation responsible for atrial fibrillation and short QT syndrome in utero. *Cardiovasc Res.* **68**, 433-440 (2005).

48. Manderfield, L. J., Daniels, M. A., Vanoye, C. G. & George, A. L. KCNE4 domains required for inhibition of KCNQ1. *J Physiol.* **587**, 303-314 (2009).

49. Takumi, T. *et al.* Alteration of channel activities and gating by mutations of slow I_{SK}. *J Biol Chem* **266**, 22192-22198 (1991).

50. Tapper, A. R. & George, A. L. J. MinK subdomains that mediate modulation of and association with KvLQT1. *J Gen Physiol* **116**, 379-390 (2000).

51. Gage, S. D. & Kobertz, W. R. KCNE3 truncation mutants reveal a bipartite modulation of KCNQ1 K+ channels. *J Gen. Physiol.* **124**, 759-771 (2004).

52. Manderfield, L. J. & George, A. L., Jr. KCNE4 can co-associate with the I(Ks) (KCNQ1-KCNE1) channel complex. *FEBS J.* **275**, 1336-1349 (2008).

53. Lundquist, A. L., Turner, C. L., Ballester, L. Y. & George, A. L., Jr. Expression and transcriptional control of human KCNE genes. *Genomics* **87**, 119-128 (2006).

54. Chen, H., Sesti, F. & Goldstein, S. A. Pore- and State-Dependent Cadmium Block of I(Ks) Channels Formed with MinK-55C and Wild-Type KCNQ1 Subunits. *Biophys. J* **84**, 3679-3689 (2003).

55. Piccini, M. *et al.* KCNE1-like gene is deleted in AMME contiguous gene syndrome: identification and characterization of the human and mouse homologs. *Genomics* **60**, 251-257 (1999).

56. Franco, D. *et al.* Divergent expression of delayed rectifier K(+) channel subunits during mouse heart development. *Cardiovasc Res.* **52**, 65-75 (2001).

57. Romey, G. *et al.* Molecular mechanism and functional significance of the MinK control of the KvLQT1 channel activity. *J Biol Chem.* **272**, 16713-16716 (1997).

58. Demolombe, S. *et al.* Differential expression of KvLQT1 and its regulator IsK in mouse epithelia. *Am J Physiol Cell Physiol* **280**, C359-C372 (2001).

59. Chouabe, C. *et al.* Properties of KvLQT1 K$^+$ channel mutations in Romano-Ward and Jervell and Lange-Nielsen inherited cardiac arrhythmias. *EMBO J* **16**, 5472-5479 (1997).

60. Felipe, A., Knittle, T. J., Doyle, K. L., Snyders, D. J. & Tamkun, M. M. Differential expression of Isk mRNAs in mouse tissue during development and pregnancy. *Am. J. Physiol* **267**, C700-C705 (1994).

61. Warth, R. & Barhanin, J. The multifaceted phenotype of the knockout mouse for the KCNE1 potassium channel gene. *Am J Physiol Regul. Integr. Comp Physiol* **282**, R639-R648 (2002).

62. Ohya, S., Asakura, K., Muraki, K., Watanabe, M. & Imaizumi, Y. Molecular and functional characterization of ERG, KCNQ, and KCNE subtypes in rat stomach smooth muscle. *Am. J. Physiol Gastrointest. Liver Physiol* **282**, G277-G287 (2002).

63. Heitzmann, D. *et al.* Heteromeric KCNE2/KCNQ1 potassium channels in the luminal membrane of gastric parietal cells. *J. Physiol* **561**, 547-557 (2004).

64. MacVinish, L. J., Guo, Y., Dixon, A. K., Murrell-Lagnado, R. D. & Cuthbert, A. W. Xe991 reveals differences in K(+) channels regulating chloride secretion in murine airway and colonic epithelium. *Mol. Pharmacol.* **60**, 753-760 (2001).

65. Abbott, G. W. *et al.* MiRP2 forms potassium channels in skeletal muscle with Kv3.4 and is associated with periodic paralysis. *Cell* **104**, 217-231 (2001).

66. McCrossan, Z. A. *et al.* MinK-Related Peptide 2 Modulates Kv2.1 and Kv3.1 Potassium Channels in Mammalian Brain. *J Neurosci* **23**, 8077-8091 (2003).

67. Grahammer, F., Warth, R., Barhanin, J., Bleich, M. & Hug, M. J. The small conductance K+ channel, KCNQ1: expression, function, and subunit composition in murine trachea. *J Biol Chem.* **276**, 42268-42275 (2001).

68. Ohya, S., Horowitz, B. & Greenwood, I. A. Functional and molecular identification of ERG channels in murine portal vein myocytes. *Am. J. Physiol Cell Physiol* **283**, C866-C877 (2002).

69. Akar, F. G., Yan, G. X., Antzelevitch, C. & Rosenbaum, D. S. Unique topographical distribution of M cells underlies reentrant mechanism of torsade de pointes in the long-QT syndrome. *Circ* **105**, 1247-1253 (2002).

70. Lundquist, A. L. *et al.* Expression of multiple KCNE genes in human heart may enable variable modulation of I_{Ks}. *J. Mol. Cell Cardiol.* **38**, 277-287 (2005).

71. Wang, Q. *et al.* Positional cloning of a novel potassium channel gene: KVLQT1 mutations cause cardiac arrhythmias. *Nature Genet* **12**, 17-23 (1996).

72. Splawski, I. *et al.* Spectrum of mutations in long-QT syndrome genes. *KVLQT1, HERG, SCN5A, KCNE1*, and *KCNE2. Circ* **102**, 1178-1185 (2000).

73. Sanguinetti, M. C., Jiang, C., Curran, M. E. & Keating, M. T. A mechanistic link between an inherited and an acquired cardiac arrhythmia: *HERG* encodes the I_{Kr} potassium channel. *Cell* **81**, 299-307 (1995).

74. Trudeau, M. C., Warmke, J. W., Ganetzky, B. & Robertson, G. A. *HERG*, a human inward rectifier in the voltage-gated potassium channel family. *Science* **269**, 92-95 (1995).

75. Curran, M. E. *et al.* A molecular basis for cardiac arrhythmia: *HERG* mutations cause long QT syndrome. *Cell* **80**, 795-803 (1995).

76. Veldkamp, M. W., van Ginneken, A. C., Opthof, T. & Bouman, L. N. Delayed rectifier channels in human ventricular myocytes. *Circ* **92**, 3497-3504 (1995).

77. Howarth, F. C., Levi, A. J. & Hancox, J. C. Characteristics of the delayed rectifier K current compared in myocytes isolated from the atrioventricular node and ventricle of the rabbit heart. *Pflugers Arch.* **431**, 713-722 (1996).

78. Spector, P. S., Curran, M. E., Keating, M. T. & Sanguinetti, M. C. Class III antiarrhythmic drugs block HERG, a human cardiac delayed rectifier K+ channel. Open-channel block by methanesulfonanilides. *Circ. Res.* **78**, 499-503 (1996).

79. Zou, A., Curran, M. E., Keating, M. T. & Sanguinetti, M. C. Single HERG delayed rectifier K+ channels expressed in Xenopus oocytes. *Am. J. Physiol* **272**, H1309-H1314 (1997).

80. Ho, W. K., Kim, I., Lee, C. O. & Earm, Y. E. Voltage-dependent blockade of HERG channels expressed in *Xenopus* oocytes by external Ca^{2+} and Mg^{2+}. *J. Physiol. (Lond.)* **507**, 631-638 (1998).

81. Zhou, Z. *et al.* Properties of HERG channels stably expressed in HEK 293 cells studied at physiological temperature. *Biophys J* **74**, 230-241 (1998).

82. Mcdonald, T. V. *et al.* A minK-HERG complex regulates the cardiac potassium current I_{Kr}. *Nature* **388**, 289-292 (1997).

83. Finley, M. R. *et al.* Expression and coassociation of ERG1, KCNQ1, and KCNE1 potassium channel proteins in horse heart. *Am J Physiol Heart Circ. Physiol* **283**, H126-H138 (2002).

84. Abbott, G. W. *et al.* MiRP1 forms I_{Kr} potassium channels with HERG and is associated with cardiac arrhythmia. *Cell* **97**, 175-187 (1999).

85. Jiang, M. *et al.* KCNE2 protein is expressed in ventricles of different species, and changes in its expression contribute to electrical remodeling in diseased hearts. *Circ* **109**, 1783-1788 (2004).

86. Splawski, I., Tristani-Firouzi, M., Lehmann, M. H., Sanguinetti, M. C. & Keating, M. T. Mutations in the hminK gene cause long QT syndrome and suppress I_{Ks} function. *Nature Genet* **17**, 338-340 (1997).

87. Sesti, F. *et al.* A common polymorphism associated with antibiotic-induced cardiac arrhythmia. *Proc. Natl. Acad. Sci. U. S. A* **97**, 10613-10618 (2000).

88. Isbrandt, D. *et al.* Identification and functional characterization of a novel KCNE2 (MiRP1) mutation that alters HERG channel kinetics. *J Mol. Med* **80**, 524-532 (2002).

89. Tyson, J. *et al.* IsK and KVLQT1: mutation in either of the two subunits of the slow component of the delayed rectifier potassium channel can cause Jervell and Lange-Nielsen syndrome. *Hum Mol Genet* **6**, 2179-2185 (1997).

90. Gordon, E. *et al.* A KCNE2 mutation in a patient with cardiac arrhythmia induced by auditory stimuli and serum electrolyte imbalance. *Cardiovasc. Res.* **77**, 98-106 (2008).

91. Guo, W., Xu, H., London, B. & Nerbonne, J. M. Molecular basis of transient outward K+ current diversity in mouse ventricular myocytes. *J Physiol (London)* **521 Pt 3**, 587-599 (1999).

92. Rosati, B. *et al.* Regulation of KChIP2 potassium channel beta subunit gene expression underlies the gradient of transient outward current in canine and human ventricle. *J Physiol (London)* **533**, 119-125 (2001).

93. Niwa, N. & Nerbonne, J. M. Molecular Determinants of Cardiac Transient Outward Potassium Current (Ito) Expression and Regulation. *J Mol. Cell Cardiol.* (2009).

94. Kuo, H. C. *et al.* A defect in the Kv channel-interacting protein 2 (KChIP2) gene leads to a complete loss of I(to) and confers susceptibility to ventricular tachycardia. *Cell* **107**, 801-813 (2001).

95. Roepke, T. K. *et al.* Targeted deletion of kcne2 impairs ventricular repolarization via disruption of IK,slow1 and Ito,f. *FASEB J.* ., (2008).

96. Ohno, S. *et al.* Novel KCNE3 mutation reduces repolarizing potassium current and associated with long QT syndrome. *Hum. Mutat.* **30**, 557-563 (2009).

97. Levy, D. I. *et al.* MiRP3 regulates Kv4.2 channels in a KChIP-dependent manner. *J Physiol.* (2010).

98. Radicke, S. *et al.* Functional modulation of the transient outward current Ito by KCNE beta-subunits and regional distribution in human non-failing and failing hearts. *Cardiovasc. Res.* **71**, 695-703 (2006).

99. Lerche, C. *et al.* Molecular cloning and functional expression of KCNQ5, a potassium channel subunit that may contribute to neuronal M-current diversity. *J. Biol. Chem.* **275**, 22395-22400 (2000).

100. Singh, N. A. *et al.* A novel potassium channel gene, *KCNQ2,* is mutated in an inherited epilepsy of newborns. *Nature Genet* **18**, 25-29 (1998).

101. Charlier, C. *et al.* A pore mutation in a novel KQT-like potassium channel gene in an idiopathic epilepsy family. *Nature Genet* **18**, 53-55 (1998).

102. Biervert, C. *et al.* A potassium channel mutation in neonatal human epilepsy. *Science* **279**, 403-406 (1998).

103. Tinel, N. *et al.* M-type KCNQ2-KCNQ3 potassium channels are modulated by the KCNE2 subunit. *FEBS Lett.* **480**, 137-141 (2000).

104. Lewis, A., McCrossan, Z. A. & Abbott, G. W. MinK, MiRP1, and MiRP2 diversify Kv3.1 and Kv3.2 potassium channel gating. *J Biol Chem.* **279**, 7884-7892 (2004).

105. Grunnet, M., Rasmussen, H. B., Hay-Schmidt, A., Rosenstierne, M. & Klaerke, D. A. KCNE4 is an inhibitory subunit to Kv1.1 and Kv1.3 potassium channels. *Biophys J* **85**, 1525-1537 (2003).

106. McCallum, L. A., Greenwood, I. A. & Tribe, R. M. Expression and function of K(v)7 channels in murine myometrium throughout oestrous cycle. *Pflugers Arch.* **457**, 1111-1120 (2009).

107. Grahammer F *et al.* The cardiac K+ channel KCNQ1 is essential for gastric acid secretion. *Gastroenterology* **120**, 1363-1371 (2001).

108. Roepke T.K. *et al.* The KCNE2 potassium channel ancillary subunit is essential for gastric acid secretion. *J Biol Chem.* **281**, 23740-23747 (2006).

109. Schroeder B.C. *et al.* A constitutively open potassium channel formed by KCNQ1 and KCNE3. *Nature* **403**, 196-199 (2000).

110. Roepke, T. K. *et al.* Kcne2 deletion uncovers its crucial role in thyroid hormone biosynthesis. *Nat. Med.* **%20.**, (2009).

111. Vallon, V. *et al.* Role of KCNE1-dependent K+ fluxes in mouse proximal tubule. *J Am Soc. Nephrol.* **12**, 2003-2011 (2001).

112. Levy, D. I., Wanderling, S., Biemesderfer, D. & Goldstein, S. A. MiRP3 acts as an accessory subunit with the BK potassium channel. *Am. J. Physiol Renal Physiol* **295**, F380-F387 (2008).

113. Nicolas, M., Dememes, D., Martin, A., Kupershmidt, S. & Barhanin, J. KCNQ1/KCNE1 potassium channels in mammalian vestibular dark cells. *Hear. Res.* **153**, 132-145 (2001).

114. Vetter, D. E. *et al.* Inner ear defects induced by null mutation of the isk gene. *Neuron.* **17**, 1251-1264 (1996).

115. Fetchko, M. & Stagljar, I. Application of the split-ubiquitin membrane yeast two-hybrid system to investigate membrane protein interactions. *Methods* **32**, 349-362 (2004).

116. Iyer, K. *et al.* Utilizing the split-ubiquitin membrane yeast two-hybrid system to identify protein-protein interactions of integral membrane proteins. *Sci. STKE.* **2005**, l3 (2005).

117. Johnsson, N. & Varshavsky, A. Split ubiquitin as a sensor of protein interactions in vivo. *Proc. Natl. Acad. Sci. U. S. A* **91**, 10340-10344 (1994).

118. Dunnwald, M., Varshavsky, A. & Johnsson, N. Detection of transient in vivo interactions between substrate and transporter during protein translocation into the endoplasmic reticulum. *Mol. Biol. Cell* **10**, 329-344 (1999).

119. Miller, J. P. *et al.* Large-scale identification of yeast integral membrane protein interactions. *Proc. Natl. Acad. Sci. U. S. A* **102**, 12123-12128 (2005).

120. Suter B, Auerbach D & Stagljar I. Yeast-based functional genomics and proteomics technologies: the first 15 years and beyond. *Biotechniques* **40**, 625-644 (2006).

121. Wang B, Pelletier J, Massaad M.J., Herscovics A & Shore G.C. The yeast split-ubiquitin membrane protein two-hybrid screen identifies BAP31 as a regulator of the turnover of endoplasmic reticulum-associated protein tyrosine phosphatase-like B. *Mol Cell Biol.* **27**, 2767-2778 (2004).

122. Yan, A., Wu, E. & Lennarz, W. J. Studies of yeast oligosaccharyl transferase subunits using the split-ubiquitin system: topological features and in vivo interactions. *Proc. Natl. Acad. Sci. U. S. A* **102**, 7121-7126 (2005).

123. Pandey, S. & Assmann, S. M. The Arabidopsis putative G protein-coupled receptor GCR1 interacts with the G protein alpha subunit GPA1 and regulates abscisic acid signaling. *Plant Cell* **16**, 1616-1632 (2004).

124. Matsuda, S. *et al.* The familial dementia BRI2 gene binds the Alzheimer gene amyloid-beta precursor protein and inhibits amyloid-beta production. *J. Biol. Chem.* **280**, 28912-28916 (2005).

125. Obrdlik P *et al.* K+ channel interactions detected by a genetic system optimized for systematic studies of membrane protein interactions. *Proc Natl Acad Sci USA* **101**, 12242-12247 (2004).

126. Peterson, B. Z., DeMaria, C. D., Adelman, J. P. & Yue, D. T. Calmodulin is the Ca2+ sensor for Ca2+ -dependent inactivation of L-type calcium channels. *Neuron* **22**, 549-558 (1999).

127. Sarhan, M. F., Van, P. F. & Ahern, C. A. A double tyrosine motif in the cardiac sodium channel domain III-IV linker couples calcium dependent calmodulin binding to inactivation gating. *J Biol. Chem.* (2009).

128. Shah, V. N. *et al.* Calcium-dependent regulation of the voltage-gated sodium channel hH1: Intrinsic and extrinsic sensors use a common molecular switch. *Proc. Natl. Acad. Sci. U. S. A.* **103**, 3592-3597 (2006).

129. Wen, H. & Levitan, I. B. Calmodulin Is an Auxiliary Subunit of KCNQ2/3 Potassium Channels. *J Neurosci* **22**, 7991-8001 (2002).

130. Gomez-Ospina, N., Tsuruta, F., Barreto-Chang, O., Hu, L. & Dolmetsch, R. The C terminus of the L-type voltage-gated calcium channel Ca(V)1.2 encodes a transcription factor. *Cell* **127**, 591-606 (2006).

131. McCrossan, Z. A. & Abbott, G. W. The MinK-related peptides. *Neuropharmacology* **47**, 787-821 (2004).

132. Li, Y., Um, S. Y. & Mcdonald, T. V. Voltage-gated potassium channels: regulation by accessory subunits. *Neuroscientist.* **12**, 199-210 (2006).

133. Abbott, G. W. & Goldstein, S. A. Disease-associated mutations in KCNE potassium channel subunits (MiRPs) reveal promiscuous disruption of multiple currents and conservation of mechanism. *FASEB J* **16**, 390-400 (2002).

134. Yang, Y. *et al.* Identification of a KCNE2 gain-of-function mutation in patients with familial atrial fibrillation. *Am. J. Hum. Genet.* **75**, 899-905 (2004).

135. Ma, K. J. *et al.* Modulation of KCNQ1 current by atrial fibrillation-associated KCNE4 (145E/D) gene polymorphism. *Chin Med J (Engl.).* **120**, 150-154 (2007).

136. Lundby, A. *et al.* KCNE3 Mutation V17M Identified in a Patient with Lone Atrial Fibrillation. *Cell Physiol Biochem.* **21**, 47-54 (2008).

137. Ravn, L. S. *et al.* Gain of function in I(Ks) secondary to a mutation in KCNE5 associated with atrial fibrillation. *Heart Rhythm.* **5**, 427-435 (2008).

138. Kurokawa, J., Chen, L. & Kass, R. S. Requirement of subunit expression for cAMP-mediated regulation of a heart potassium channel. *Proc Natl Acad Sci U S A* **100**, 2122-2127 (2003).

139. Kurokawa, J. *et al.* KCNE variants reveal a critical role of the beta subunit carboxyl terminus in PKA-dependent regulation of the IKs potassium channel. *Channels (Austin.).* **3**, 16-24 (2009).

140. Haitin, Y. *et al.* S1 constrains S4 in the voltage sensor domain of Kv7.1 K+ channels. *PLoS. ONE.* **3**, e1935 (2008).

141. Shen, Z. & Marcus, D. C. Divalent cations inhibit IsK/KvLQT1 channels in excised membrane patches of strial marginal cells. *Hear. Res.* **123**, 157-167 (1998).

142. Kerst, G. *et al.* Properties and function of KCNQ1 K+ channels isolated from the rectal gland of Squalus acanthias. *Pflugers Arch.* **443**, 146-154 (2001).

143. Boucherot, A., Schreiber, R. & Kunzelmann, K. Regulation and properties of KCNQ1 (K(V)LQT1) and impact of the cystic fibrosis transmembrane conductance regulator. *J Membr. Biol* **182**, 39-47 (2001).

144. Gamper, N., Li, Y. & Shapiro, M. S. Structural requirements for differential sensitivity of KCNQ K+ channels to modulation by Ca2+/calmodulin. *Mol Biol Cell* **16**, 3538-3551 (2005).

145. Kahlig, K. M. *et al.* Multiplexed transposon-mediated stable gene transfer in human cells. *Proc. Natl. Acad. Sci. U. S. A.* **107**, 1343-1348 (2010).

146. Torok, K. *et al.* Inhibition of calmodulin-activated smooth-muscle myosin light-chain kinase by calmodulin-binding peptides and fluorescent (phosphodiesterase-activating) calmodulin derivatives. *Biochemistry* **37**, 6188-6198 (1998).

147. Payne, M. E. *et al.* Calcium/calmodulin-dependent protein kinase II. Characterization of distinct calmodulin binding and inhibitory domains. *J. Biol. Chem.* **263**, 7190-7195 (1988).

148. Hamill, O. P., Marty, A., Neher, E., Sakmann, B. & Sigworth, F. J. Improved patch-clamp techniques for high-resolution current recording from cells and cell-free membrane patches. *Pflügers Arch* **391**, 85-100 (1981).

149. Lindau, M. & Neher, E. Patch-clamp techniques for time-resolved capacitance measurements in single cells. *Pflugers Arch.* **411**, 137-146 (1988).

150. Rhoads, A. R. & Friedberg, F. Sequence motifs for calmodulin recognition. *FASEB J* **11**, 331-340 (1997).

151. Terrenoire, C., Houslay, M. D., Baillie, G. S. & Kass, R. S. The cardiac IKs potassium channel macromolecular complex includes the phosphodiesterase PDE4D3. *J Biol. Chem.* **284**, 9140-9146 (2009).

152. Vanoye, C. G. *et al.* Distinct subdomains of the KCNQ1 S6 segment determine channel modulation by different KCNE subunits. *J Gen Physiol* **134**, 207-217 (2009).

153. Martin-Nieto, J. & Villalobo, A. The human epidermal growth factor receptor contains a juxtamembrane calmodulin-binding site. *Biochemistry* **37**, 227-236 (1998).

154. Li, H. & Villalobo, A. Evidence for the direct interaction between calmodulin and the human epidermal growth factor receptor. *Biochem J* **362**, 499-505 (2002).

155. Li, H., Ruano, M. J. & Villalobo, A. Endogenous calmodulin interacts with the epidermal growth factor receptor in living cells. *FEBS Lett.* **559**, 175-180 (2004).

156. Sah, R., Ramirez, R. J., Kaprielian, R. & Backx, P. H. Alterations in action potential profile enhance excitation-contraction coupling in rat cardiac myocytes. *J Physiol (London)* **533**, 201-214 (2001).

157. Bianchi, L. *et al.* Cellular dysfunction of LQT5-minK mutants: abnormalities of I_{Ks}, I_{Kr} and trafficking in long QT syndrome. *Hum Mol Genet* **8**, 1499-1507 (1999).

158. Dias Da Silva, M. R., Cerutti, J. M., Arnaldi, L. A. & Maciel, R. M. A mutation in the KCNE3 potassium channel gene is associated with susceptibility to thyrotoxic hypokalemic periodic paralysis. *J Clin Endocrinol Metab* **87**, 4881-4884 (2002).

159. Zeng, Z. *et al.* The Single Nucleotide Polymorphisms of I(Ks) Potassium Channel Genes and Their Association with Atrial Fibrillation in a Chinese Population. *Cardiology.* **108**, 97-103 (2006).

160. Schroeder B.C. *et al.* A constitutively open potassium channel formed by KCNQ1 and KCNE3. *Nature* **403**, 196-199 (2000).

161. Nerbonne, J. M. Studying cardiac arrhythmias in the mouse--a reasonable model for probing mechanisms? *Trends Cardiovasc Med* **14**, 83-93 (2004).

162. Baker, L. C., London, B., Choi, B. R., Koren, G. & Salama, G. Enhanced dispersion of repolarization and refractoriness in transgenic mouse hearts promotes reentrant ventricular tachycardia. *Circ. Res.* **86**, 396-407 (2000).

163. Barry, D. M., Xu, H., Schuessler, R. B. & Nerbonne, J. M. Functional knockout of the transient outward current, long-QT syndrome, and cardiac remodeling in mice expressing a dominant-negative Kv4 alpha subunit. *Circ. Res.* **83**, 560-567 (1998).

164. Brunner, M. *et al.* Characterization of mice with a combined suppression of I(to) and I(K,slow). *Am J Physiol Heart Circ. Physiol* **281**, H1201-H1209 (2001).

165. Demolombe, S. *et al.* Transgenic mice overexpressing human KvLQT1 dominant-negative isoform. Part I: Phenotypic characterisation. *Cardiovasc. Res.* **50**, 314-327 (2001).

166. Guo, W., Li, H., London, B. & Nerbonne, J. M. Functional consequences of elimination of i(to,f) and i(to,s): early afterdepolarizations, atrioventricular block, and ventricular arrhythmias in mice lacking Kv1.4 and expressing a dominant-negative Kv4 alpha subunit. *Circ. Res.* **87**, 73-79 (2000).

167. Jeron, A. *et al.* Inducible polymorphic ventricular tachyarrhythmias in a transgenic mouse model with a long Q-T phenotype. *Am. J. Physiol Heart Circ. Physiol* **278**, H1891-H1898 (2000).

168. Kodirov, S. A. *et al.* Attenuation of I(K,slow1) and I(K,slow2) in Kv1/Kv2DN mice prolongs APD and QT intervals but does not suppress spontaneous or inducible arrhythmias. *Am. J. Physiol Heart Circ. Physiol* **286**, H368-H374 (2004).

169. London, B. *et al.* Long QT and ventricular arrhythmias in transgenic mice expressing the N terminus and first transmembrane segment of a voltage-gated potassium channel. *Proc. Natl. Acad. Sci. U. S. A* **95**, 2926-2931 (1998).

170. Babenko, A. P., Aguilar-Bryan, L. & Bryan, J. A view of sur/KIR6.X, KATP channels. *Annu. Rev. Physiol* **60**, 667-687 (1998).

171. Flagg, T. P. *et al.* Arrhythmia susceptibility and premature death in transgenic mice overexpressing both SUR1 and Kir6.2[{Delta}N30,K185Q] in the heart. *Am J Physiol Heart Circ. Physiol.* **%20;.**, (2007).

172. Chu, V. *et al.* Method for non-invasively recording electrocardiograms in conscious mice. *BMC. Physiol* **1**, 6 (2001).

173. Bouchard, R. A., Clark, R. B. & Giles, W. R. Effects of action potential duration on excitation-contraction coupling in rat ventricular myocytes. Action potential voltage-clamp measurements. *Circ. Res.* **76**, 790-801 (1995).

174. Kaprielian, R. *et al.* Relationship between K+ channel down-regulation and [Ca2+]i in rat ventricular myocytes following myocardial infarction. *J Physiol (London)* **517 (Pt 1)**, 229-245 (1999).

175. Kaprielian, R., Sah, R., Nguyen, T., Wickenden, A. D. & Backx, P. H. Myocardial infarction in rat eliminates regional heterogeneity of AP profiles, I(to) K(+) currents, and [Ca(2+)](i) transients. *Am J Physiol Heart Circ. Physiol* **283**, H1157-H1168 (2002).

176. Sah, R. *et al.* Inhibition of calcineurin and sarcolemmal Ca2+ influx protects cardiac morphology and ventricular function in K(v)4.2N transgenic mice. *Circ* **105**, 1850-1856 (2002).

177. Lu, Z., Kamiya, K., Opthof, T., Yasui, K. & Kodama, I. Density and kinetics of I(Kr) and I(Ks) in guinea pig and rabbit ventricular myocytes explain different efficacy of I(Ks) blockade at high heart rate in guinea pig and rabbit: implications for arrhythmogenesis in humans. *Circ* **104**, 951-956 (2001).

178. Virag, L. *et al.* The slow component of the delayed rectifier potassium current in undiseased human ventricular myocytes. *Cardiovasc. Res.* **49**, 790-797 (2001).

179. Sah, R. *et al.* Regulation of cardiac excitation-contraction coupling by action potential repolarization: role of the transient outward potassium current (I(to)). *J Physiol (London)* **546**, 5-18 (2003).

180. Lopez-Lopez, J. R., Shacklock, P. S., Balke, C. W. & Wier, W. G. Local, stochastic release of Ca2+ in voltage-clamped rat heart cells: visualization with confocal microscopy. *J Physiol (London)* **480 (Pt 1)**, 21-29 (1994).

181. Lopez-Lopez, J. R., Shacklock, P. S., Balke, C. W. & Wier, W. G. Local calcium transients triggered by single L-type calcium channel currents in cardiac cells. *Science* **268**, 1042-1045 (1995).

182. Cannell, M. B., Cheng, H. & Lederer, W. J. The control of calcium release in heart muscle. *Science* **268**, 1045-1049 (1995).

183. Fiset, C., Clark, R. B., Larsen, T. S. & Giles, W. R. A rapidly activating sustained K+ current modulates repolarization and excitation-contraction coupling in adult mouse ventricle. *J Physiol (London)* **504 (Pt 3)**, 557-563 (1997).

184. Sah, R., Ramirez, R. J. & Backx, P. H. Modulation of Ca(2+) release in cardiac myocytes by changes in repolarization rate: role of phase-1 action potential repolarization in excitation-contraction coupling. *Circ. Res.* **90**, 165-173 (2002).

185. Jerng, H. H., Shahidullah, M. & Covarrubias, M. Inactivation gating of Kv4 potassium channels: molecular interactions involving the inner vestibule of the pore. *J Gen Physiol* **113**, 641-660 (1999).

186. Nerbonne, J. M. Molecular basis of functional voltage-gated K+ channel diversity in the mammalian myocardium. *J Physiol (London)* **525 Pt 2**, 285-298 (2000).

187. Jan, L. Y. & Jan, Y. N. Structural elements involved in specific K+ channel functions. *Annu. Rev. Physiol* **54**, 537-555 (1992).

188. Kong, W. *et al.* Isolation and characterization of the human gene encoding Ito: further diversity by alternative mRNA splicing. *Am J Physiol* **275**, H1963-H1970 (1998).

189. Ohya, S. *et al.* Molecular cloning and tissue distribution of an alternatively spliced variant of an A-type K+ channel alpha-subunit, Kv4.3 in the rat. *FEBS Lett.* **420**, 47-53 (1997).

190. Johns, D. C., Nuss, H. B. & Marban, E. Suppression of neuronal and cardiac transient outward currents by viral gene transfer of dominant-negative Kv4.2 constructs. *J Biol Chem.* **272**, 31598-31603 (1997).

191. Kassiri, Z., Hajjar, R. & Backx, P. H. Molecular components of transient outward potassium current in cultured neonatal rat ventricular myocytes. *J Mol Med.* **80**, 351-358 (2002).

192. Bou-Abboud, E. & Nerbonne, J. M. Molecular correlates of the calcium-independent, depolarization-activated K+ currents in rat atrial myocytes. *J Physiol (London)* **517 (Pt 2)**, 407-420 (1999).

193. Wickenden, A. D. *et al.* Targeted expression of a dominant-negative K(v)4.2 K(+) channel subunit in the mouse heart. *Circ. Res.* **85**, 1067-1076 (1999).

194. Xu, H., Guo, W. & Nerbonne, J. M. Four kinetically distinct depolarization-activated K+ currents in adult mouse ventricular myocytes. *J Gen Physiol* **113**, 661-678 (1999).

195. Nabauer, M., Beuckelmann, D. J., Uberfuhr, P. & Steinbeck, G. Regional differences in current density and rate-dependent properties of the transient

outward current in subepicardial and subendocardial myocytes of human left ventricle. *Circ* **93**, 168-177 (1996).

196. Fedida, D. & Giles, W. R. Regional variations in action potentials and transient outward current in myocytes isolated from rabbit left ventricle. *J Physiol (London)* **442**, 191-209 (1991).

197. Wickenden, A. D., Jegla, T. J., Kaprielian, R. & Backx, P. H. Regional contributions of Kv1.4, Kv4.2, and Kv4.3 to transient outward K+ current in rat ventricle. *Am J Physiol* **276**, H1599-H1607 (1999).

198. Liew, C. C. & Dzau, V. J. Molecular genetics and genomics of heart failure. *Nat. Rev. Genet.* **5**, 811-825 (2004).

199. Knollmann, B. C. *et al.* Casq2 deletion causes sarcoplasmic reticulum volume increase, premature Ca2+ release, and catecholaminergic polymorphic ventricular tachycardia. *J Clin. Invest.* **116**, 2510-2520 (2006).

200. Wang, Z., Fermini, B. & Nattel, S. Effects of flecainide, quinidine, and 4-aminopyridine on transient outward and ultrarapid delayed rectifier currents in human atrial myocytes. *J Pharmacol Exp Ther.* **272**, 184-196 (1995).

201. Wang, L., Swirp, S. & Duff, H. Age-dependent response of the electrocardiogram to K(+) channel blockers in mice. *Am J Physiol Cell Physiol* **278**, C73-C80 (2000).